Multiple-tracer based characterisation of a river catchment in the Pamir Mountains

Dissertation
zur Erlangung des
Doktorgrades der Naturwissenschaften (Dr. rer. nat.)

der

Naturwissenschaftlichen Fakultät III
Agrar- und Ernährungswissenschaften,
Geowissenschaften und Informatik

der Martin-Luther-Universität Halle-Wittenberg

vorgelegt

von Frau Christiane Meier
geb. am 25.12.1983 in Rodewisch

1. Gutachter: Prof. Dr. Ralf Merz
2. Gutachter: Prof. Dr. Michael Zech

Tag der Verteidigung: 05.05.2020

Für meine Familie

Acknowledgements

Abstract

The Pamir Mountains in Tajikistan are part of a semi- to cold-arid mountain region in Central Asia. Its snow and glacier deposits are the source of one of the largest Central Asian rivers - the Amu Darya. The development of the further availability of these important fresh water resources depending on high impact from factors such as climate change is in the central focus of this study. For this, the actual hydrological condition of the high-alpine catchment of the Gunt river is supposed exemplary for the Pamir. By application of hydrochemical tracers (major ions and physico-chemical parameters) and isotope hydrological methods (δ^2H, ^{3}H, δ^{18}O, δ^7Li, ^{87}Sr/^{86}Sr, noble gases) basic hydrological processes are identified and described. This multi-tracer approach allows to get a detailed picture on the flow regime and chemical evolution of the river water of two to three circles of season and gives the fact that the catchment area of the Gunt is a geomorphologically young catchment area, which reacts fast on hydrological changes due to its climatically, geological and geomorphological conditions. There are clear regional and seasonal variations in all investigated parameters. The catchment area can be subdivided into northern catchment areas, southern catchment areas, the eastern plateau, which is mainly characterized by the lake Yashilkul and the main river Gunt collecting all hydrogeochemical signals. In data of the δ^{18}O and δ^2H values and the major anions and cations, a clear annual cycle is recognizable. This has shown that snow melting and glacier melting are the dominant processes for runoff formation and that runoff is less strongly fed by large groundwater deposits. By determining the transit time with ^{3}H/^{3}He, it became clear that at exemplary cold springs the transit time is less than two years, and in wells in the steep northern subcatchments and in the southern subbasins and the Gunt river itself the transit time is less than ten years. Only the hot springs show transit times of at least twenty years and more. Therefore, it can be assumed that the meltwater is not strongly retained in deeper aquifers. The glaciers in the catchment area of the Gunt are also affected by strong melting processes. This in turn would mean that the investigated catchment is very sensitive to any changes of water input from the available current glacier decreases and the current meteorological circulations containing poor precipitation from the Atlantic, the Mediterranean, the Caspian Sea and the Persian Gulf and it also would be affected by increasing water scarcity in the next decades.

Zusammenfassung

Das Pamirgebirge in Tadschikistan ist Teil einer semi- bis kaltariden Bergregion in Zentralasien. Seine Schnee- und Gletscherablagerungen sind die Quelle eines der größten zentralasiatischen Flüsse - des Amu Darya. Die Entwicklung der weiteren Verfügbarkeit dieser wichtigen Süßwasserressourcen in Hinblick auf bevorstehende Veränderungen durch den Klimawandel steht im Mittelpunkt dieser Studie. Dazu wird der tatsächliche hydrologische Zustand des hochalpinen Einzugsgebietes des Gunt Flusses exemplarisch für den Pamir beschrieben. Durch den Einsatz von hydrochemischen Tracern (Hauptionen und physikalisch-chemische Parameter) und isotopenhydrologischen Methoden ($\delta^{18}O$, δ^2H, δ^7Li, $^{87}Sr/^{86}Sr$, $^3H/^3He$) werden grundlegende hydrologische Prozesse identifiziert und beschrieben. Dieser Multi-Tracer-Ansatz ermöglicht es, ein detailliertes Bild über das Abflussregime und die chemische Entwicklung des Flusswassers über zwei bis drei hydrologische Jahre zu erhalten und zeigt, dass das Einzugsgebiet des Gunt ein geomorphologisch junges Einzugsgebiet ist, das aufgrund seiner klimatischen, geologischen und geomorphologischen Bedingungen schnell reagiert. Bei allen untersuchten Parametern gibt es deutliche regionale und saisonale Schwankungen. Das Einzugsgebiet lässt sich klar unterteilen in nördliche Einzugsgebiete, südliche Einzugsgebiete, das östliche Plateau, welches hauptsächlich durch den See Yashilkul geprägt ist, und den Hauptfluss Gunt, der alle Signale in sich vereint. Sowohl in den $\delta^{18}O$ und δ^2H Werten sowie in den Hauptan- und kationen ist ein klarer Jahreszyklus erkennbar. Dies zeigt, dass Schnee- und Gletscherschmelze die dominierenden Prozesse für die Abflussbildung sind und dass der Abfluss weniger stark von großen Grundwasservorkommen gespeist wird. Durch die Bestimmung der Verweilzeit mit $^3H/^3He$ wird deutlich, dass die mittlere Verweilzeit an ausgewählten kalten Quellen und Brunnen der steilen nördlichen Teileinzugsgebiete weniger als zwei Jahre beträgt sowie in den südlichen Einzugsgebieten und dem Fluss Gunt selbst die mittlere Verweilzeit weniger als zehn Jahre beträgt. Nur die heißen Quellen weisen durchschnittliche Verweilzeiten von mindestens zwanzig Jahren und mehr auf. Daher ist davon auszugehen, dass das Schmelzwasser nicht in tieferen Grundwasserleitern stark zurückgehalten wird. Auch die Gletscher im Einzugsgebiet des Gunt sind von starken Schmelzprozessen betroffen. Dies wiederum bedeutet, dass das untersuchte Einzugsgebiet sehr empfindlich auf Veränderungen der hydrologischen Rahmenbedingungen, wie zum Beispiel das Abschmelzen der Gletscher und die aktuellen meteorologischen Zirkulationen mit geringen Niederschlägen aus dem Atlantik, dem Mittelmeer, dem Kaspischen Meer und dem Persischen Golf, reagiert und es in den nächsten Jahrzehnten von der zunehmender Wasserknappheit betroffen sein wird.

Table of contents

List of figures

List of tables

Index to Appendices

List of abbreviations

a.s.l. – above sea level	meq – milliequivalents
AMJJAS – April, May, June, July, August, September	MM/YYYY – Date (month/year)
BMBF – Federal Ministry of Education and Research	NIST – National Institute of Standards and Technology
CAME – Monsoon Dynamics and Geo-Ecosystems	PBL – planetary boundary layer
d – deuterium excess	PE – Polyethylene
DEM – digital elevation model	Q – Discharge (min = minimum, max = maximum, mean)
EC – Electric conductivity	RH – relative humidity
FAO – Food and Agriculture Organization of the United Nation	RT – residence time
GBAO – Province Gorno-Badakhshan	SI – saturation index
GDAS – Global Data Assimilation System	SLAP – Standard Light Antarctic Precipitation
GMWL – Global Meteoric Water Line	SPM – Suspended Particulate Matter
GNIP – Global Network of Isotopes in Precipitation	SST – sea surface temperature
HCl – hydrochloric acid	T – Temperature
HDPE – high-density polyethylene	TIMS – thermal ion mass spectrometry
HF – hydrofluoric acid	TPE – Third Pole Environment
HNO_3 – nitric acid	TT – Transit Time resp. MRT (Mean Residence Time)
HYSPLIT – Hybrid Single Particle Lagrangian Integrated Trajectory Model	TU – tritium unit
IAEA – International Atomic Energy Agency	TUBA – University of Resources Freiberg
ICP-OES – inductively coupled plasma optical emission spectrometry	UFZ – Helmholtz Centre for Environmental Research
IQR – Interquartile range	USAF – United States Air Force
IRIS – isotope ratio infrared spectroscopy	USGS – U.S. Geological Survey
ISM – Indian Summer Monsoon	VSMOW – Vienna Standard Mean Ocean Water
LMWL – Local Meteoric Water Line	W/Q ratio – weathering/precipitation ratio

(MC)-ICP-MS – (Multi-collector) inductively coupled plasma mass spectrometer	WRI – water rock interaction

1   Introduction

The high mountains are widely called as the water towers of the world (Viviroli and Weingartner 2004). As a result of plate tectonics, the high mountain range of the ongoing Earth forming crust built the characteristic shape of the planet Earth. The high mountains are very important fresh water suppliers for the mountain region itself and for the surrounding valleys and plains. From highland watersheds, 32 % to 95 % of freshwater can be provided via various hydrological processes (Meybeck et al. 2001; Viviroli and Weingartner 2004). On the one hand, due to the orographic effect, in the upper layers along the mountain slopes more condensation and precipitation takes place. Therefore, more precipitation falls in the mountains than in the plains. This precipitation can then either fall in form of rain creating direct surface runoff or of snow, which is stored during the cold season until snow melt takes place during change of season. Accordingly, precipitation resulting in runoff becomes available to the population for various hydrological aspects, e.g. as drinking water, irrigation water, water power. However, not only precipitation contributes to runoff in the mountain regions: In the high mountains, glaciers also play an important role in hydrology. Due to climate change, these important water reservoirs are particularly affected by increased melting and will most likely no longer be available for water supply in the future. Other compartments that can contribute to runoff are outflowing groundwater resources that feed surface waters or melting permafrost deposits.

However, the importance of the influence of the mountains on the water supply of the lowlands depends to a large extent on their geographical location. Mountains in humid regions of the Earth are less important for the water supply of the surrounding lowlands than mountains in arid or semi-arid areas (Viviroli and Weingartner 2004). If one compares the importance of the mountain discharge for the surrounding lowlands worldwide, the Amu Darya stands for Asia in first place (Viviroli et al. 2003). The two tributaries of the Amu Darya, the Vakhsh and the Panj, have their origin in the Pamir Mountains, which are also called "roof of the world" (Brockhaus 1928).

The Pamir, with its surrounding mountains and sedimentary basins, is a key region for research into the climatic changes of recent years and the geological history (paleoclimatology). This makes it one of the world's most interesting regions for climatic and hydrological studies alongside the polar regions and is part of the so-called "Third Pole Environment – TPE" (Yao et al. 2012). The TPE extends from the Pamir in the west over the Tibet Plateau to the Hengduan Mountains in the east.

This predominantly semi-arid region is home to the world's highest mountains, which are very sensitive to climatic changes and human influences.

The Food and agriculture organization of the United Nation (2017) states that water abstraction exceeds recharge rates and water bodies are overexploited in Central Asia. This has a negative impact on aquatic ecosystems and also hinder socio-economic development. Due to climate change, a shortage of water is forecasted for the TPE, partly due to the decline in glacier deposits. Especially for the Central Asian states, which are all together riparian states of the Amu Darya and, in minor extend, the Syr Darya, a strong population growth and

a predicted increasing water shortage are expected. In view of the increased demand for water in the individual Central Asian states, the resource water thus represents an enormous potential for conflict.

In order to estimate how much water is actually available in the region, how water resources are distributed and what impact climate change has on the region and water resources, the Federal Ministry of Education and Research (BMBF) initiated a research program entitled "Central Asia – Monsoon Dynamics and Geo-Ecosystems (CAME)", which funded a total of 54 individual projects. A subproject of this project group is the project "PAMIR water - influence of climate change on the water balance of a river basin in the Pamir", in which the present dissertation is embedded. The aim of the project PAMIR water is to record hydro(geo)logical processes such as runoff and groundwater recharge in an exemplary high-alpine catchment of the Pamir in Tajikistan, to model the effects of climate change and to transfer them to the whole Pamir region.

Objective

In this dissertation an exemplary catchment area for the Pamir is characterized hydro(geo)logically by means of environmental tracers. The specific investigated high-alpine catchment of the Pamir comprises the extensions of the river Gunt. The aim is to describe the water cycle in the Gunt river basin at different places and different times and to uncover causal relationships to the natural conditions of the individual tributaries. In order to carry out an initial hydrogeological characterisation of the catchment area, various tracer methods were selected and applied to different hydrological components. To describe origins of precipitation and to link precipitation with runoff stable isotopes of water (δ^{18}O and δ^{2}H) were selected. Hydrochemical data of major ions were used to describe the hydrochemical system of surface water and to decipher influences on runoff generation. Additionally, lithium isotopes were used to describe the groundwater compartment and within this the interactions between water and rock.

Specific objectives are set by the following questions under the framework of the three before mentioned particular aspects:

Aspect 1 – Characterization of precipitation and river water by using oxygen and hydrogen isotopes

- How can seasonal precipitation impacts be identified in the main stream and its tributaries?
- Are there local differences between the sub catchments?
- What is the main contribution to the head water?

Aspect 2 – Assessment of the hydrochemical system using statistical analysis methods

- Are there differences of water chemistry between the tributaries and main stream and how are they related to aspects of background geology and morphology?
- Are there seasonal changes of water chemistry identifiable and what are they based on?

Aspect 3 – Description of water-rock interactions with lithium isotopes in respect of residence times (RT)

- Are there differences in river water evolution in the Gunt catchment?
- Can a development of water chemistry along the flow path be traced?
- How long are the residence times (RTs) of the river?

In order to characterize the water resources in the catchment area, samples of precipitation and river water were taken monthly over a period of three years. In addition, random samples of different groundwater leaks (hot and cold springs), stagnant waters and glacier samples were obtained. These samples were examined for their hydrochemical composition. Among other things, the stable isotopes of the water (δ^2H and δ^{18}O) and hydrochemical parameters (electrical conductivity, pH value, water temperature and major ions) were analyzed. Li and Sr isotope investigations were also used as a natural tracer for a specific issue and linked to transit times that were obtained by applying the ^{3}H/^{3}He dating method. Descriptive and multivariate statistical methods were used to evaluate and interpret the measured data. Furthermore, a backtracking model was used to track precipitation origins as well as a reactive transport model to clarify the process understanding with regard to the water-rock interactions.

2 Study area – the Gunt catchment

2.1 Geography

Tajikistan is a landlocked state in the southeastern part of Central Asia. Bordering states are Kyrgyzstan in the north, China in the east, Afghanistan in the south and Uzbekistan in the west. The investigation area is the river Gunt catchment, which is situated in the Amu Darya headwaters (Figure 1). It is part of the Pamir Mountains and lies in the south-eastern part of Tajikistan in the province Gorno-Badakhshan (GBAO). The Pamir is surrounded by large and high mountain ranges – the Karakorum Range in the south east, the Kunlun Mountains in the south, and the Tien-Shan in the north east.

Figure 1: General map of Central Asia showing Tajikistan and the Gunt catchment (pink), source of world borders from: thematicmapping.org.

The Tajik Pamir can be divided into the Eastern and Western Pamirs. Typical for the Eastern Pamir are comparatively smooth relief forms, plateaus and pastures (Figure 3, right). The West-Pamir is characterized by steep relief with deep river valleys (Bill and Schreiber 2010) (Figure 3, left). The Gunt catchment is a high alpine east-west running basin covering with an area of about 14,000 km² ca. 1/10 of the whole country (Figure 2). It belongs both to the Eastern and to the Western Pamirs. The catchment shows an altitudinal range between circa 2000 m at the Gunt's mouth in Khorog and more than 6500 m a.s.l. at the highest peaks (Pik Karl Marx 6726 m a.s.l. and Pik Engels 6510 m a.s.l.), whereas the mean altitude is at about 4300 m a.s.l.. The catchment is characterised in the East by a high alpine plateau (ca. 4000 m a.s.l.) with broad and flat valleys; the western sub basin represents a steep landscape with a high relief dynamic, as it is typical for the both Pamir regions, respectively. Almost 10 % of the Pamir Mountains are covered by glaciers (Knoche et al. 2017). The Gunt catchment showed in 2011 a glaciation of about 4.5 % (Lindner 2014).
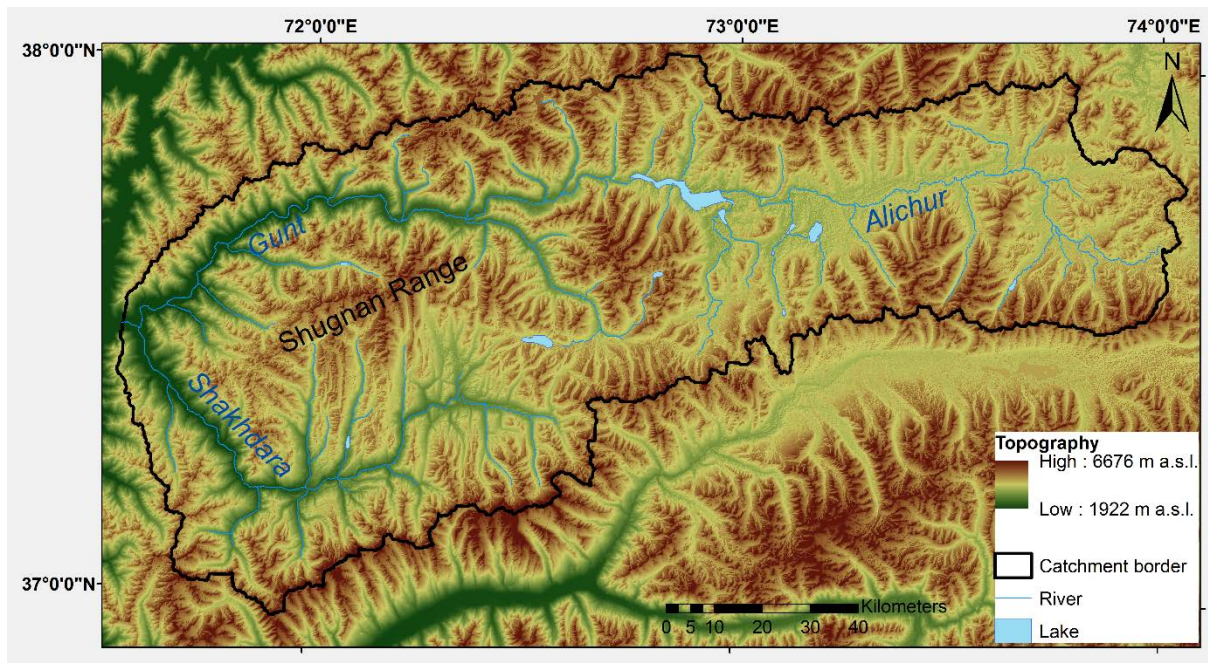
Figure 2: Topography of the Gunt catchment.

Furthermore, Tajikistan has over 200 lakes of different origins. The largest lake in the Pa-mirs is the Karakul Salt Lake. The lakes Yashilkul and Bulunkul are located in the valley of the river Alichur, a tributary of river Gunt that discharges the Eastern part of the catchment. The Pamir also has more than 80 springs, many of them are hot and contain sulphur, sodium and potassium. The most famous thermal springs in the Gunt catchment are the hot springs in Djelondi (Figure 5, right) between Alichur and Khorog (Bill and Schreiber 2010).

Figure 3: Changing relief types. Left: West Pamir with steep valleys. Right: High plateau in East Pamir.

The Afghan-Tajik border river Panj belongs to the longest rivers in Tadjikistan and is located in the south of Tajikistan. The investigated Gunt (Figure 5, middle) is a tributary of the Panj and has together with river Alichur a length of 296 km. The Alichur flows through the lake Yashilkul (Figure 5, left), and afterwards as river Gunt it takes up the water of the river Shakhdara shortly before Khorog and flows into the Panj after the city.

The discharge at the hydrological station at the river outflow in Khorog shows a mean annual runoff of 105 m³/s with strong intra-annual variations. From October to March the discharge is very low ($Q_{mean} \approx 44$ m³/s) and continuously declining to its minimum discharge in March ($Q_{min} \approx 30$ m³/s). In April, the melting season starts and thus, discharge rapidly increases and shows its maximum value in July ($Q_{max} \approx 290$ m³/s), whereas the average discharge for the summer period (AMJJAS) is about 164 m³/s (Pohl et al. 2015). Pohl et al. (2015) also stated that the interannual variations of the summer hydrograph are strong, whereas the winter hydrograph shows a low and rather constant pattern (Figure 4).
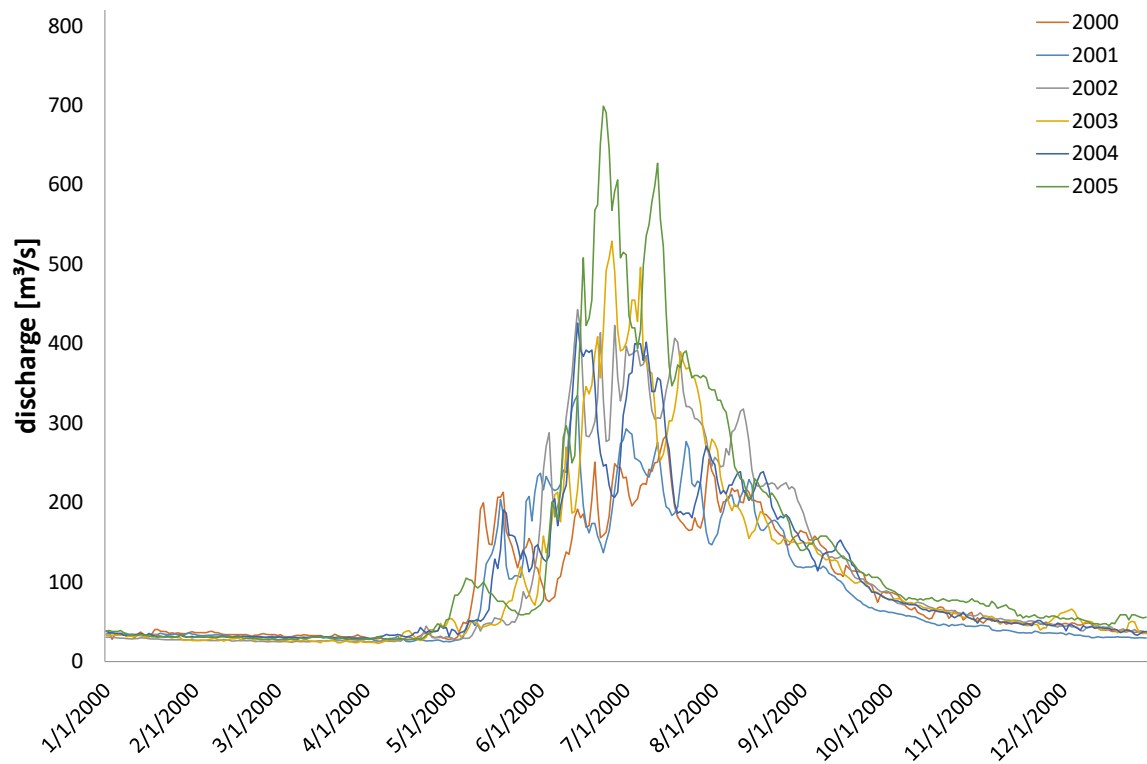
Figure 4: Discharge patterns for the years 2000-2005 of the river Gunt at the hydrological station in Khorog.

This suggests that snow and glacier melt is important for the discharge in summer. However, in winter groundwater runoff has a significant and constant impact on runoff generation (Knoche et al. 2017).

Figure 5: Hydrological situation in the Pamir Mountains. Left: Lake Yashilkul, middle: River Gunt near Sardem, right: hot spring in Djelondi.

2.2   Climate

In general, Tajikistan is influenced by a pronounced continental climate with long, hot summers and short mild winters (Bill and Schreiber 2010). The Pamirs instead show a semiarid to cold-arid climate. The Western Pamir is characterized by a semiarid climate with hot dry summers and a precipitation maximum in the winter months. However, the Eastern Pamir shows cold-arid climate conditions (Peel et al. 2007). In contrast to the Himalayas that receive their precipitation mainly from the Indian summer monsoon (ISM), the Pamirs lie in the transition zone of different atmospheric circulation systems (Aizen et al. 2009; Zech et al. 2005; Fuchs et al. 2013). Primarily, the Pamir is influenced by the westerlies. This leads on the one hand to a west-east gradient in the precipitation (sum of annual precipitation: Khorog = 200 mm/a, Bulunkul = 100 mm/a) and on the other hand to a precipitation maximum in winter, which is dominated by snow (Maussion et al. 2014). Only in the easternmost part of the Gunt catchment it is supposed that the influence of the Indian monsoon increases. One evidence for the increasing ISM influence could be the shift of the maximum precipitation into summer (Aizen et al. 2009; Fuchs et al. 2013)(see Figure 6). However, this hypothesis is still subject of controversial discussions (Pohl et al. 2015; Meier et al. 2013). Knoche et al. (2017) supports the assumption of Aizen et al. (2009) that also polar air masses have an influence on precipitation in the far eastern part of GBAO. In addition, the area is characterized by a very high potential evaporation of 600-1000 mm/a (Gorbunov 1990) and a significant decrease in the average temperatures from west to east (Figure 6).
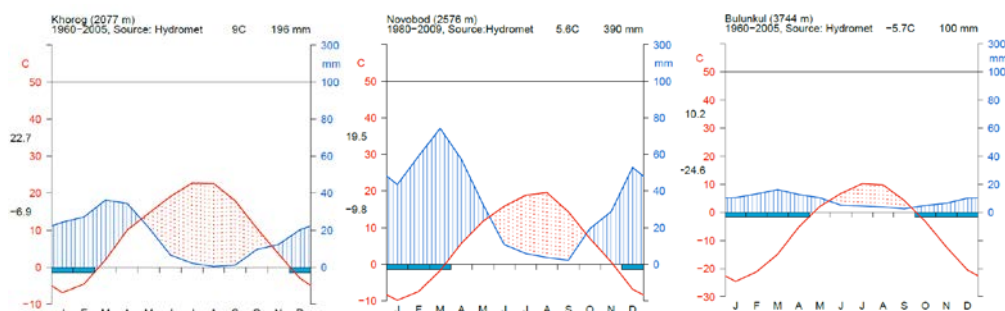
Figure 6: Climate diagrams from three meteorological stations (Khorog, Navabad and Bulunkul) in the Gunt catchment from west (left) to east (right) (Lindner 2014).

2.3   Vegetation

The vegetation in the Pamir is very sparse (Pohl et al. 2015) and is characterized above all by different kinds of juniper trees in the western, lower and humid mountainous areas. In addition, numerous shrubs and bushes such as honeysuckle, maple, rose hip, hawthorn, barberry and sea buckthorn are also part of typical vegetation. Lichens and herbs, such as wild rosemary, are also native to the area. Up to an altitude of 2200 m a.s.l. there are occasional walnut trees; juniper trees grow up to 3000 m a.s.l.. Along the rivers and at the springs in western Pamir there are birches and willows. The East Pamir is extremely dry, the vegetation accordingly sparse. Besides bush plants, feverfew and grasses, there are some dwarf and half-shrub species. The high pastures up to ~4000 m above sea level are characterized by low grass plants. Half shrub also grows in high and dry areas and is an important winter

food source for the animals. In the rocky landscape >4500 m above sea level only very low plants and some fungi remain (Bill and Schreiber 2010).

2.4 Geology

The mountain massifs and high plateaus of the Pamir were created together with the Himalaya in the broadest sense through the collision of two continental plates: the Indian Plate in the south and the Eurasian Plate in the north (Schwab et al. 2004; Robinson et al. 2004). Topographically, the Pamir forms the northwestern extension of the Tibetan Plateau (Fuchs et al. 2013). The mountain can be geologically divided into three areas: the North Pamir, the Central Pamir and the South Pamir (Burtman and Molnar 1993)(Figure 7).

The study area is mainly located in the South Pamir, which is geologically subdivided into the North Alichur and South Alichur areas and is traversed in the east by the northwest-southeast running dextral Aksu-Murghab disorder (Figure 7). In the north follows the relatively narrow Rushan-Pshart zone of ophiolite sequences, which are also represented in the form of small cliffs in southern Pamir.
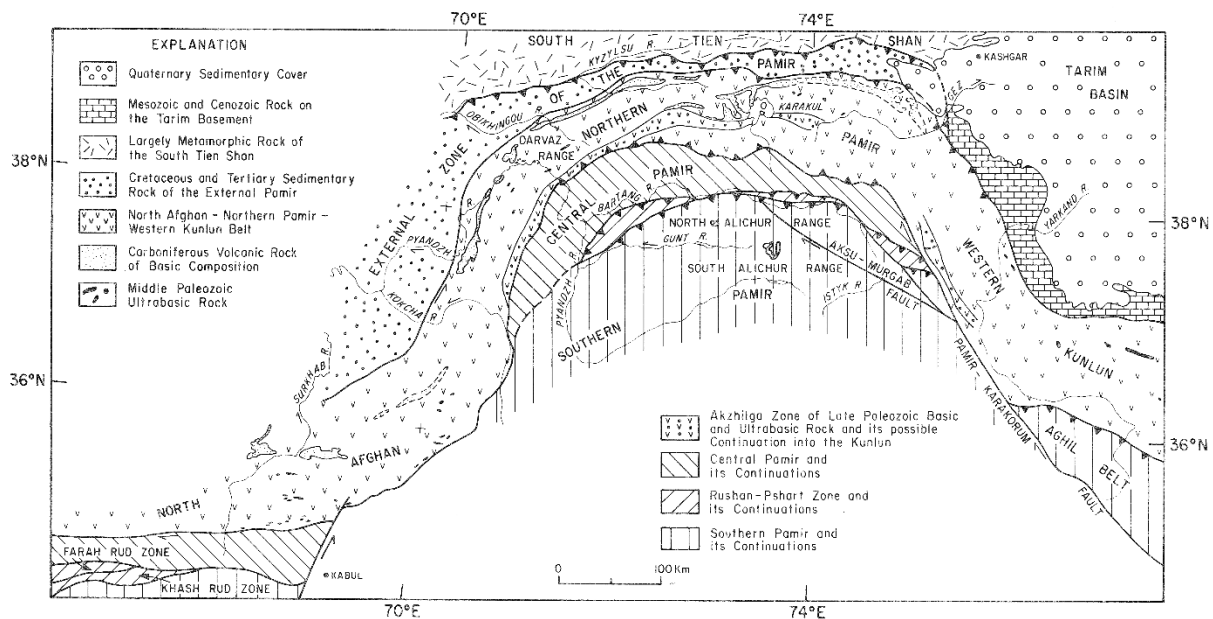
Figure 7: Geological overview with tectonic units, the Pamir regions as well as Palaeozoic and Mesozoic overthrust paths (Burtman and Molnar 1993).

This Rushan-Pshart zone contains rocks of the Palaeozoic, which are discordantly overlaid by late Carboniferous and early Permian sandstones, limestones and marl (Figure 8). These are detritic and carbonatic sediments of a former shallow water zone in the area of the passive continental margin. These are superimposed by carbonic and palaeogenic sediments without noticeable unconformity. Most areas have the entire sequence of rocks from carbon to palaeogen with partly some lacks of the late Jurassic and early Cretaceous.
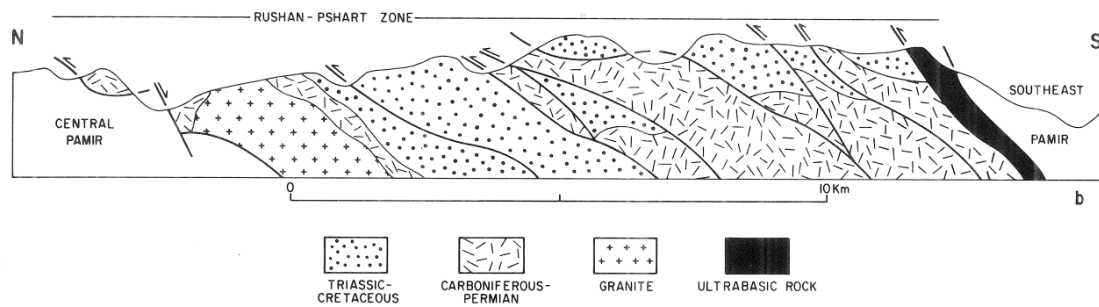
Figure 8: Profile section through the Rushan-Pshart zone (Burtman and Molnar 1993).

In the North Alichur region, metamorphic rocks of the Southwest Pamir are covered by basalt, picrit and tufa, which also contain Triassic limestones. This ceiling, which was pushed up in the late Triassic period, is covered by Jurassic sediments. Significantly thicker layers of Mesozoic ophiolites can be found in the southern Alichur region, near the border between southeast and southwest Pamir. These are also stored on metamorphic rocks and are superimposed by Jurassic sediments. The lower part of the ophiolites consists of ultramafic tectonites, overlaid by alkali-olivin basalts and tholeit basalt with layers of siliceous slate and tuffs. Further up in the sequence are included lava, tuffs and olisthostromes with blocks of Permian and Triassic.

The South Pamir is subdivided by very different rock sequences into a southeast part and a southwest part. The southwestern consists of Precambrian metamorphites with Mesozoic and palaeogenic granite intrusions (Leonov et al. 2017). In the southeast, the oldest rocks are Carboniferous to Permian sandstone, siltstone, claystone and limestone (Figure 9). The Triassic sequence of limestones, radiolarites and claystones contains little basalt lava and tuffs, such as those of the Rushan-Pshart zone. These layers are overlaid by Jurassic reef limestones and Cretaceous sediments containing alternating layers of conglomerates, dacites, andesites, tuffs and limestones. Folding in the southeast Pamir and the Rushan-Pshart zone took place in the Jura up to possibly the early Cretaceous; however, all tectonic structures were reactivated during the Cenozoic deformation processes (Burtman and Molnar 1993).
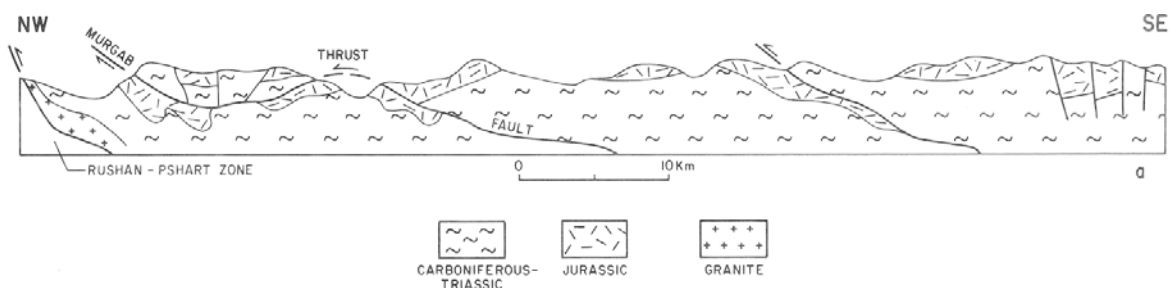
Figure 9: Profile section through the Murghab disturbance in southeast Pamir (Burtman and Molnar 1993).
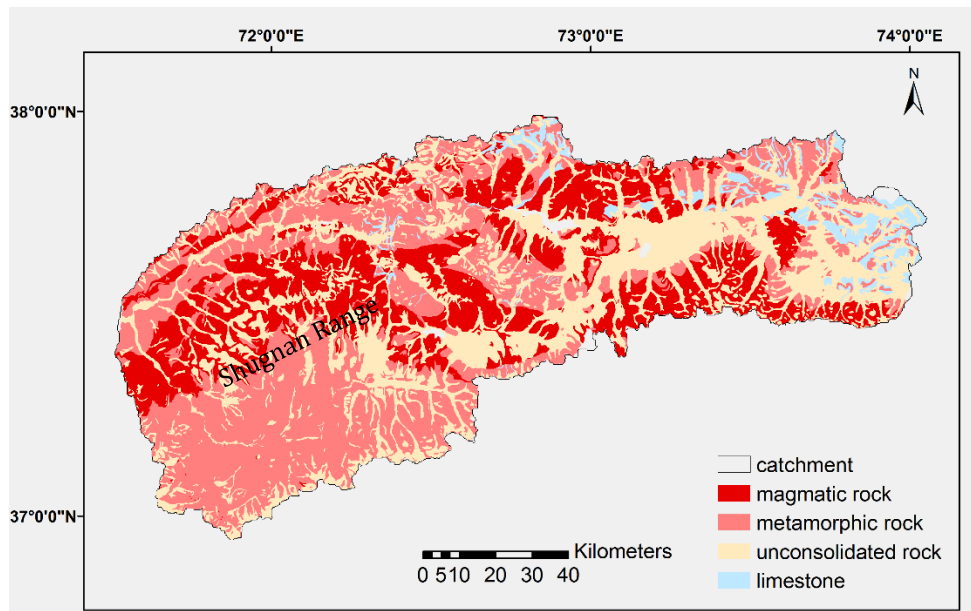
Figure 10: Lithological units in the Gunt catchment.

According to the geological map (Figure 10) the lithology of the Pamirs can be grouped into four lithological units: "unconsolidated rock", "limestone", "magmatic rock" and "metamorphic rock". The group "unconsolidated rock" contains Eocene and Oligocene boulders and the entire Quaternary sediments. The second group consists of Permian, Jurassic and Triassic limestones and Proterozoic marbles. The crystalline rock can be divided into "magmatites" and "metamorphites", whereas granites, granodiorites and diorites from Mesozoic intrusions can be generally combined to "magmatites". The group "metamorphites" includes Precambrian gneiss as well as Palaeozoic mica schist and Mesozoic schist, clay slate and phyllite.

The distribution of lithological units follows in the western part arching belts of metamorphic and igneous rocks, e.g. granite, granodiorite and gneiss. In the northern side of the catchment the bedrock consists mainly of granite, migmatite and biotite rich rocks, southerly a band of biotite rich gneisses follows; the Shugnan Range is represented by a huge granitic intrusion, and in the southernmost belt the band of biotite rich gneisses continues. Only in the eastern high plain unconsolidated rock like marl and moraine material as well as limestone and schist can be found.

3   Material and Methods

This chapter presents the sampling strategies and the hydrochemical tracers that were applied.

All analytical results of the samples as well the calculated transit times are documented in the (Appendix).

3.1   Sampling

In several field campaigns in August 2011, October 2011, March and August 2013 and September 2014 a high number of surface and groundwater samples was taken from water reservoirs in the Gunt catchment. 96 locations were chosen to collect water samples from e.g. the main stream Gunt, its accessible tributaries, Lake Yashilkul and Lake Bulunkul, hot and cold springs, wells and glacier melt (see Figure 11, Appendix Figure 1 and Appendix Table 1). A monthly monitoring program involving local technicians has been in place from October 2011 until November 2014. River water samples were taken from the middle stream of the rivers wherever possible. All water samples were immediately filtered through a 0.45 µm cellulose acetate filter paper.
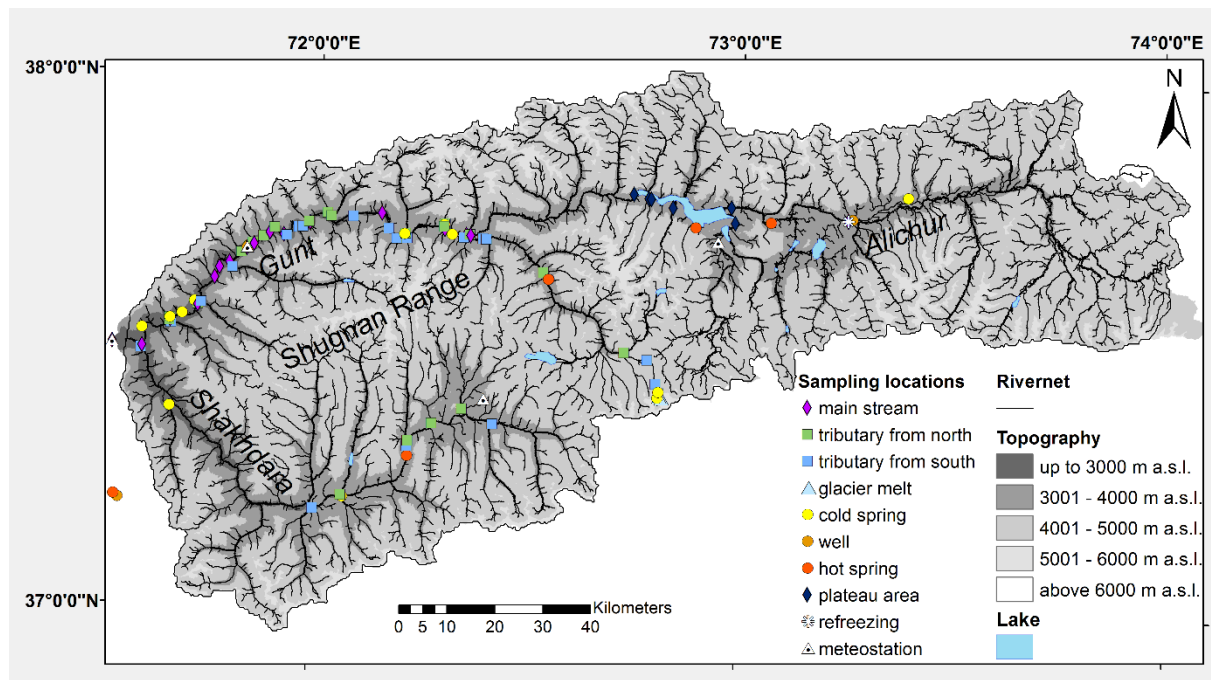
Figure 11: Location of the study area including all sampling locations.

Precipitation was collected at four sites but only two of these sites, Khorog and Navabad, which are 34 km apart, will be discussed further. Over the course of 15 months, 19 monthly-integrated samples were collected in 2012 and 2013. Subsequently, sampling of single rain events took place in 2013 and 2014, resulting in further 89 event samples collected over a period of 13 months (Appendix Table 2).

The monthly-integrated precipitation samples were collected from Hellmann-type rain gauges. To avoid evaporation effects, samples were collected at least twice per day, stored in

high-density polyethylene (HDPE) bottles, and conflated to monthly samples. Event samples were transferred from the Hellman rain gauges into durable PE bags (Whirl-Pak™, Nasco, Fort Atkinson, WI, USA). These water-filled bags were put into HDPE bottles for shipping.

Samples for stable isotope analysis of $\delta^{18}O$ and δ^2H were stored in clean 30 ml HDPE bottles. Before filling the bottle with the sample, the bottle was rinsed three times with the filtrated water sample. The bottles were filled to the rim to protect the sample against evaporation and exchange with atmospheric steam. These samples were also used for anion analysis; the water in the bottles was not acidified. The samples for the cation analysis were filled after rinsing to the rim into clean 30 ml HDPE bottles, acidified with ca. 20 µL HNO_3 and tightly closed to avoid contamination.

For lithium and strontium isotopes 250 ml HDPE bottles were pre-cleaned with ultrapure HCl. The bottles were filled to the rim, acidified with HNO_3 and tightly closed to avoid contamination.

A total of 1279 water samples from the Gunt catchment area were collected and partially analyzed for the following parameters:

- Stable isotopes of oxygen lithium strontium
- Stable and radioactive isotopes of hydrogen
- Noble gases
- Major cations and anions and trace elements
- Physico-chemical parameters (pH, electrical conductivity (EC), water temperature (T))

All analytical results that were used for evaluation are reported in the (Appendix).

In addition, scientists of the University of Resources (TUBA) Freiberg (Germany), Institute of Geology, Department of Tectonophysics, collected a variety of rock materials to represent the regional geology; 15 rock samples were selected for this study. Over a period of three months in 2013, the suspended particulate matter (SPM) samples were taken daily at three gauging stations in the catchment area: in Khorog from the main river Gunt, in Khabost from the main tributary Shakhdara and at the gauging station from the Patkhur River, the tributary of the most glaciated sub catchment. If possible, SPM-samples were taken from the central canal of the rivers, often from bridges. For SPM-samples five liter of river water were taken and passed through a filter. For laboratory analysis monthly integrated SPM-samples were generated by mixing of all available daily SPM-samples of one month.

3.2   Analytics

The samples from the field campaigns were immediately after the field trip shipped to Germany. All water samples of the monitoring program performed by technicians from Tajikistan were shipped to Germany every two months.

3.2.1   Stable isotopes of oxygen and hydrogen

Water samples were analyzed for $\delta^{18}O$ and δ^2H in the stable isotope laboratory of the Catchment Hydrology Department of the Helmholtz Centre for Environmental Research – UFZ in Halle (Saale).

Before measurement, all precipitation samples were filtered through a 0.45 µm cellulose acetate filter paper. The analysis of stable oxygen and hydrogen isotopes was performed with an isotope ratio infrared spectroscopy (IRIS) analyser, based on wavelength-scanned cavity ring-down spectroscopy (L2120-i, Picarro Inc., Santa Clara, CA, USA). All measurements of $\delta^{18}O$ and δ^2H were scale normalized with laboratory standards that are calibrated against the high and low international reference materials Vienna Standard Mean Ocean Water (V-SMOW) and Standard Light Antarctic Precipitation (SLAP) from the International Atomic Energy Agency (IAEA). The stable hydrogen and oxygen isotopic compositions of SLAP are expressed as delta values relative to VSMOW with $\delta^{18}O$ = -55.5±0.02‰ and δ^2H = -427.5±0.3‰ (Gröning et al. 2010). The two-point calibration was controlled by a third laboratory standard water. To exclude memory effects, each sample is measured with nine injections while the first three injections are discarded. All values are reported in the standard δ notation in per mil (‰) vs. V-SMOW according to Equation 1.

$$\delta^{18}O \ (‰) \ = \ \left(\frac{\left(\frac{^{18}O}{^{16}O} \right)_{sample}}{\left(\frac{^{18}O}{^{16}O} \right)_{standard}} - 1 \right) * 1000$$

Equation 1: Delta notation demonstrated with the isotopes of oxygen, ^{16}O and ^{18}O.

Values had an overall reproducibility of ±0.4 ‰ and ±1.5 ‰ (±2σ) for $\delta^{18}O$ and δ^2H, respectively.

3.2.2   Lithium isotopes

Sample preparation for measurement of lithium isotopes was done in the institute for geosciences, petrology and geochemistry at the Goethe University Frankfurt (Germany) according to (Seitz et al. 2004). For the water samples this preparation method was adapted to the liquid matrix. So, no pulping of the sample by hydrofluoric acid (HF) was necessary. Lithium was separated on a cation exchange column.

Lithium isotope ratios were determined with a multi-collector inductively coupled plasma mass spectrometer (MC-ICP-MS; Neptune, Thermo Scientific). All measurements were fulfilled after the sample-standard-bracketing method by measuring of at least two replicates per sample (n≥2), because lithium analysis with MC-ICP-MS produces a large fractionation and requires therefore a correction using bracketing standards. The isotopic compositions of the samples are given in delta notation (Equation 1).

The primary standard is the NIST L-SVEC SRM 8545, a high purified Li_2CO_3 reference material from the National Institute of Standards and Technology (NIST), which has a

^{7}Li/^{6}Li = 12.02±0.03 (Flesch et al. 1973). The total precision of the Li measurements in this study is: 2σ = 1 ‰.

3.2.3 Major ion concentrations, trace elements and field parameters

All water samples were shipped to Germany to be analyzed for the ion concentrations in the Department Catchment Hydrology and the Department of Analytics in the Helmholtz Centre for Environmental Research – UFZ in Halle and Leipzig, respectively. Cation concentrations of the dissolved loads were done by spectroscopy with an ICP-OES – Spectro Ciros CCD (Spectro Analytical Instruments, Germany), anion concentrations by ion chromatography (IC), and trace elements by inductively coupled plasma mass spectrometer (ICP-MS). Alkalinity was instantly determined in the laboratory via titration with HCl. All concentrations were transferred to meq/L under consideration of the ionic masses and the ion charge of each parameter. To evaluate the quality of major ion analysis the calculation of cation-anion balances was used according to DIN 38402-62 (Equation 2):

$$\Delta_{meq} = \frac{(\sum meq^{+} - \sum meq^{-})}{(\sum meq^{+} + \sum meq^{-})} * 100\%$$

Equation 2: Calculation of cation-anion balance.

The ion balances of the whole data set show balances > 50 %. Therefore, alkalinity was calculated as the total anion charge deficit. For all further investigations the calculated alkalinity is used.

All physico-chemical parameters (EC, T, pH) were measured in-situ by using WTW 350i (WTW, Germany).

3.2.4 Strontium isotopes

The measurement of strontium isotopes was carried out in the isotope laboratory of the chair of "Isotope Geochemistry at the Institute of Mineralogy and Geodynamics" at the University of Tübingen and in the Laboratory for Isotope Geochemistry and Geochronology at the Mineralogical Institute of the University of Resources (TUBA) Freiberg. Before the measurement the water samples are evaporated and the residue is used for ion chromatographic separation of strontium with HNO$_{3}$ (ultrapure). For analysis, the strontium is applied to the filament of the TIMS device. Analyses of the ^{87}Sr/^{86}Sr isotope ratio of water samples are performed by thermal ion mass spectrometry – TIMS (Finnigan MAT 262). The measurement of the ^{87}Sr/^{86}Sr-ratio is done in reference to the international standard NBS SRM 987. The ^{87}Sr/^{86}Sr-ratio of the NBS SRM 987 standard is about 0.710259±0.000018 (Tichomirowa et al. 2010). The total precision of the Sr measurements in this study is: 2σ = 0.00002.

3.2.5 Noble gases and ^{3}H

Travel times were estimated by applying the Tritium-Helium dating method (^{3}H/^{3}He-Method) (Appendix Table 10). For that, helium isotopes dissolved in groundwater and other noble gases (^{4}He, Ne) were taken with the use of diffusion samplers (Aeschbach-Hertig and

Solomon 2013). The diffusion samplers consist of two copper pipes connected by a gas-permeable silicone hose. For sampling they were placed in the groundwater outlet. After two days, equilibrium between the gas composition inside the sampler and the gases dissolved in the groundwater was established under stationary conditions. In order to be able to measure gas contents representative of groundwater, the diffusion samplers must be placed at locations with sufficient water depth and flow velocity. Assuming a laminar flow when the spring water emerges from the sediment/solid rock, at a maximum storage time of 7 days a minimum water height of about 10 cm is necessary to prevent the exchange of gases across the water surface.

The analysis of the noble gases and in particular of the helium isotopes, which was used for dating, was carried out at the Institute for Environmental Physics at the University of Heidelberg by application of mass spectrometry.

3.2.6   Additional data

3.2.6.1 Geographical data

The calculation of the natural spatial parameters (height distributions, slope inclinations, exposure etc.) was carried out by Brehme (2014) and was based on an SRTM-3 data set, which is freely available for download from the USGS (U.S. Geological Survey) and is available in the form of a digital elevation model (DEM). Information on the lithological subsurface was provided by a geological map, which was digitized by the project partner of the University of Resources (TUBA) Freiberg. The glacier distribution in the catchment area of the Gunt was calculated as part of a master thesis (Lindner 2014) and could also be used directly in the form of a shape file.

3.2.6.2 Data from the GNIP database

To access isotope data, the Global Network of Isotopes in Precipitation (GNIP) was used in a first step (International Atomic Energy Agency (IAEA) 2018). Additional isotope data were collected and evaluated from numerous publications for areas with sparse spatial coverage by GNIP stations. A full list of GNIP stations and additional data from publications used in this study can be found in (Appendix Table 3).

3.2.6.3 Statistical analysis

The statistical analyses were mainly carried out using the commercial software Statistica (Version 13, TBICO Software Inc. Copyright 1984-2017), partly also with Excel 2010 (© Microsoft Corporation 2010). Piper plots were created with the open source software GWChart Version 1.29.0.0 (U.S. Geological Survey 2015).

3.2.6.3.1   Box-Whisker-Plot

The Box-Whisker-Plot (short: Boxplot) is one of the most important graphical tools for describing a data set. Within the "box" the median value, the 25 % quartile and the 75 % quartile are displayed. The dispersion of the data is represented by the 1.5-fold interquartile range (IQR) ("whisker"). Outside these ranges there are outliers and distances greater than

three times the IQR is referred as an extreme value. This type of data representation enables the illustration of data location and dispersion. The shape of the box plot provides information about the normal distribution and possible skewness of the data. The size ratio between the box and the whisker allows statements to be made about the extent of the data. Regular or systematic outliers can, for example, be an indication of a high extent.

3.2.6.3.2 Histogram

Essentially, a histogram is a visualized frequency table. The measured-values are displayed in intervals against their absolute or relative frequencies. The selection of intervals or categories is decisive for the meaningfulness of such a diagram.

3.2.6.3.3 Piper-Plot

The presentation of hydrochemical data or the ratios of ion concentrations is usually done according to (Piper 1944) using the water types (Furtak and Langguth 1967). The Piper representation is a combination of ternary plots and a square diagram. A diamond is formed by inclination, on the lower sides of which two triangular diagrams are attached. Cations (alkaline earths $Ca^{2+} + Mg^{2+}$ and alkalis $Na^+ + K^+$ and anions ($SO_4^{2-} + Cl^- + HCO_3^-$) are represented in the diamond. The triangle diagrams show the proportions of cations and anions separately. Figure 12 shows the classification of (Furtak and Langguth 1967).
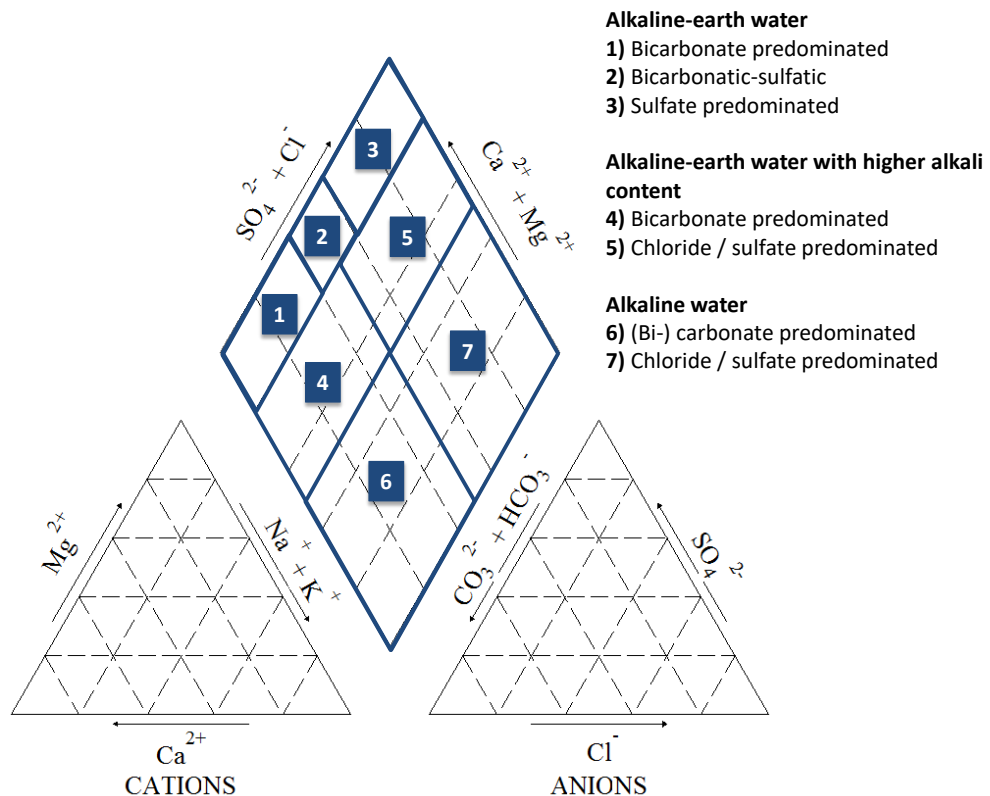
Figure 12: Piper Plot (Piper 1944) with classification after (Furtak and Langguth 1967).

3.2.6.3.4 Product moment correlation

The correlation is suitable for uncovering pairwise relationships of the variables x and y between (n) several observations. The correlation coefficient r describes the strength and direction of a relationship numerically and is defined as:

$$r_{x,y} = \frac{n \sum xy - \sum x \sum y}{\sqrt{[n \sum x^2 - (\sum x)^2][n \sum y^2 - (\sum y)^2]}}$$

Equation 3: Correlation

Since the correlation coefficient is symmetrical, it does not matter which variable is chosen first and which second: $r_{x,y} = r_{y,x}$. It is normalized and gives values from $-1 \leq r \leq 1$. A value r close to 1 represents a strong relationship, a value close to 0 a small one or no relationship. The sign indicates the direction of the correlation. In a correlation with $r = \pm 1$, the linear relationship exists: $y = ax + b$. Since the method only measures linear dependencies, independence cannot be automatically inferred from no correlation (i.e. $r = 0$). However, if there is a correlation between two variables x and y, this can be interpreted in the following causal sense:

- x influences y causally
- y influences x causally
- x and y are causally influenced by one or more other variables
- x and y influence each other causally.

4   Stable isotopes of hydrogen and oxygen in water

The composition of the stable isotopes of water (δ^2H and δ^{18}O) act as an ideal conservative tracer of water sources and mixing processes (Yurtsever and Gat 1981; Joussaume et al. 1984; Rozanski et al. 1993; Bowen and Revenaugh 2003; Terzer et al. 2013; Stumpp et al. 2014; Galewsky et al. 2016). Isotope patterns are a powerful tool which can give insights into natural hydrological processes, such as evaporation (Craig and Gordon 1965; Gibson et al. 2016) and transpiration (Dongmann et al. 1974; Helliker and Ehleringer 2000) over large spatial and/or temporal scales (West et al. 2009).

Choosing the oceanic reservoir as a starting point of the hydrologic cycle, evaporation of iso-topically relatively uniform ocean water enriches the resulting water vapour in light iso-topes. Condensation of this water vapour in clouds during formation of rain is assumed to be an isotopic equilibrium process, which only depends on temperature. Consequently, the iso-topic composition of precipitation is subject to several effects that mostly depend on the temperature during condensation. They include the altitude effect, the latitude effect, and seasonality. It also correlates with travel distance, and thus continentality because of Ray-leigh fractionation during subsequent rainout events (Clark and Fritz 1997; Gat 2000). On a global scale, these effects average the isotope abundance of oxygen and hydrogen in precipi-tation to a linear relationship, which has been termed the Global Meteoric Water Line (GMWL) and defined by Craig (1961) as:

$$\delta^2H \; = \; 8 * \delta^{18}O + 10‰$$

Equation 4: GMWL defined by Craig (1961)

and was later specified by Rozanski et al. (1993) as:

$$\delta^2H \; = \; 8.13 * \delta^{18}O + 10.8‰$$

Equation 5: GMWL specified by Rozanski et al. (1993)

To reduce the number of effects that have to be taken into account during the evolution from ocean water to precipitation, Dansgaard (1964) introduced the concept of a deuterium ex-cess value (*d*) (see chapter 5.1.1), which ideally should not be altered by isotope equilibrium effects.

It is defined as

$$d \; = \; \delta^2H - 8 * \delta^{18}O$$

Equation 6: *d*-excess

and can be visualized as the intercept of a line with slope 8 which crosses the given isotope pair in a dual isotope plot of δ^{18}O vs. δ^2H. Thus, the GMWL connects points of *d* = 10 ‰. Evaporation as a non-equilibrium process is generally assumed to be the major modifier of d-values, allowing direct comparison of oceanic water vapour and moisture precipitating from clouds (Merlivat and Jouzel 1979). On large scales and assuming a closed water cycle, d-values of average oceanic water vapour are mainly controlled by relative humidity (RH) and sea surface temperature (SST). Precipitation along the GMWL is generated for RH and

SST values of 85 % and 25 °C, respectively (Clark and Fritz 1997). Based on the closure assumption of the water cycle, simple linear relationships between d and RH, and d and SST were introduced to use source values of d as a 'fingerprint' to trace water in the atmosphere up to its point of rainout (Rindsberger et al. 1983; Johnsen et al. 1989; Pfahl and Sodemann 2014).

An example for one of these linear relationships at the location of evaporation is expressed as

$$d = 0.33 \, {}^{\text{‰}}\!/_{C} \cdot \text{SST} - 0.44 \, {}^{\text{‰}}\!/_{\%} \cdot \text{RH} + 37‰$$

Equation 7: Relationship between SST, RH and d

with d in ‰, SST in °C, and RH in % (Aemisegger et al. 2014).

Note that after the condensation of water vapour in clouds, rain droplets can be subject to additional evaporation during their fall through a warm and dry air column which shifts their d-value from its original vapour composition (Friedman et al. 1962; Stewart 1975). This effect is more pronounced for small rain amounts and can be accounted for if precipitation amount weighted d-values are considered (Lee and Fung 2008). These theoretical basics enable applications to estimate contributions of recycled inland water to precipitation (Froehlich et al. 2008; Aemisegger et al. 2014; Parkes et al. 2017). They may also discern and compare meteorological patterns (Liotta et al. 2006; Guan et al. 2013), and enable the paleoclimate interpretation of ice cores (Jouzel et al. 1982; Steffensen et al. 2008).

Some of the highest natural deuterium excess values in precipitation have been recorded in the Mediterranean, with maximum long-term mean values of 22 ‰ (Gat and Carmi 1970). High d water vapour is produced when cold dry air from the surrounding continents interacts with the warm Mediterranean seawater and enhances isotope fractionation during evaporation (Gat and Carmi 1970; Gat et al. 1996). This high d signal is transported eastward, mainly by prevailing westerlies. Extending from countries with direct contact to the Mediterranean, several studies from countries further away refer to Mediterranean moisture as an explanation of unusually high d-values in precipitation and surface waters. These include studies from Syria (Kattan 1997; Al Charideh and Abou Zakhem 2010), Jordan (Bajjali 2012), Saudi-Arabia (Alyamani 2001; Michelsen et al. 2015), Iraq (Hamamin and Ali 2013; Ali et al. 2015), Iran (Osati et al. 2014; Parizi and Samani 2014), Pakistan (Hussain et al. 2015), Tajikistan (Liu et al. 2015a), northern India (Jeelani et al. 2013; Jeelani et al. 2017), and western China (Yao et al. 2013; Wang et al. 2015). Moreover, the moisture source of precipitation in Central Asia was discussed by several studies, which identified several air travel pathways and identified Mediterranean moisture as one of the potential main sources for precipitation in Central Asia (Aizen et al. 1995; Kreutz et al. 2003; Tian et al. 2007) while other studies identified the Indian Ocean as another major moisture source (Aizen et al. 1996; Karim and Veizer 2002; Jeelani et al. 2017). Additional proposed pathways include polar air masses (Tian et al. 2007) and more continental Westerlies (Aizen et al. 1996; Meier et al. 2013; Pang et al. 2014).

However, the global network for isotopes in precipitation (GNIP), which was established from the International Atomic Energy Agency (IAEA) together with the world meteorological organization (WMO) and that provides long-term isotope signals in precipitation over large parts of the world, possesses an almost blank spot on the map in the Central Asian mountains, especially just here in the Pamirs (Araguás-Araguás et al. 1998).

To cover this gap and to understand the controls of precipitation and different runoff components in the Tajik Pamir we have undertaken a stable isotope study in an exemplary drainage basin (river Gunt; Figure 13) in the headwaters of the Amu Darya.
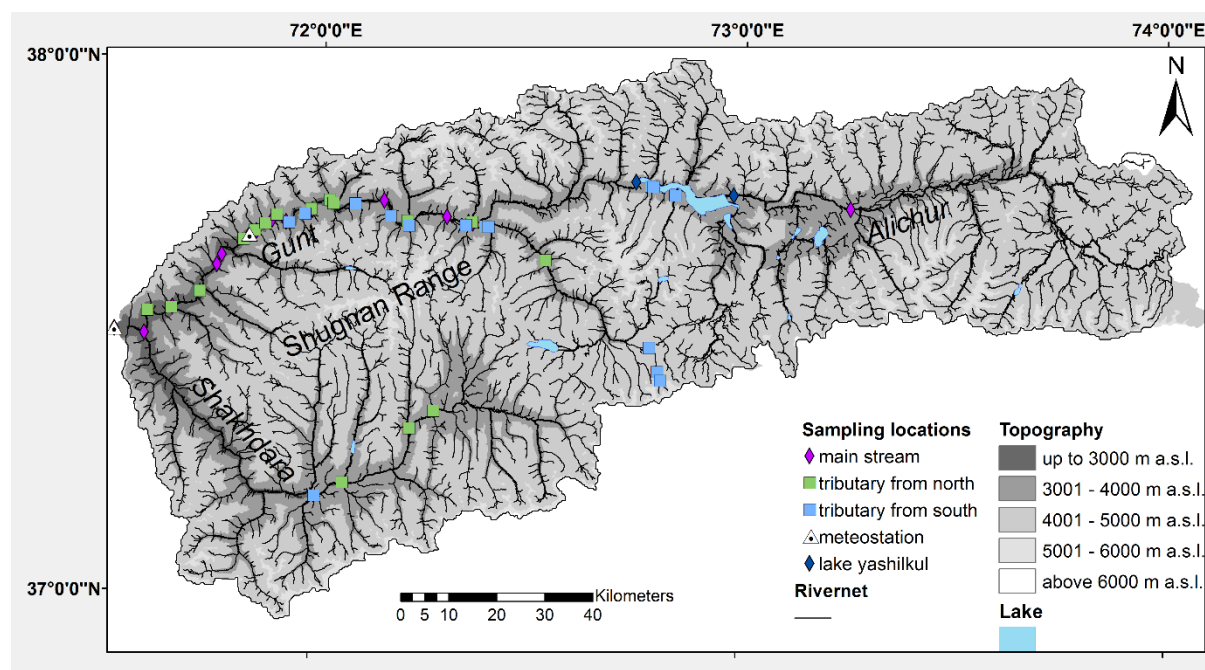
Figure 13: Location of all sampling stations for $\delta^{18}O$ and δ^2H analysis.

This chapter offers an insight into stable isotope patterns of surface water and precipitation in the Pamir Mountains and approaches to governing the processes responsible so that we can delineate the different origins of water which contribute to the hydrological regime.

4.1   Precipitation[1]

The precipitation, which is an important initial parameter for the isotopic composition of waters in the catchment area, shows that it comes from various wind systems (westerly winds, monsoons, southern cyclones). Deuterium excesses in precipitation of more than 10 ‰ indicate precipitation by re-evaporation and thus an origin in the Caspian and/or Mediterranean Sea. Within the catchment area, the surface water samples from the sub-basins can be grouped according to the deuterium surplus in their waters. This reinforces the assumption that different wind systems have different influences.

---

[1]This work was published as Juhlke et al. 2019; Juhlke, T. R. and Meier, C. contributed equally to this work.

4.1.1 Results of stable isotopes ($\delta^{18}O$ and $\delta^{2}H$) in precipitation

4.1.1.1.1 Monthly integrated samples

The results of monthly integrated samples for oxygen and hydrogen stable isotopes are shown in a dual isotope plot of $\delta^{2}H$ against $\delta^{18}O$ (Figure 14). Values for $\delta^{18}O$ range between –24.4 ‰ and –2.0 ‰, whereby minimum values are reached in the cold season (boreal winter), while maximum values were observed during warm season (boreal summer) (Appendix Table 2). The Local Meteoric Water Line (LMWL) calculated from the samples (Figure 14) has the following equation (Equation 8), which is quite similar to the GMWL (Equation 4):

$\delta^{2}H = 8.1(\pm0.1) \cdot \delta^{18}O + 13.6(\pm1.8)$ ‰.

Equation 8: LMWL

As outlined in the introduction, several effects occurring during transport of atmospheric moisture and rainout have an impact on the isotopic composition of any precipitation sample. Therefore, the detailed discussion is limited to the deuterium excess parameter, which should be less affected by these processes and thus a better indicator for moisture transport.
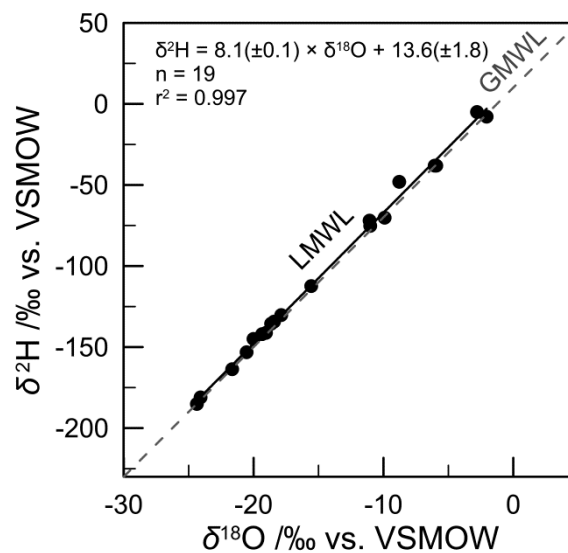
Figure 14: Dual isotope plot of $\delta^{2}H$ against $\delta^{18}O$ (VSMOW) for monthly integrated isotope samples of the Western Pamir Mountains. Grey dotted line is the Global Meteoric Water Line (GMWL, see Equation 5). Black solid line is the Local Meteoric Water Line (LMWL) as calculated from the samples.

In order to cope with the coarser temporal resolution of integrated precipitation samples, their *d*-values are compared to monthly *d* averages of isotope precipitation monitoring stations along the route of commonly assumed air travel pathways. This comparative data was taken from the GNIP database and additional literature studies (see chapter 5.1.6.2).

All isotope data were clustered and subdivided into ten regional classes based on their geographical position: W Mediterranean, E Mediterranean, Levant, Middle East, Caspian Sea, Polar, Persian Gulf, N India, Kabul & Kashmir, and Western Pamir (Figure 15). From monthly *d*-values for all stations in one class, two types of averages were calculated for each month: the arithmetic mean $\bar{d}_m$

$$\overline{d}_m = \frac{\sum d_m}{n}$$

Equation 9: arithmetic mean

and the precipitation amount-weighted arithmetic mean $\overline{d}_{p,m}$

$$\overline{d}_{\mathrm{p,m}} = \frac{\sum(d_{\mathrm{m}} \cdot p_{\mathrm{m}})}{\sum p_{\mathrm{m}}}$$

Equation 10: amount-weighted arithmetic mean

where d_m is the d value of month m for one regional class, p_m is the precipitation amount, and n is the number of monthly values. This approach will unveil similarities and differences concerning extreme values of d and their seasonal distributions.
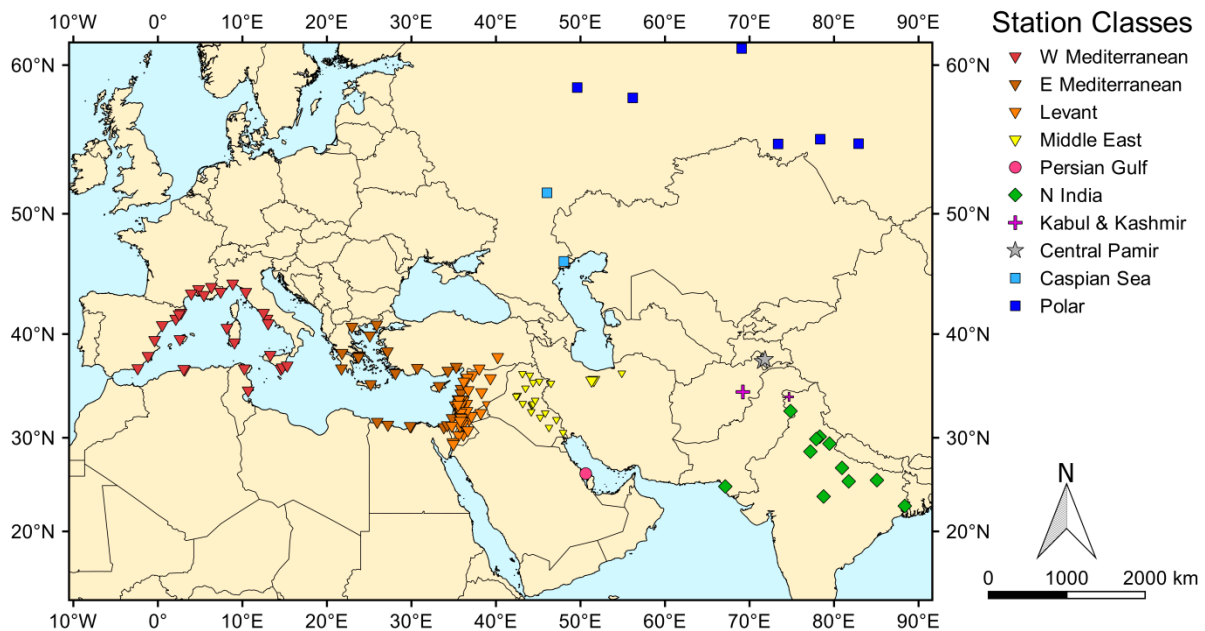
Figure 15: Map of GNIP stations (larger symbols) and additional data (smaller symbols) used for calculation of regional deuterium excess averages. Grey stars show sampling sites of this study in the Western Pamir Mountains.

The monthly d-values of the precipitation samples collected in the Gunt catchment and additional data associated with each of the ten regional classes are summarized in Figure 16
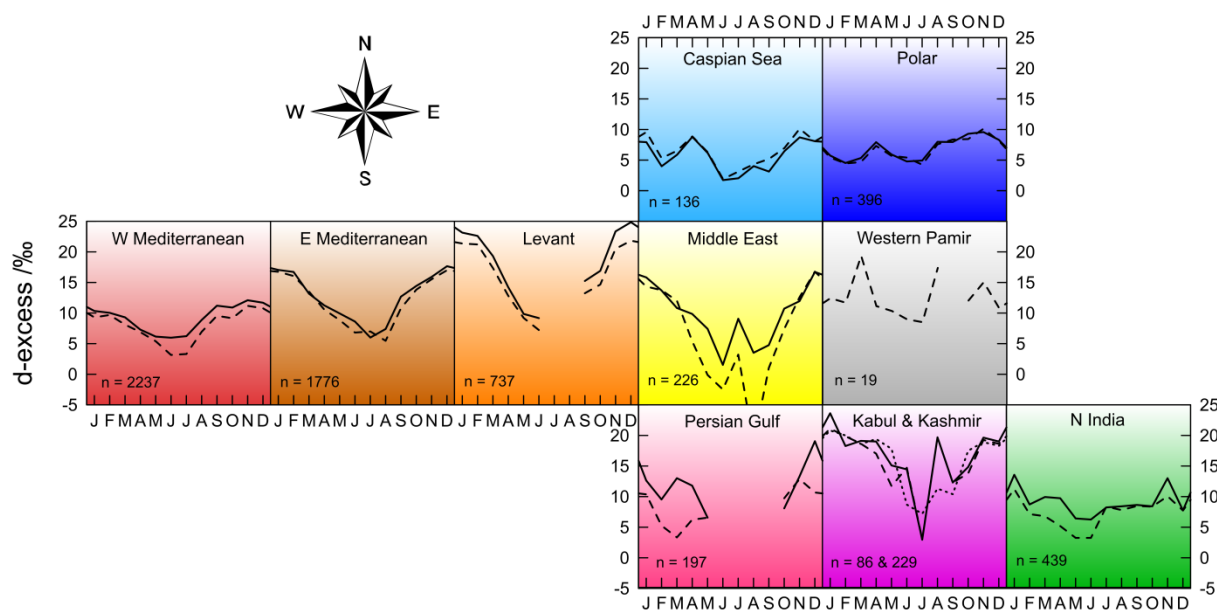
Figure 16: Monthly deuterium excess (*d*) values for regional classes, corresponding to stations in Figure 15. Plots are arranged in their respective geographic setting. Solid lines are precipitation amount weighted *d*-averages (Equation 10), dashed lines are non-weighted arithmetic means (Equation 9). The dotted line in the "Kabul and Kashmir" subplot is the non-weighted arithmetic mean of the Kashmir valley after Jeelani et al. (2017). Sample size is shown in lower left corner of each subplot.

The first region to consider along the proposed W–E transect is the Western Mediterranean. Stations in this region have an average deuterium excess of 10 to 12 ‰ in the cold season and around 3 ‰ in the warm season (Figure 16). The seasonal evolution is a smooth sinusoidal course between those two extremes. The differences between precipitation weighted and non-weighted averages increase from 1 ‰ in the cold season to 3 ‰ in the warm season.

This seasonal pattern continues in eastward direction in the eastern Mediterranean and Levant where cold season values reached 17 and 22 ‰, respectively (Figure 16). Warm season values scatter around 6 to 7 ‰, which results in a more pronounced seasonal oscillation in the Levant region when compared with the eastern Mediterranean. For July and August, no monthly isotope values were recorded in the Levant region because of the absence of rain.

Precipitation amount-weighted to non-weighted differences increase from cold to warm seasons in the eastern Mediterranean. However, these differences decrease in the Levant region. For all those three Mediterranean-influenced regions, the spatial and temporal resolution of isotope data is very good and averages of *d*-values can be assumed to be representative for their respective region.

The Middle East region (for extent of this region as defined in this study see Figure 15) is dominated by data from the GNIP station at Teheran (Iran), while additional measurements are mainly single monthly values from various sampling sites in Iraq (Figure 15). The seasonal variations of *d*-values are similar to the regions located to the west (W and E Mediterranean, Levant) described above (Figure 16), however, they show more variable values for late summer due to low volume sample sizes. An approximate difference between cold and

warm seasons of about 15 ‰ in *d*-values is comparable to the seasonal differences in the Levant region. The Middle East absolute values range from about 0 to about 17 ‰ (Figure 16), while *d*-values observed in Levant range from ∼7 to ∼22 ‰.

South of the Middle East region landmass, the Persian Gulf acts as a moisture source for passing air masses. In this region, the only available GNIP station of Bahrain exhibits *d*-values between 19 ‰ in the cold season and 7 ‰ at the beginning of the warm season (Figure 16). A strong difference between precipitation-weighted and non-weighted *d* averages was found here. Moreover, in summer, absence of precipitation leaves a gap in the *d*-record. In general, the seasonal *d*-value patterns of the region around the Persian Gulf are comparable to the *d*-values of the Middle East region. Following the transect further eastwards, a distribution between cold and warm seasons similar to the Mediterranean can also be observed in the GNIP station of Kabul (Afghanistan). This is also reflected in precipitation samples of Jeelani et al. (2017) that were collected from the Kashmir Valley (India), with high *d*-values of ∼21 ‰ in the cold season and low values of 3 to 7 ‰ in the warm season (Figure 16). The *d*-values of stations in Northern India are less variable than those of stations described so far, with a minimum-maximum difference of around 8 ‰ (Figure 16). Precipitation weighted-values generally decrease from January with 14 ‰ to 6 ‰ in June. From July to October *d*-values are stable around 8 ‰. A notable difference between precipitation weighted and unweighted averages can be observed from March to June.

Stations that were assigned here to the Polar class show *d*-values between 4 and 10 ‰ (Figure 16). Contrary to the seasonal distribution pattern with a single summer minimum that is observed eastward from the Mediterranean, this Polar class has two minima in February and July with low *d*-values around 4 ‰. A first maximum is found in April with around 7 ‰. From July to November *d*-values steadily increase to a second peak of ∼10 ‰. Two stations to the northwest of the Pamir Mountains were assigned to the Caspian Sea class, that exhibit a similar seasonal evolution when compared to the Polar class stations. However, they show increased amplitudes with minimum and maximum values of 2 ‰ and 10 ‰ in June and November (Figure 16). Integrated samples (unweighted monthly means here) from the Western Pamir Mountains display *d*-values between 9 and 19 ‰ (Figure 16). Note that September values are missing, because of lack of precipitation. A first maximum in March of ∼19 ‰ is followed by a steady decrease to 9 ‰ in July. Another peak of around 17 ‰ is observed in August. December holds another minimum around 9 ‰, after which values increase until March.

4.1.1.1.2 Possible moisture uptake along air mass trajectories

d-values of event samples are more easily allocated to specific air travel pathways via computed backward air mass trajectory models, such as HYSPLIT (Stein et al. 2015). The necessary user input for these trajectory models consists of a location and a date of the associated precipitation event. From gridded meteorological data, such as the Global Data Assimilation System (GDAS) (NOAA 2018), HYSPLIT computes regularly spaced data points along trajectories which include additional parameters such as elevation of the air parcel, specific humidity of the air parcel and elevation of the planetary boundary layer (PBL). These parame-

ters can be used to categorize the resulting trajectories into the wedge-shaped or radial regional classes that were pre-defined to represent areas of possible moisture origin. Note that classes for *integrated* and *event* samples are not necessarily identical. They may differ in shape, where classes for integrated samples form proximity-related clumps of stations and event sample classes are radial sectors with the sampling site as centre. The classes of integrated monthly samples aggregate multiple, spatially close station and represent the regions where precipitation collection took place. Event samples were divided into classes that correspond to possible main moisture sources. They are wedge shaped due to the central starting point of the calculated trajectories.

Four of the 89 events that were sampled at Khorog and Navabad in the Western Pamir Mountains showed *d*-values below -10 ‰, which hints at sample alteration (Michelsen et al. 2018). These events were excluded from further calculations. For the remaining 85 single precipitation events, backward air mass trajectories were calculated for each location with the Hybrid Single-Particle Lagrangian Integrated Trajectory model (HYSPLIT) of the National Oceanic and Atmospheric Administration (NOAA) Air Resources Laboratory (Stein et al. 2015; Rolph et al. 2017). GDAS1 grids with 1°x1° resolution from the National Oceanic and Atmospheric Administration and National Centers for Environmental Prediction (NOAA/NCEP) were used as meteorological input data. Starting times for the trajectories were chosen in accordance with precipitation records of the United States Air Force (USAF) station in Khorog (Tajikistan; station ID 389540). The time period for all trajectories covered by this model was set to seven days, and hourly data points along the backward trajectories were produced. In order to follow the specific air mass that produced precipitation at the sampling site, the trajectory starting altitude should correspond to the altitude of the rain clouds during sampled events. Since this cloud altitude was not measured, eight different trajectory starting altitudes were used as inputs with 150, 300, 500, 1000, 1500, 2000, 2500, and 3000 meters above ground level, thus generating eight trajectories per event. In order to select one of the eight starting altitudes for further evaluation, the evolution of specific humidity along each trajectory was assessed. For air mass altitudes below the height of the PBL derived from the HYSPLIT model, an increase in specific humidity was assumed to correspond to evaporation from the underlying ground area, and a decrease in specific humidity was assumed to correspond to precipitation (Bottyán et al. 2017). For air mass altitudes above the height of the PBL, humidity changes were assumed to be not due to ground surface interaction and consequently ignored. From the eight trajectories per event, the one with the largest sum of specific humidity increase below the PBL height along a trajectory was selected. This selection ensured that the trajectory that represents one precipitation event has a history of maximum moisture uptake and thus is regarded as the most representative for the sampled precipitation (Bottyán et al. 2017). To evaluate the origin of moisture in these 85 selected trajectories, radial regional classes around the precipitation collection site were constructed (Figure 17). Each trajectory was allocated to one of these radial classes. The class boundaries were chosen to include larger bodies of surface water that may act as moisture sources (Mediterranean Sea, Caspian Sea, and northern Indian Ocean). If a trajectory crossed areas of several classes, it was associated with the class where most of the moisture entered the air parcel according to the model. Since the boundaries of the con-

structed wedge-shaped classes all converge to the sampling locations in the Pamir Mountains, a correct classification of air parcels that receive their moisture close to the sampling site is difficult. For this reason, an additional 'local' class was defined for air parcels that received most of their moisture in close proximity (<3° distance, ≈300 km) to the sampling sites. Further classes were introduced, because some trajectories originated, and had their moisture uptake, outside the reasonable boundaries of the area of the radial classes. This eventually resulted in 9 classes: Polar, Caspian Sea, Mediterranean, Persian Gulf, N Indian Ocean, Local, Africa, W Atlantic, and E Atlantic (Figure 17).
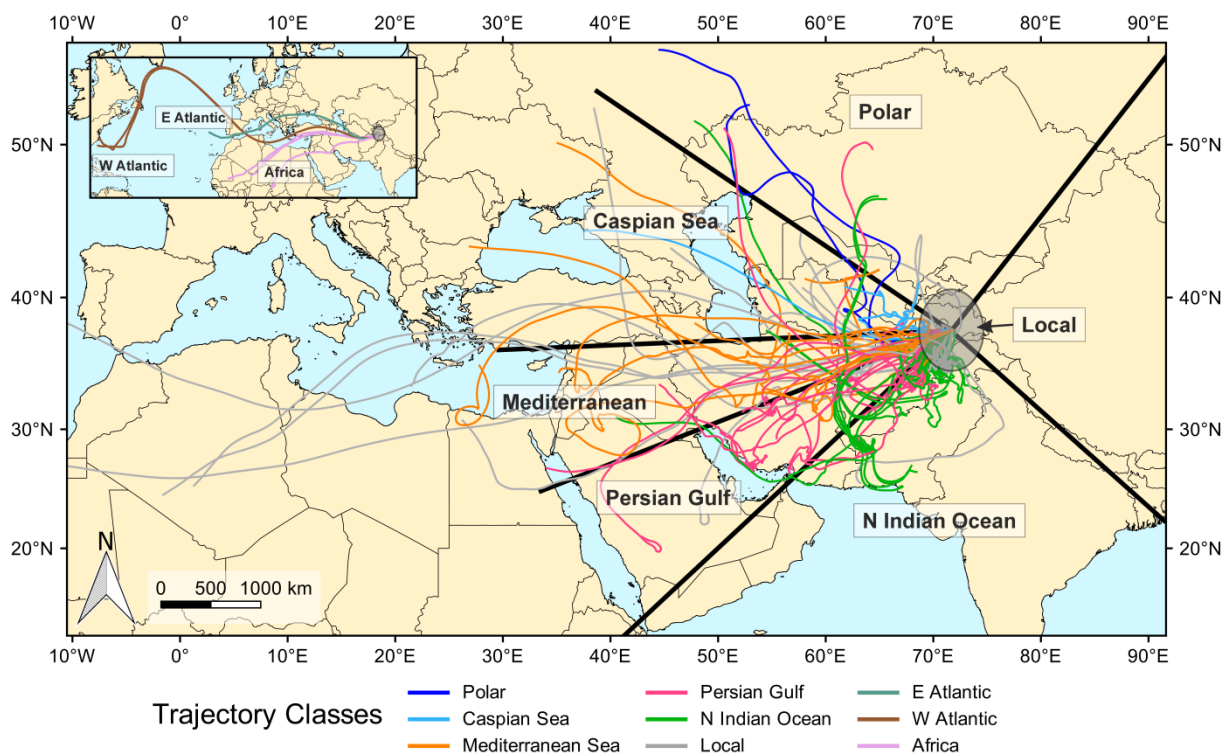
Figure 17: Map of air mass trajectories leading up to rain events in the Western Pamir Mountains. Different classes of moisture origin are color-coded. Small insert displays long distance trajectories.

The calculated air mass trajectories leading up to each sampled rain event in the Western Pamir Mountains are shown in Figure 17. Note that none of the calculated trajectories for the sampling sites arrived from an eastern direction. Some of the trajectories had the majority of their moisture uptake and their origin beyond the reasonable boundaries of the radial classes introduced in the methods section. These six long-distance trajectories (Figure 17, small box; Figure 18a) include pathways with main moisture uptake over the northeastern Atlantic Ocean in January, from the western Atlantic Ocean in March, and from northern Africa in January and December.
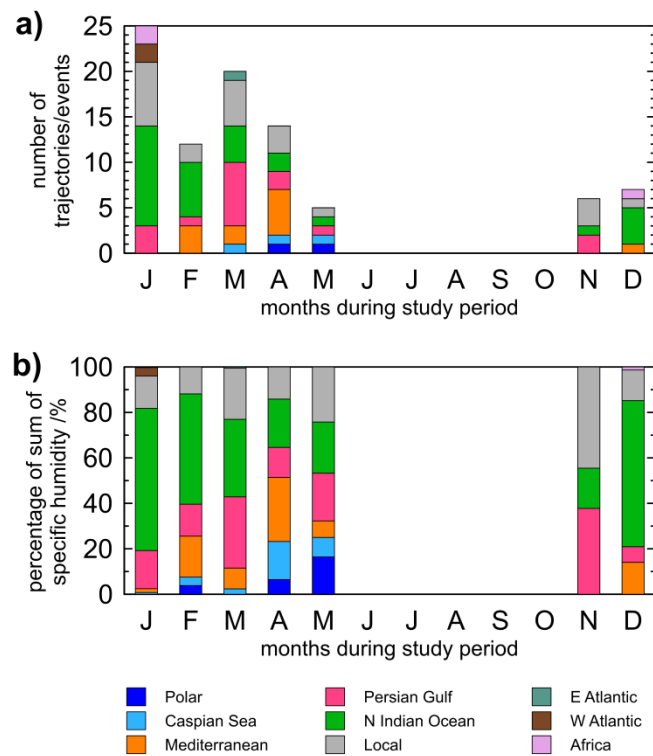
Figure 18: Statistics of air mass trajectories. a) Number of trajectories per month that had the majority of their moisture uptake in the area of a certain class. b) Monthly percentage of the total amount of specific humidity that arrived at the measurement site via the calculated trajectories.

Statistics of events or trajectories per class and month are shown in Figure 18a. January holds the annual maximum of 25 sampled precipitation events, while June to October was dry and no precipitation was collected. Events assigned to the N Indian Ocean class are most frequent in January with a decrease in spring and an increase from November to January. If the Persian Gulf and the Mediterranean class are combined, they show a similar distribution, but with a maximum of precipitation events in March. Polar and Caspian Sea class precipitation events are rare and only obvious in late spring. Figure 18b was generated using the specific humidity information along the trajectories.

It is assumed that an increase in specific humidity below the PBL corresponds to additional moisture uptake from the ground surface along the pathway of transported water vapour. Consequently, each point along the trajectories, where an increase in specific humidity is detected, is considered an additional source for the precipitation at the sampled rain event. For the month of January, the increase in specific humidity of all points of one class was added up. This sum of specific humidity increase of one class was expressed as a percentage relative to the sum of specific humidity increase of all classes, during the month of January. This operation was repeated for each month and enables to untangle the moisture contribution of the different classes to precipitation at the sampling site. Moisture contribution of the N Indian Ocean class varies between 15 and 60 %. The sum of Persian Gulf and Mediterranean moisture fluctuates between 20 and 40 %. Moisture from the Caspian Sea and Polar class each has maximum contributions of 15 %. Each trajectory eventually leads up to a rain event, for which the d-value was calculated according to Equation 6. The d-values of the Western Pamir Mountain rain events are summarized as monthly boxplots in Figure 19a. In

order to compare different classes and to retain a seasonal resolution, an average of *d*-values for each month and class was calculated. Thus, Figure 19b shows one point per class for each month, if at least one trajectory was assigned to this class.
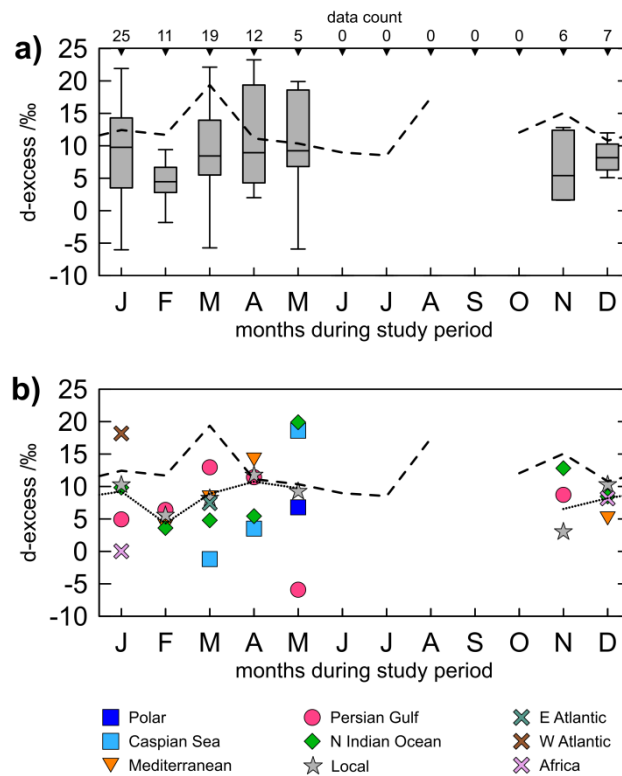
Figure 19: Deuterium excess of rain events at the termination of air mass trajectories. a) Boxplot of all event samples (whiskers end at last values inside 1.5 IQR), including sample size for each box at the top axis. b) Monthly averages for event samples of every class. For number of trajectories per plot symbol refer to Figure 18a. Dashed line represents monthly *d-values* of the Western Pamir class of monthly-integrated samples (see grey plot of Figure 16), dotted line represents monthly average of all event values.

4.1.2 Discussion of stable isotopes (δ¹⁸O and δ²H) in precipitation

4.1.2.1.1 Monthly averaged-values

The evolution of *d*-values along the considered transect from the Mediterranean to Central Asia is initiated by Atlantic moisture, which arrives at the western Mediterranean. In winter, the deuterium excess of 10 to 12 ‰ is near the value of the GMWL and consistent with average moisture produced over the Atlantic Ocean (Dansgaard 1964). Additional local moisture from evaporated water of the Mediterranean Sea strongly depends on the season. The atmospheric conditions during the cold season favour the formation of water vapour with higher *d*-values, when cold and dry air from the continent prevails (Gat and Carmi 1970; Rindsberger et al. 1983; Liotta et al. 2006). In the warmer season more humid air prevents high *d*-values. Additionally, warm season sub-cloud evaporation of falling water droplets enhances *d*-value decrease, which results in even lower *d*-values (Stewart 1975). This trend manifests itself in positive deviations of precipitation-weighted from non-weighted monthly averages, because lighter rain events, which increasingly suffer from sub-cloud evaporation, contribute less to precipitation-weighted averages. The general increase of *d*-values in pre-

cipitation from the western to the eastern Mediterranean is consistent with the meteorological evolution, where air becomes drier the further eastwards it moves. The warmer season d-values in the eastern Mediterranean are comparable to the western Mediterranean, whereas winter values increase eastward. This winter increase is due to stronger evaporation in the eastern, more enclosed part of the Mediterranean basin. There, continental influences of cold, dry air are increased (Gat and Carmi 1970). This can also be observed in the residual seawater that undergoes a d-value shift from ~ -3 ‰ in the western Mediterranean to ~ -5 ‰ in the eastern Mediterranean. As local seawater serves as a source for precipitation, this shift is also transposed to the rainout trajectories.

Compared to the Mediterranean, the Levant region is subject to increased continental influence with warmer summers and colder winters (Kalnay et al. (1996); their long term monthly mean temperature data), which increases the overall d-value together with its seasonal amplitude.

In the Middle East this trend does not continue, which can result from various influences. First, mixing of Mediterranean moisture with other less-enriched moisture sources (e.g. Black Sea; International Atomic Energy Agency (IAEA) (2005)) can account for a decrease in average d-values. Second, another important factor is the lower relative humidity compared with the Eastern Mediterranean that can induce a more pronounced sub-cloud evaporation. Notably smaller rain amounts in the Middle East also increase this observable effect of the amount driven sub-cloud evaporation.

In the Persian Gulf, the GNIP station in Bahrain is dominated by dry air, which is also manifested by missing summer precipitation and large differences between amount-weighted and averaged d-values. These d-values are similar to those of the Eastern Mediterranean; however, the seasonal evolution does not show the smooth sinusoidal evolution of the Mediterranean stations and is noisier. One potential interpretation is that nearby local evaporation of Persian Gulf seawater plays a major part in the precipitation of this station. Further possible influences of moisture from the Indian Ocean were proposed by (Rizk and Alsharhan 2003).

In Northern India, the seasonal distribution pattern of d-values differs clearly from the simple sinusoidal trough-peak distribution of the Mediterranean. Since India is strongly influenced by air from the Indian Ocean, the seasons in this region differ from European ones and are comprised by winter, summer, monsoon, and post-monsoon season. The generally increased d-values in winter have been interpreted as of Mediterranean or generally western origin from where moisture is transported eastward by so-called Western Disturbances. These wind patterns are extra-tropical cyclones (Dimri et al. 2015; Dimri and Chevuturi 2016) in high-altitude air masses (Jeelani et al. 2017). The warm season from March to June is hot and dry, a fact that causes decreasing d-values and a more pronounced sub-cloud evaporation effect. During the monsoon season from July to September d-values are stable around 8.5 ‰ and no difference between amount-weighted and non-weighted could be observed. This is due to heavy rainfall events that saturate the air quickly with moisture and prevent pronounced sub-cloud evaporation (Peng et al. 2005).

The GNIP station in Kabul and a site in the Kashmir valley (Jeelani et al. 2017), both located south of the Pamir Mountains, are located at the crossway of proposed Mediterranean and Monsoon air mass influences. Cold season values can be ascribed to moisture of Mediterranean origin with a high probability due to the extreme high d-values of around 20 ‰. Around July, monsoon and Mediterranean precipitation both show similar values and cannot be differentiated from monthly d-values. As a result, the overall annual d-value pattern is more similar to Mediterranean stations than to Indian ones (Figure 16).

GNIP stations to the North and Northwest of the sampling site (Caspian Sea and Polar class in Figure 16) are located in cooler and more continental settings. Stations in both regions exhibit a similar seasonal d-value distribution. Their seasonal amplitude is smaller compared to more maritime stations and below 10 ‰ year-round.

The seasonal evolution in the Western Pamir Mountains is not so obvious with respect to the possible influence of the discussed sources or transit paths. The shape of the seasonal distribution in the Western Pamir is different from the simple sinusoidal trend westward and in Kabul and Kashmir (Figure 16). The annual weighted average of d of 13 ‰ is higher than the 10 ‰ of average global precipitation, which suggests influence of enriched moisture.

From October to February, during the cold season, values range between 10 and 12 ‰, with the exception of 15 ‰ in November. This is lower than the cold season values for the Eastern Mediterranean, and regions eastward, and suggests a divers and not exclusively Mediterranean moisture origin. The d-values of March and August are positive outlier with 19 ‰ and 17 ‰. Similar positive excursion could be observed in Bahrain in March, albeit only reaching 13 ‰, and in Kabul in August with 20 ‰. However, a causal connection between these month-long irregularities is highly speculative. During summer months, d-values decrease to a range between 8 and 9 ‰ in July that are comparable to the Kashmir Valley and Northern India during the monsoon season. Northern moisture with year-round d-values below 10 ‰ does not seem to exert significant influences on those in the Western Pamir Mountains with d-values above 10 ‰ during most of the year.

4.1.2.1.2   Event trajectories

Air mass trajectories give a good indication from where the moisture for a specific precipitation event originated. During the sampled period, a dry period from June to October made it difficult to analyse general year-round source variabilities. For the rest of the year, however, moisture sources were variable (Figure 18). Most of the time, moisture from each sector contributed to precipitation in the Pamir Mountains.

Long-distance trajectories from Africa or the W Atlantic occurred with a higher frequency in December and January (Figure 18a). This can be due to the prevailing west wind zone in temperate latitudes during winter, where air can be transported westward over long distances. The accompanying d-values are diverse and range between 0 ‰ and 18 ‰. They also do not show a seasonal trend (Figure 19b). Because of the low number of occurrences, d-values of the long-distance trajectories are not further discussed here. Moisture from northern and northwestern areas arriving in the Western Pamir Mountains could mainly be detected from March to May (Figure 18). In March, moisture from the Caspian Sea class has

slightly negative d-values (Figure 19b). The evolution to May with notably increasing d-values is consistent with average air temperature and relative humidity.

Temperatures near 0 °C and high relative humidity keep d-values near 0 ‰ in winter. During spring, temperatures increase and the air becomes drier. This in turn increases the d-value of evaporated Caspian Sea water as well as the possible contribution of recycled water from soils and other surface water bodies.

The contribution of N Indian Ocean moisture decreases from January to May from around 60 % to 20 %, which can result from the hot and dry Indian summer season climate around March, April, and May (Figure 18b). Another hint to this Indian summer dryness are the notably lower d-values of ~5 ‰, compared to 9 to 13 ‰ in the cold season (Figure 19b).

After the monsoon season, air from the N Indian Ocean adds increasingly more moisture and dominates the winter months in the Western Pamir Mountains. Additionally, the d-averages of monthly integrated samples (dashed lines, Figure 16 Western Pamir plot, and Figure 19b) compare relatively well with the averages of event samples from the N Indian Ocean (green diamonds, Figure 19b) during November, December, and January, which also points to a cold season dominance of N Indian Ocean moisture.

Mediterranean and Persian Gulf moisture do not show a simple distribution concerning the contribution to the total amount of specific humidity in the Western Pamir Mountains. If both are summed up and subsequently interpreted as 'western' moisture, an increase from January to April and a subsequent decrease to May can be found (Figure 18b). In December, January, and February, moisture contributions from 'western' classes were as low as 20 to 30 %, while a maximum of around 40 % occurred in March and April. This observation is in contrast to several other studies in the wider region (Aizen et al. 1995; Kreutz et al. 2003; Tian et al. 2007), where Mediterranean moisture is often proposed to be a major source of precipitation and influences d-values during winter months. Especially in the notch formed by Himalaya and Hindu Kush Mountains, Western Disturbances contribute to the formation of a low pressure area in winter, resulting in precipitation events enriched in the heavy isotopes ^{18}O and ^{2}H (Lang and Barros 2004).

Regions on the southern flank of the Hindu Kush and Karakoram Mountains receive more Mediterranean moisture, which is indicated by high d-values of around 20 ‰ in the cold season (Figure 16, Kabul and Kashmir region).

The Western Pamir Mountains seem to be less influenced by these high d-values of Mediterranean origin. This tendency is even clearer when the type of precipitation in the Western Pamir Mountains is considered. In contrast to rain, snow formation in clouds happens under non-equilibrium conditions (Lamb et al. 2017) and tends to elevate the d-values of the resulting snow above the water vapour it was formed from (Jouzel and Merlivat 1984; Uemura et al. 2005). Thus, snow samples derived from Mediterranean moisture should show even higher d-values. Since at least part of the precipitation during the winter months falls in the form of snow, a connection to high d-values of Mediterranean origin should be expected to be expressed more clearly.

Precipitation events that were assigned to the 'local' moisture source class represent moisture from within 3° radial distance. The d-values of these events are in the same range as N Indian Ocean and western moisture (Figure 19b).

Moisture from the proximity of the measurement stations ultimately also originates from evaporated vapour of different seas. Therefore, a comparison between its d-value and those of other source area classes can help to understand the moisture source of a wider region. In November, local moisture is a major contributor (Figure 18b) with low d-values (Figure 19b). From December to February, 'local' d-values are in the range of N Indian Ocean values. This changes from February to April when they resemble western d-values more closely. This behavior correlates well with the seasonal specific humidity contribution, where most moisture stems from the N Indian Ocean in December and January, and western moisture takes the lead in March. Over the course of the year, d-values of the 'local' class are closely related to the overall average of event samples (dotted line in Figure 19b). This indicates that moisture in the 3° proximity to the sampling stations is well represented by the average of all discussed moisture sources at the sampling site. This shows that the sampled precipitation events are representative of a wider region.

4.2 River water[2]

4.2.1 Results of stable isotopes (δ^{18}O and δ^2H) in river water

The distribution of the δ^2H and δ^{18}O values of the Gunt river and its tributaries is shown in a common δ^2H-δ^{18}O plot in Figure 20. The δ^2H and δ^{18}O values are in the range of -136.3 ‰ to -92.6 ‰ for δ^2H and -18.5 ‰ to -13.2 ‰ for δ^{18}O, respectively (Appendix Table 4). In their mean, the monitoring data from samples of the western part of the catchment show a wider range in δ^2H (from −136.3 ‰ to −97.6 ‰) and δ^{18}O values (from −18.5 ‰ to −14.3 ‰), than in the higher elevations of the eastern basin at the plateau area around the lake Yashilkul (δ^2H: −125.9 to −118.0 ‰, δ^{18}O: −16.6 to −15.3 ‰). These low stable isotope values are in the ranges typical for high mountainous regions, as observed for example in the Andes (Stern and Blisniuk 2002; Ohlanders et al. 2012), the Himalaya (Pande et al. 2000) or Mount Kenya as well as Kilimanjaro (Niewodniczanski et al. 1981). A short summary of the mean δ^2H and δ^{18}O values is given in Table 1. Herein, data is divided into samples from the main stream, from tributaries that have a flow direction from north to south (northern tributaries) and from south to north (southern tributaries), respectively. The plateau area includes all samples that were taken from streams flowing in the plateau region and lake water.

Table 1: Short summary of distribution of δ^2H and δ^{18}O values in water samples of the Gunt catchment. Reasons for differentiation into main stream, northern tributaries, southern tributaries and plateau are given in the text.

[2] This work was published as Meier et al. 2013.

Water type		$\delta^{18}O$ (‰)	δ^2H (‰)	d excess (‰)	Number of samples (n)
Main stream	Min	-17.4	-129.5	3.0	393
	Max	-15.1	-106.2	18.1	
	Mean	-16.2	-119.3	10.1	
Northern tributary	Min	-17.4	-127.9	8.1	294
	Max	-13.2	-92.6	26.8	
	Mean	-15.2	-106.1	15.8	
Southern tributary	Min	-18.5	-136.3	8.0	286
	Max	-14.5	-102.1	27.5	
	Mean	-16.1	-115.6	13.3	
Plateau	Min	-16.6	-125.9	4.1	6
	Max	-15.3	-118.0	7.5	
	Mean	-16.0	-122.3	6.0	
total	Min	-18.5	-136.3	3.0	998
	Max	-13.2	-92.6	27.5	
	Mean	-15.9	-116.4	12.1	

The different river water samples indicate a regression line given by Equation 11 for the tributaries and Equation 12 for the Gunt river

$$\delta^2H = 8.7(\pm 0.1)*\delta^{18}O + 26.3 \pm 1.7 \text{ ‰ with } R^2 = 0.92 \text{ and } n = 580$$

Equation 11: regression tributaries

$$\delta^2H = 5.1(\pm 0.3)*\delta^{18}O - 37.4 \pm 5.2 \text{ ‰ with } R^2 = 0.38 \text{ and } n = 393.$$

Equation 12: regression main stream

It is obvious that both the slope and the intercept of the tributaries' regression line are higher than those of the Global Meteoric Water Line (GMWL) (Equation 4).
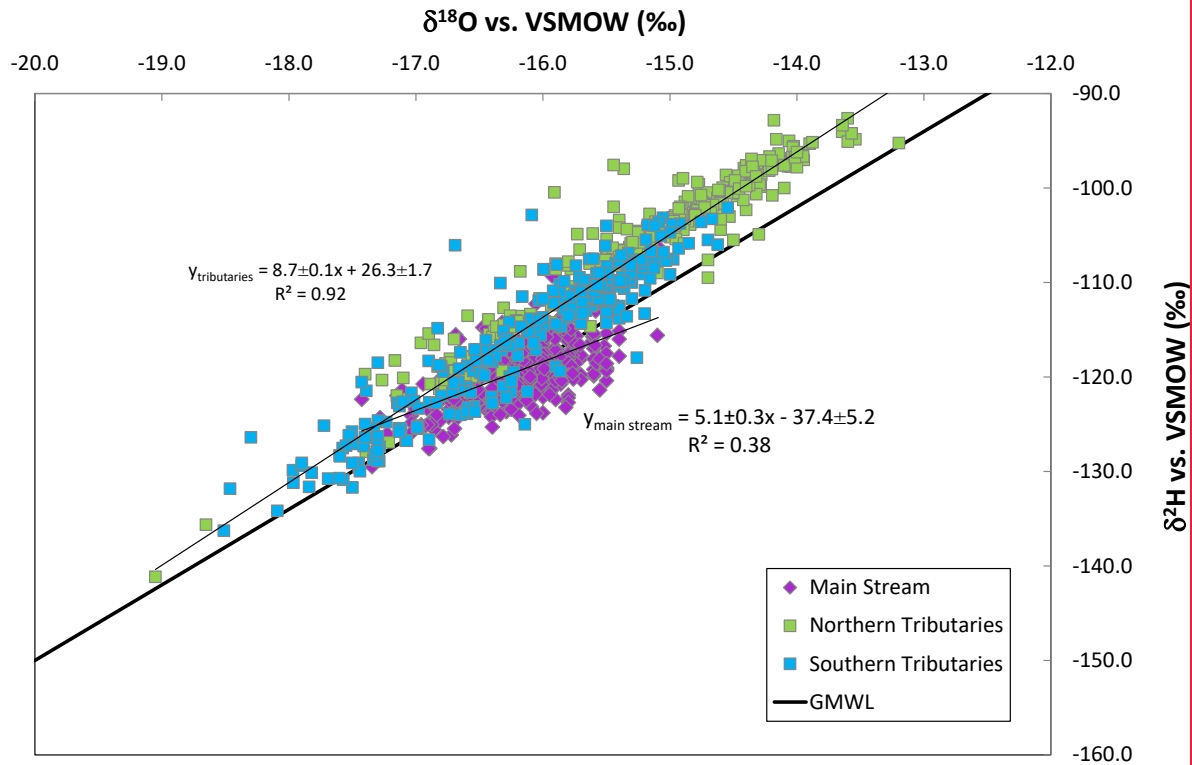
Figure 20: δ^2H-$\delta^{18}O$-Plot showing isotope values of the Gunt river and its tributaries vs. the Global Meteoric Water Line. Purple diamonds = main stream (Gunt river) water samples; green squares = northern tributaries; blue squares = southern tributaries; black bold line = Global Meteoric Water Line (GMWL); thin lines = regression lines for the two main sampling classes (main stream and tributaries).

4.2.2 Discussion of stable isotopes ($\delta^{18}O$ and δ^2H) in river water

4.2.2.1.1 Local characteristics

As a first pattern differences in the isotope ratios of the tributaries on the left bank of the Gunt river are found, in the following called southern tributaries, compared to the tributaries on the right bank of the stream, in the following called northern tributaries. An enrichment of heavier stable isotopes in the tributaries flowing from the northern boundary to the main stream compared to those originating in the south of the catchment (Figure 21) is identified.
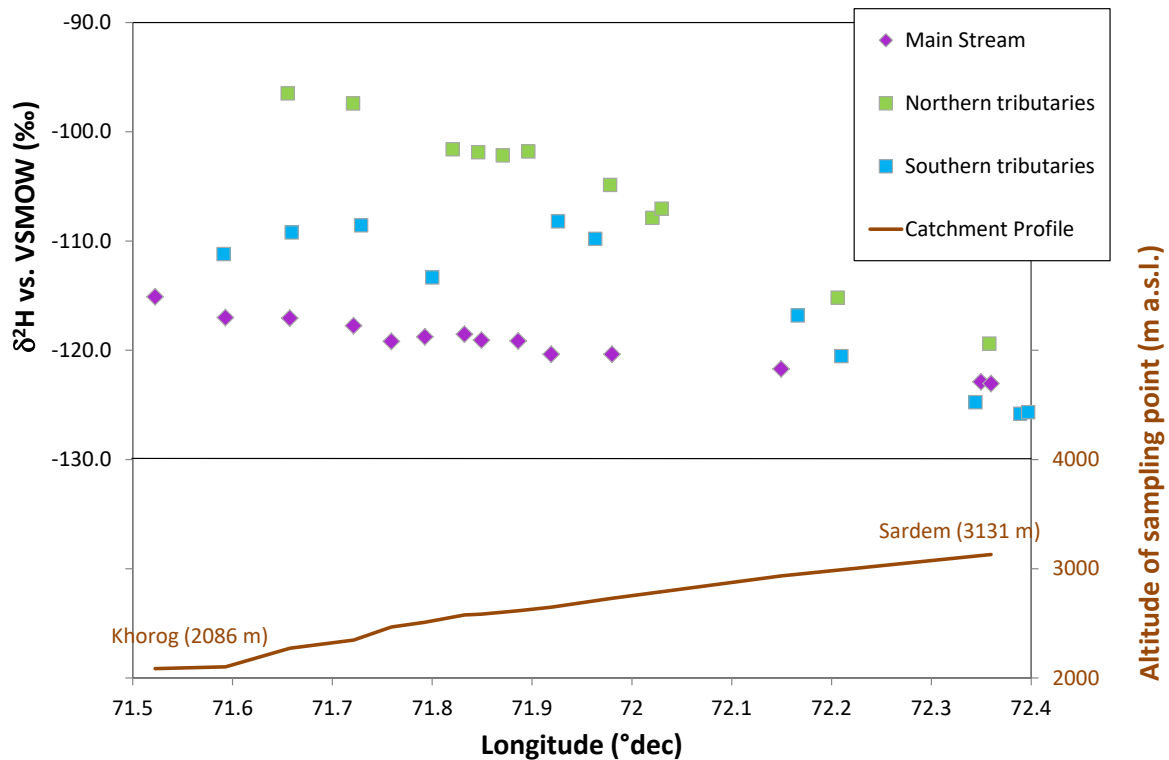
Figure 21: Development of mean δ^2H values of water samples along the main river profile, i.e. the western part of the catchment. Purple diamonds = main Stream; blue squares = southern tributaries; green squares = northern tributaries; brown line = river profile from west to east. Longitude is given in °dec east.

As it is known from hydrological observation data in this catchment (Baidulloeva August 2011), the main source of runoff is melt water, whose source is without much doubt local precipitation and glacier melt water. It can be concluded that the Local Meteoric Water Line (LMWL) is likewise given by Equation 8. The Local River Water Line for the tributaries (Equation 11) is similar to the LMWL. These observations are in line with Pande et al. (2000), who observed a similar steep slope of the Local Meteoric Water Line of the Ladakh region (India) as it is done in the Gunt catchment, while other publications focusing on stable isotopes in high altitude regions in Central Asia, for example publications about the Yamuna river (Dalai et al. 2002), the Ganges river (Ramesh and Sarin 1992) or precipitation in the Himalaya (Kang et al. 2002), often publish a slope of the Local Meteoric Water Line respectively Local River Water Line around eight or less.

Pande stated that the effect of the steeper slope is a local phenomenon of the Ladakh region (India). The results of this catchment and other studies in Central Asia, for example (Ricketts et al. 2001), show that a slope of around nine tend to be no exception or a specific local behaviour only of the Ladakh region and may be a result of a combination of different processes. Indeed, the steeper slope of 8.75 in our region must be explained as follows:

The regression line for the waters of the Gunt river (Equation 12) differs significantly from those of its tributaries (Equation 11). A strong evaporation signal in the river Gunt's isotopic composition is found, which is generated in the whole eastern Pamir plateau. The tributaries to this lake, mainly the Alichur river and the outflow of the lake Bulunkul, already show

evaporative trends in their waters. Additionally, the lake itself underlies a strong evaporation, e.g. due to low air humidity and high expose to wind from the West.

In Figure 22 the catchment is subdivided into four regions, according to the percentage of glaciation, the topography of the subcatchments (like mean altitude and slope) and following the flow direction of the tributaries as well as due to differences in the stable isotope parameters (δ^2H and δ^{18}O) (Figure 23).
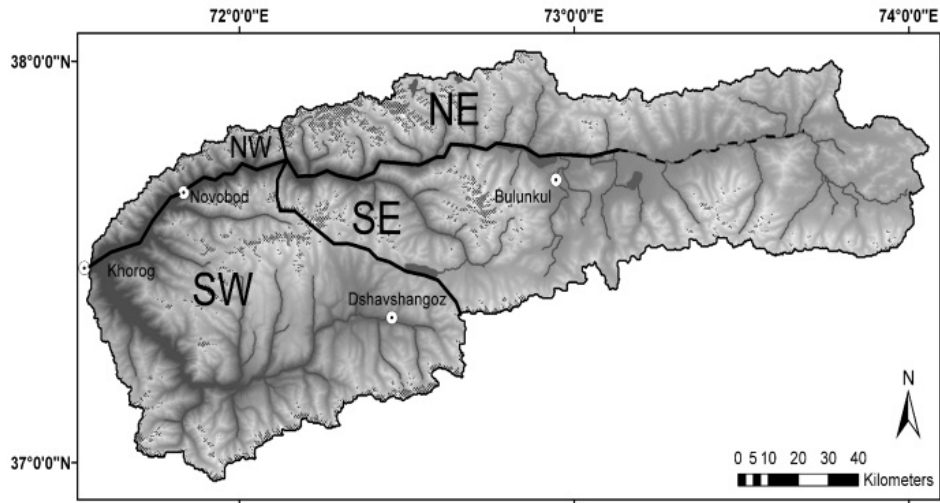
Figure 22: Regional classification of the western and middle part of the catchment into four sub-regions (NW = North West, NE = North East, SW = South West and SE = South East). Lines = borders of the sub-regions; cross hatch signature = glacier extend 2011.
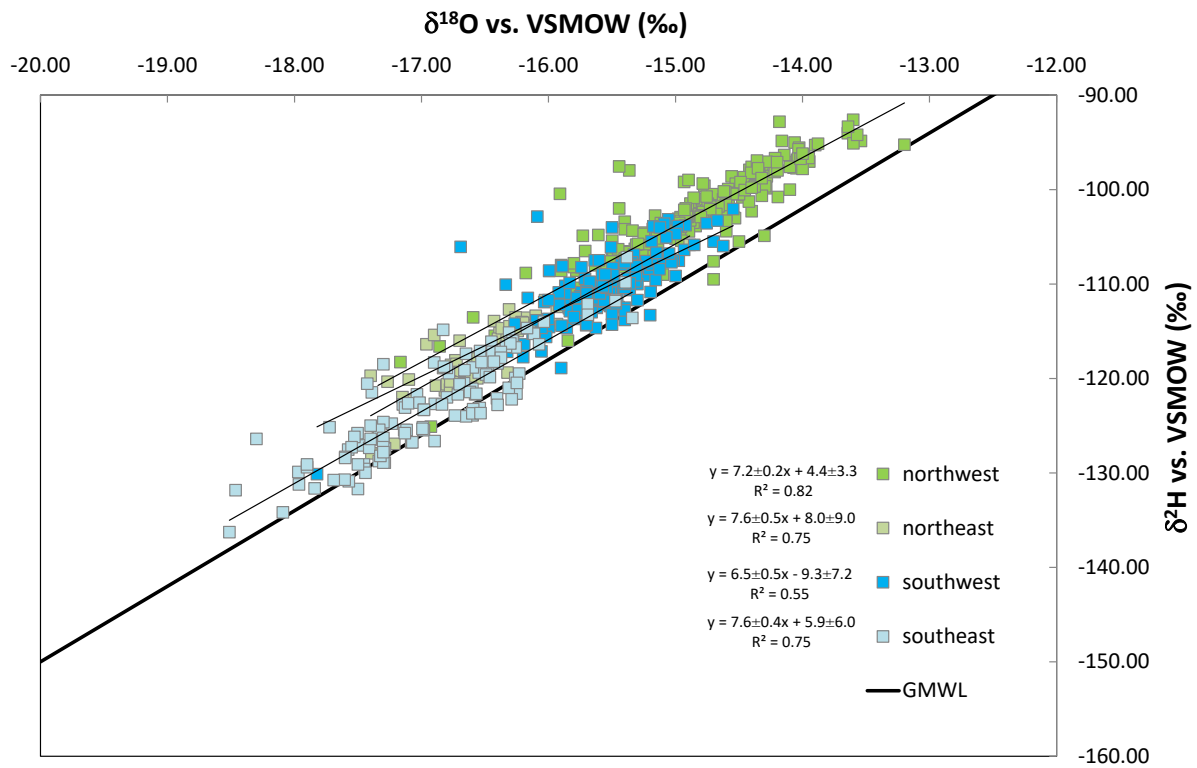
Figure 23: δ^2H-δ^{18}O-Plot showing regionalized isotope values of the tributaries vs. the Global Meteoric Water; green squares = northern tributaries; blue squares = southern tributaries; black bold line = GMWL

As it was done for the Gunt river itself, for each of these four regions a Local River Water Line can be defined. The Local River Water Line for the north-western tributaries is given in Equation 13 for the north-eastern tributaries in Equation 14, for the south-western tributaries in Equation 15 and for the south-eastern tributaries in Equation 16:

$$\delta^2H = 7.2\pm0.2*\delta^{18}O + 4.4\pm.3. \text{ \textperthousand with } R^2 = 0.82$$

Equation 13: regression line north-western tributaries

$$\delta^2H = 7.6\pm0.5*\delta^{18}O + 8.0\pm9.0 \text{ \textperthousand with } R^2 = 0.75$$

Equation 14: regression line north-eastern tributaries

$$\delta^2H = 6.5\pm0.5*\delta^{18}O - 9.3\pm7.2 \text{ \textperthousand with } R^2 = 0.55$$

Equation 15: regression line south-western tributaries

$$\delta^2H = 7.6\pm0.4*\delta^{18}O + 5.9\pm6.0 \text{ \textperthousand with } R^2 = 0.75.$$

Equation 16: regression line south-eastern tributaries

With this information it is revealed that the slope tending to nine of the Local River Water Line of the whole data set of the Gunt catchment as defined before is just an artefact of the different intercepts of each single tributary. The regions itself instead reflect a slope that is almost in the range of the GMWL and shows slight tendencies towards evaporation signals. Therefore, dividing the single regression line for the whole catchment into four separate Equation 13-Equation 16) leads to more detailed information.

Differences between northern and southern tributaries can usually be explained by topographical variations in the catchment. The mean area weighted altitude of the northern ranges is about 4,356 m a.s.l., the southern mountain chains show a mean altitude of 4,232 m a.s.l. Because the altitudes of the northern and southern mountain ranges are similar, one explanation for the differences in the isotope values of the northern versus the southern subcatchments is a difference in the influence of the wind systems to the northern and southern mountain slopes, respectively.

As mentioned before, the deuterium excess d gives information about the conditions during phase transitions and mixing processes (Froehlich et al. 2002). Especially precipitation with enhanced moisture recycling such as precipitation with origin in the Mediterranean Sea shows very high d-values, even above 15 ‰ (Gat et al. 2003). The data for the tributaries show mostly d-values above ten per mil while the Gunt river samples as well as the samples of the plateau area vary strongly in their d-values (Appendix Table 4). The variation of the d-values of the Gunt river and the plateau waters is based on evaporation in the lake respectively the flat plateau. However, the data show that the explanation of the high d-value cannot be found only in the Mediterranean Sea (or e.g. the Caspian Sea) as moisture source. In the Pamir region most of the annual precipitation falls as snow in the winter months during low mean monthly temperatures (<0 °C). So, the isotopic composition of the precipitation should be strongly influenced by the Jouzel-Merlivat effect during snow formation. An additional kinetic fractionation occurs during condensation in a supersaturated environment at lower temperatures and causes an increase in the d-value (Jouzel and Merlivat 1984). This effect is not clearly found in the data. Hence there should be at least three influences causing the higher d-value in the water samples compared to the GMWL: (i) most of the precipitation is transported from the Mediterranean Sea and or Persian Gulf by south-western

winds (Figure 24), (ii) precipitation is dominantly fallen as snow and (iii) enhanced moisture recycling occurs.
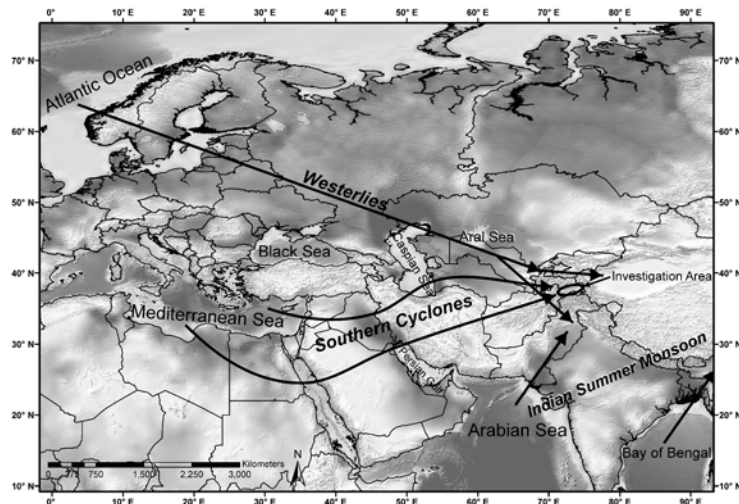
Figure 24: Presumed air mass trajectories causing the main precipitation events in the study area (Meier et al. 2013).

These assumptions are similar to a recent study of Bershaw et al. (2012) in the Himalaya and eastern Tibetan Plateau.

The *d*-value of the western Gunt catchment tributary waters is generally higher than 10, which leads to the assumption that the main humidity must come from a moisture source where moisture recycling occurred. In winter, when the catchment receives most of the annual precipitation, the westerlies bring moist air from the Atlantic with *d*-values around 10 (Dansgaard 1964). Additionally and more over south-western winds transport humid air from the Mediterranean and Caspian Sea as well as the Persian Gulf to the Pamir region (Barlow and Tippett 2008; Aizen et al. 2009). Thus, it is stated that south-western winds act as main moisture contributors.

As indicated by the different (hypothetic) local meteoric water lines represented by Equation 13-Equation 16, different parts of the catchment are dominated by different precipitation processes. Related to the catchment's topography and the wind direction major precipitation falls onto the steep southerly exposed slopes of the northern tributaries. This leads to a depletion of heavier stable isotopes in precipitation. The large southern subcatchments and therein the high regions of the north-exposed valleys receive more depleted precipitation due to the longer travel path of the precipitating moisture. Additionally there may have some intrusions of the Indian Monsoon in the Pamirs (Aizen et al. 1996; Dalai et al. 2002). However, more data on precipitation and river water is necessary to verify this hypothesis.

4.2.2.1.2 Altitude effect

As shown in Figure 21 a decrease of heavy isotope contents with increasing longitude was identified. This issue is an outcome of the altitude effect because the mean catchment elevation increases in their altitude from west to east. Thus the lapse rates lie between $\Delta\delta^2H/100$ m = -3.2 ± 0.5 ‰ and $\Delta\delta^{18}O/100$ m = -0.4 ± 0.1 ‰ for the northern tributaries

and $\Delta\delta^2H/100$ m = -3.3 ± 0.7 ‰ and $\Delta\delta^{18}O/100$ m = -0.4 ± 0.1 ‰ for the southern ones (Figure 25 and Figure 26).
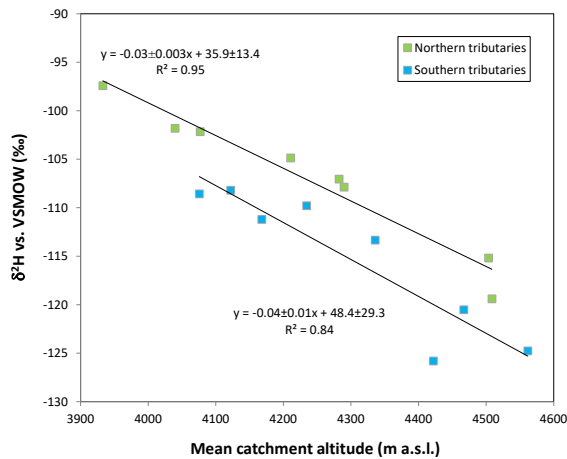
Figure 25: Altitude effect in δ^2H of the different tributaries. Blue squares = southern tributaries; green squares = northern tributaries; thin lines = regression lines for northern and southern tributaries, respectively.
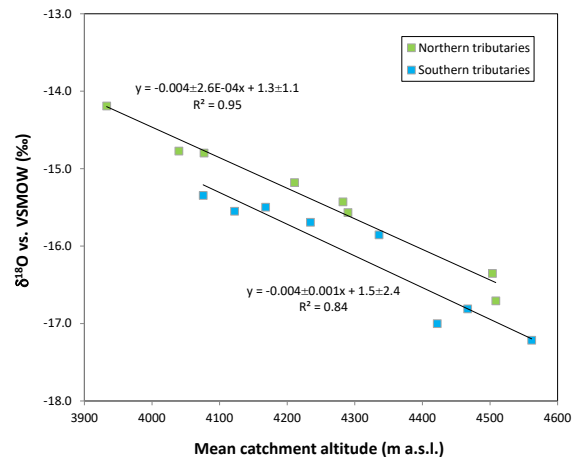
Figure 26: Altitude effect in $\delta^{18}O$ of the different tributaries. Blue squares = southern tributaries; green squares = northern tributaries; thin lines = regression lines for northern and southern tributaries, respectively.

The different behaviour of the northern tributaries compared with the southern ones was already discussed. This is also reflected in their lapse rates. The differences are in some cases from seasonal origin, where various precipitation sources influence the isotopic signal in the waters (Clark and Fritz 1997). The samples also show variations in the altitude effect throughout the year. The reason for this behaviour is founded i) in the air mass fluxes that bring precipitation and following have an impact on the catchment in different seasons and ii) in temperature and altitude dependent melting processes. Friedman and Smith (1970) demonstrated that the altitude effect is often well defined in windward sides of mountains and not well defined on leeward sides. If it is assumed that most of the precipitation is primarily delivered from western winds, the moist air should affect the northern catchments more because of their topography. The stable isotope values in the southern tributaries are wider spread than in the northern ones, and hence the altitude effect of the southern tributary range is less pronounced. This is well in line with the findings of Friedman and Smith and confirms the hypothesis that south-western winds have a major impact on the isotope patterns in the Pamirs. The southern and eastern subcatchments might also be affected by the Indian Monsoon. These facts contribute to the both diverging lapse rates and confirm the better pronounced altitude effect of the northern catchments.

4.2.2.1.3 Seasonality

In the data of Gunt river samples variations over the time (Figure 27 and Figure 28) can be observed which is caused by contributions of the tributaries to the total stream flow varying over the year. In winter the stream flow of the Gunt river is dominated by evaporation affected water from the high plains flowing through the natural landslide dam that is also partly released artificially for production of electrical power. In late autumn and winter,

when the total runoff reaches its minimum, the isotopic composition of the river Gunt water converges at the lake Yashilkul's δ^2H and δ^{18}O values (Figure 27).
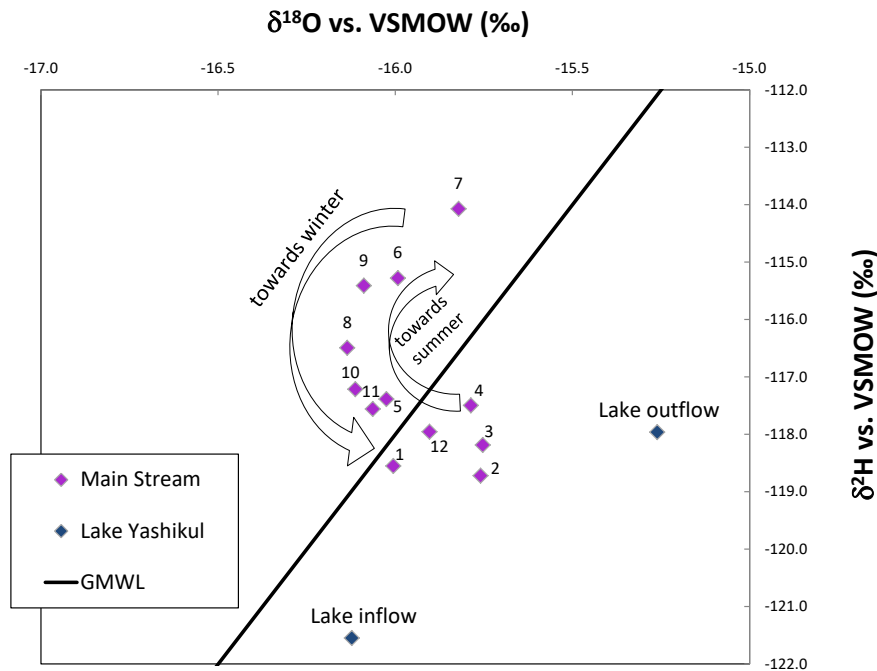
Figure 27: Mean seasonal variation of the isotopic signal of the Gunt river near the town Khorog. Purple diamonds = main stream water samples; blue diamonds = lake Yashilkul samples from 08/2011; Numbers = month of the year; black bold line = GMWL.

In late spring and summer, when the melting period is taking place, the δ^2H and δ^{18}O values are going to reflect the Local River Water Line's values. In Figure 27 we detect a difference in the melting process. Point 7 indicates a melt of more enriched solid water than the points 4–6. The hysteresis in the Gunt river samples can be explained by different evaporation rates in the Yashilkul water as explained below in more detail. So, in our catchment the lake Yashilkul and the high plains are very important for the runoff contribution over the whole year but most important in the winter time.

We see in the isotope values that the runoff of the tributaries must be diminished during the low flow period in winter (points 1–2). This is consistent with field observations. Due to the continental and altitude effect the downstream tributaries are isotopically heavier in comparison to the high plain waters. When the snowmelt starts (points 3–7), isotopically enriched snow from the downstream catchments is melted and mixed in the Gunt river with the isotopically depleted water from the high eastern plateau. The highest δ^2H and δ^{18}O values can be found in the month July, which shows also the highest discharge rates (see Figure 4). This means that we have a maximum of runoff in the tributaries. At the end of the melting period (points 8–12) the surface runoff of the tributaries decreases and at the same time the relative portion of lake- or plateau water increases. The mixing of isotopically enriched water of the tributaries with isotopically depleted water from the eastern catchment becomes apparent in Figure 21. With increasing flow length of the Gunt river we notice an enrichment

of δ^2H and δ^{18}O in the river water is observed, which is caused by the admixture of the in-flowing water of the tributaries.

Equation 12 shows the regression line for the Gunt river with a poor correlation coefficient. This is a result of the large scatter of the Gunt river data on the δ^2H-δ^{18}O plot due to seasonal variations in the runoff contributions of the different tributaries.

Not only the Gunt river's isotope ratios show a seasonal effect but also the tributaries vary in their isotopic signal with maximum values in the summer (June–August) and minimum in the winter months (December–February) (Figure 28).
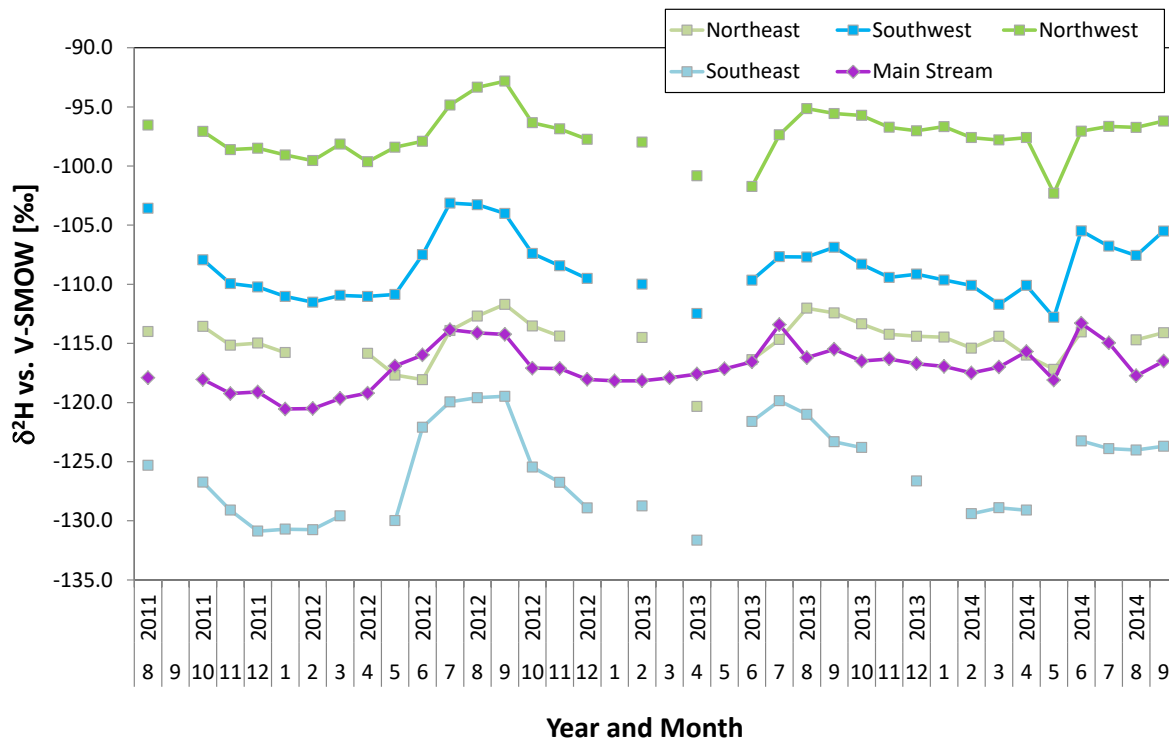
Figure 28: Seasonal variations of δ^2H over the year of each two exemplary northern (green squares; green lines) and southern tributaries (blue squares; blue lines) as well as the Main Stream (purple diamonds; purple line).

This seasonal effect in river systems is commonly associated with seasonal variations of stable isotopes in precipitation (Mook 2005; Koeniger et al. 2009; Lachniet and Patterson 2009). Seasonal variations in the Gunt river's hydrograph indicate that our drainage basin is controlled by melt water from precipitation from the recent winter or even preceding from glacier melt. Thus the suggested undulating trend in the isotopic composition of the stream water cannot be caused by the each month's precipitation but could be explained through melting processes (Stichler et al. 1986; Taylor et al. 2001; Taylor et al. 2002). With beginning of the melting period, the melt water is depleted in ^{2}H and ^{18}O. Throughout the melting period the isotopically enriched snow melts and generates relatively higher δ^2H and δ^{18}O values. The seasonality in the isotope values correlates with the seasonality in the runoff data of the main stream that show also a discharge maximum in the summer months (June–August).

4.3 Conclusions to the assessment of stable isotopes (δ^{18}O and δ^2H) in water

The derived results show that isotope measurements are a very helpful tool to investigate remote areas.

Most of the precipitation samples and river waters showed δ^2H and δ^{18}O values that are typical for high altitude regions. The stable isotope values in river water showed regional differences as well as seasonal effects. The regional variations in the isotope patterns result from differences in the catchment altitude and the precipitation distribution in the catchment.

Seasonal differences in the isotope values are caused by melting processes. The main stream Gunt is clearly affected by water arising from the high plateau and the lake Yashilkul.

Additionally, the *d*-values are mostly above ten, indicating that the Gunt catchment is a snow-dominated catchment which receives its precipitation mainly through western and south-western winds coming from the Atlantic Ocean, the Mediterranean Sea and the Persian Gulf. An influence of the Indian Monsoon cannot be denied. The data evaluation of air mass trajectories from the Western Mediterranean to the Western Pamir shows a maximum moisture contribution during March and April.

5   Hydrochemistry of river water

The hydrochemical composition of a water body depends on the geological formation through which it flows or its petrographic composition, the vegetation of the catchment and on the atmospheric input (Meybeck 1987; Schneider et al. 2003). Mason et al. (1985) also mention the type and quantity of precipitation and the relief as influencing factors on the chemistry. During weathering processes reactions between water and rock take place, which result into a change of water chemistry in regard to e.g. major ions and trace elements. Rivers are fed directly from surface runoff on the one hand, and from groundwater via infiltration processes on the other. Thus, there are other sources and sinks, such as substances washed away on the surface or infiltrated by percolating water, as well as anthropogenically infiltrated substances with different water mobility characteristics (Greifenhagen 2000). Due to the very low population density in the study area, the latter are not expected.

In the master thesis of Brehme (2014), the influences of the natural conditions on the river water composition were investigated for a limited data set from the Gunt catchment area by means of factor analysis and main component analysis. This chapter presents an evaluation of the hydrochemical parameters of the entire data set of river waters at selected locations (Figure 29). For the evaluation of the hydrochemical analyses with regard to relationships to natural conditions, the results of the geo-characteristics from Brehme (2014) were adopted.
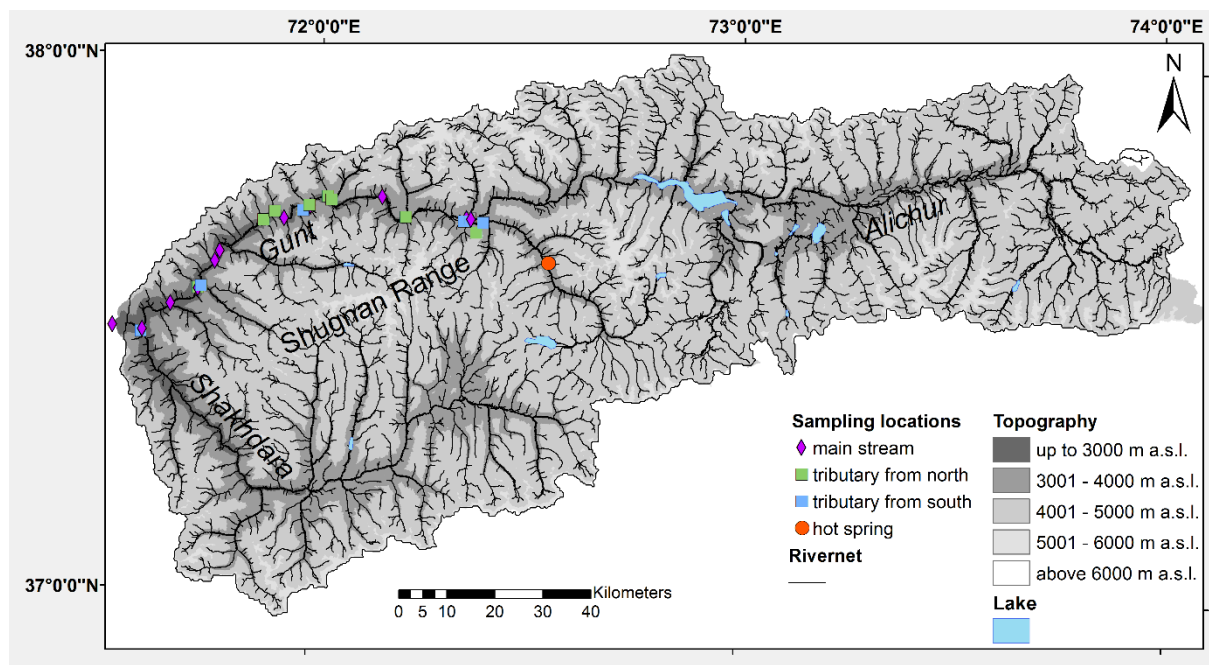
Figure 29: Location of sampling locations that were used for hydrochemical analysis.

5.1   Results of hydrochemical analysis

The data set shows that the cation distribution in the whole catchment is very divers (Appendix Table 5). The total sodium concentrations vary between 0.02 meq/L and 0.64 meq/L, with an arithmetic mean of 0.21 meq/L and a median of 0.16 meq/L (Figure 31). Most of the

sodium values are around 0.05 meq/L. However, a second grouping around-values between about 0.28 meq/L and 0.48 meq/L is also noticeable.

The potassium concentrations are between 0.01 meq/L and 0.54 meq/L with a clear maximum in the histogram at values of around 0.04 meq/L (Figure 30).

Calcium is one of the main constituents in the study area and shows concentrations between 0.22 meq/L and 2.46 meq/L (Figure 32). There are two maxima in the distribution: one high pronounced maximum around 0.8 meq/L and one less pronounced one at values of around 1.5 meq/L.

The total magnesium values vary between 0.01 meq/L and 0.58 meq/L with maxima at 0.06 meq/L, 0.18 meq/L and 0.42 meq/L (Figure 33).
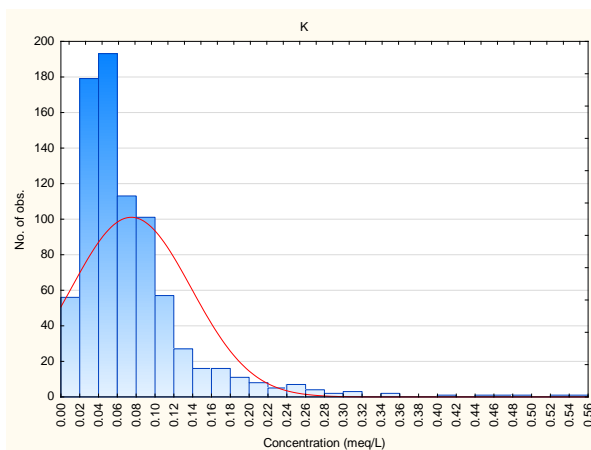
Figure 30: Histogram of K-concentrations; red line=expected normal distribution.
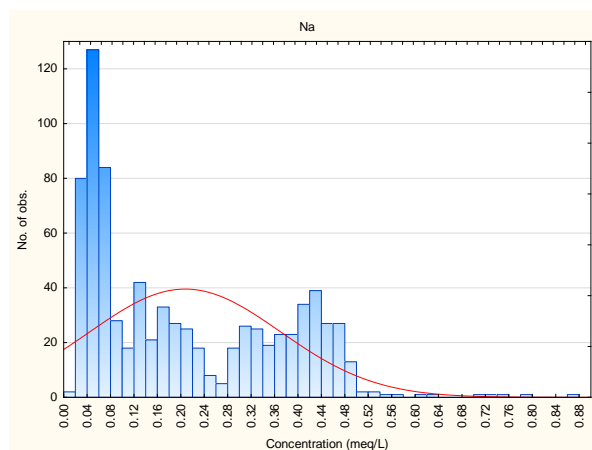
Figure 31: Histogram of Na-concentrations; red line=expected normal distribution.
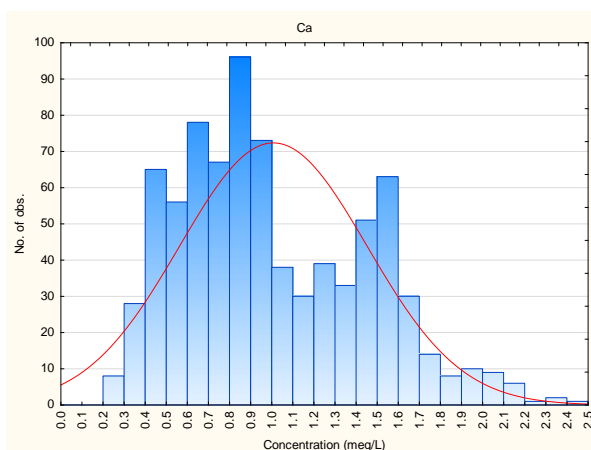
Figure 32: Histogram of Ca-concentrations; red line=expected normal distribution.
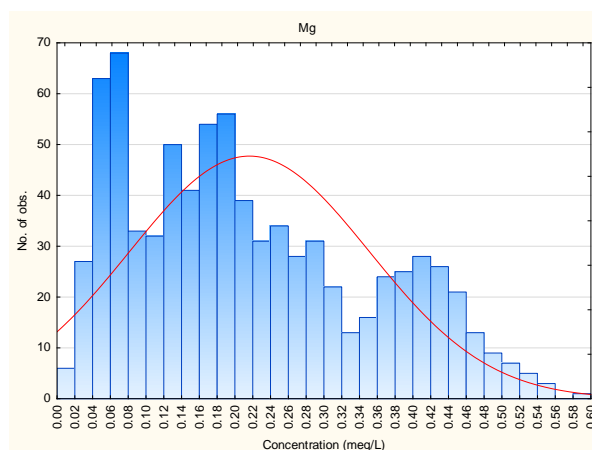
Figure 33: Histogram of Mg-concentrations; red line=expected normal distribution.

The chloride concentrations of the waters range between 0.001 meq/L and 0.89 meq/L, with a very high frequency of 0.02 meq/L (Figure 34). The distribution itself is accordingly strongly right-skewed.

The histogram of the sulphate data set also shows a right-skewed distribution with values between 0.02 meq/L and 1.17 meq/L and a maximum frequency of 0.10 meq/L as well as a tendency towards a two-capped distribution (Figure 35).

Bicarbonate is the most dominant anion of the Gunt waters and fluctuates in its calculated HCO_3 concentrations between 0.18 meq/L and 2.41 meq/L and show peaks of about 0.7 meq/L and 2.0 meq/L in the distribution (Figure 36).
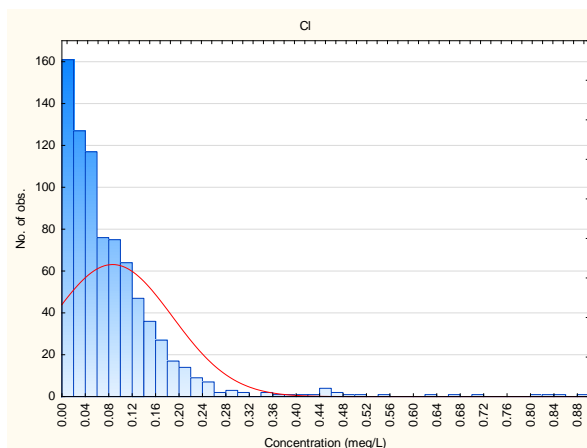
Figure 34: Histogram of Cl-concentrations; red line=expected normal distribution.
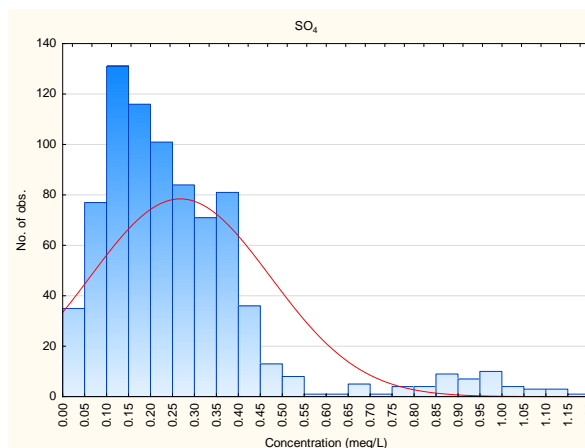
Figure 35: Histogram of SO_4-concentrations; red line=expected normal distribution.
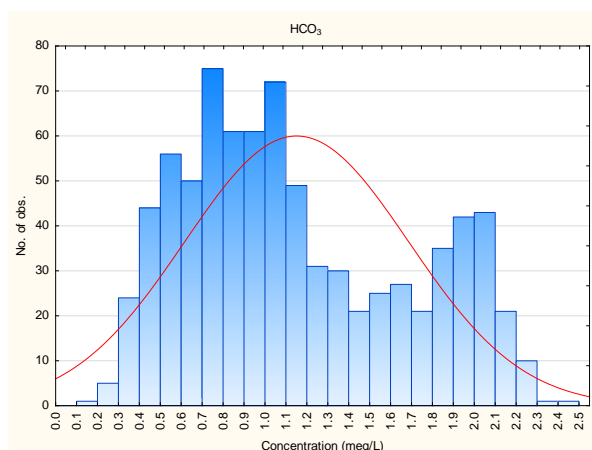
Figure 36: Histogram of HCO_3-concentrations; red line=expected normal distribution.

The electrical conductivities of the water vary at most between 19 and 400 µS/cm, the median is 143 µS/cm. The box plots – differentiated by water type – show clear differences in the distribution of values (Figure 37). The measured values of the main stream (g) cover a range of 250 µS/cm. The significantly higher fluctuation range of circa 400 µS/cm can be detected for the southern tributaries, whose median are 161 µS/cm. The lowest fluctuation range in the EC values can be found for the northern tributaries with a median value of 116 µS/cm.

In the collected data set, the water temperatures fluctuate between a minimum of 0 °C and a maximum of 17 °C. The arithmetic mean value is 6.9 °C, the median 7.6 °C. The distribution of the water temperatures compared to their origin is quite homogeneous (Figure 39).

Table 2: Descriptive statistics of the hydrochemical parameters.

Variable	N	Arith. Mean	Me-dian	Mini-mum	Maxi-mum	25 %-Quar-tile	75 %-Quar-tile	Vari-ance	Std.Dev.	Skew-ness	Kurto-sis
Electric conduc-tivity (µS/cm)	805	160.03	143.00	19.00	400.00	115.00	205.00	3370.51	58.06	0.61	0.03
Temperature (°C)	782	6.90	7.60	0.00	17.00	2.90	10.60	17.61	4.20	-0.14	-1.25
pH	805	7.15	7.11	4.52	8.81	6.80	7.52	0.27	0.52	0.06	0.52
Cl (meq/L)	806	0.09	0.06	0.00	0.89	0.03	0.11	0.01	0.10	3.70	20.11
SO$_4$ (meq/L)	806	0.27	0.22	0.02	1.17	0.13	0.35	0.04	0.21	2.05	4.87
Na (meq/L)	805	0.21	0.16	0.02	0.87	0.06	0.36	0.03	0.16	0.66	-0.54
K (meq/L)	806	0.07	0.06	0.01	0.54	0.04	0.09	0.00	0.06	3.06	14.05
Mg (meq/L)	806	0.22	0.19	0.01	0.58	0.10	0.31	0.02	0.13	0.52	-0.76
Ca (meq/L)	806	1.01	0.91	0.22	2.46	0.66	1.38	0.20	0.44	0.56	-0.41
HCO$_3$ (meq/L)	806	1.15	1.03	0.18	2.41	0.73	1.60	0.29	0.54	0.45	-0.95

The pH values in the overall data set vary between 4.5 in the minimum and 8.8 in the maximum, the arithmetic mean is 7.2 and the median is 7.1. This already shows that the data set contains not many outliers, as shown by the box plots of the individual sites (Figure 38).
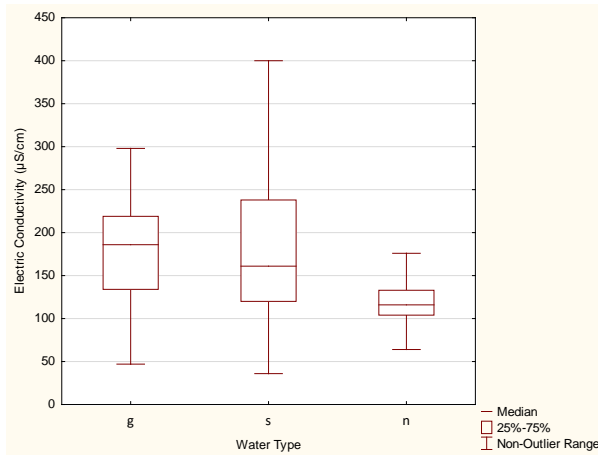
Figure 37: EC-distribution of all water samples. g = main stream (Gunt), s = southern tributaries, n = northern tributaries.
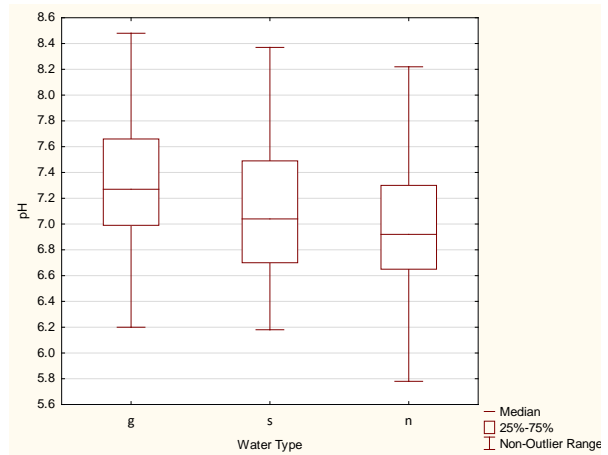
Figure 38: pH-distribution of all water samples. g = main stream (Gunt), s = southern tributaries, n = northern tributaries.
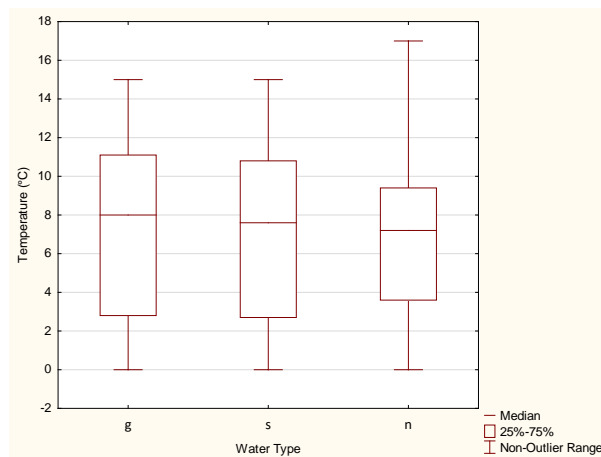
Figure 39: Temperature distribution of all water samples. g = main stream (Gunt), s = southern tributaries, n = northern tributaries.

The correlation matrix in Table 3 results from the correlation analysis of all major ions with each other. Particularly strong correlations between bicarbonate and magnesium (r = 0.91), sodium (r = 0.90) and calcium (r = 0.89) can be seen, whereby these are also strongly correlated with each other. Furthermore, calcium and sulphate (r = 0.83) and chloride and sulphate (r = 0.87) correlate with each other.

Table 3: Correlation of major ions. Correlation coefficients with p<0.05 are red.

	Cl (meq/L)	SO$_4$ (meq/L)	Na (meq/L)	K (meq/L)	Mg (meq/L)	Ca (meq/L)	HCO$_3$calc (meq/L)	EC [µS/cm]	T [℃]	pH
Cl (meq/L)	1.00	0.87	0.70	0.67	0.38	0.74	0.44	0.76	0.34	0.44
SO$_4$ (meq/L)	0.87	1.00	0.63	0.62	0.57	0.83	0.50	0.81	0.34	0.49
Na (meq/L)	0.70	0.63	1.00	0.69	0.74	0.88	0.90	0.88	0.59	0.85
K (meq/L)	0.67	0.62	0.69	1.00	0.39	0.65	0.54	0.76	0.33	0.49
Mg (meq/L)	0.38	0.57	0.74	0.39	1.00	0.84	0.91	0.72	0.49	0.85
Ca (meq/L)	0.74	0.83	0.88	0.65	0.84	1.00	0.89	0.89	0.57	0.82
HCO$_3$calc (meq/L)	0.44	0.50	0.90	0.54	0.91	0.89	1.00	0.77	0.61	0.91
EC [µS/cm]	0.76	0.81	0.88	0.76	0.72	0.89	0.77	1.00	0.57	0.74
T [℃]	0.34	0.34	0.59	0.33	0.49	0.57	0.61	0.57	1.00	0.65
pH	0.44	0.49	0.85	0.49	0.85	0.82	0.91	0.74	0.65	1.00

The correlation analysis of the natural catchment parameters (Appendix Table 7) against the seasonal mean values of the main ion concentrations of the respective catchments are given in the correlation matrix contained in Table 4.

Table 4: Correlation of major ions with catchment parameters. Correlation coefficients with p<0.05 are red.

	Cl (meq/L)	SO$_4$ (meq/L)	Na (meq/L)	K (meq/L)	Mg (meq/L)	Ca (meq/L)	HCO$_3$calc (meq/L)	EC [µS/cm]	T [℃]	pH
Altitude$_{min}$ (m a.s.l.)	-0.26	-0.31	-0.24	-0.10	-0.38	-0.29	-0.24	-0.41	-0.27	-0.39
Altitude$_{max}$ (m a.s.l.)	0.03	0.23	-0.05	0.06	-0.03	0.10	-0.04	0.12	0.30	-0.12
Altitude$_{mean}$ (m a.s.l.)	-0.23	-0.16	-0.47	-0.28	-0.49	-0.38	-0.50	-0.38	-0.09	-0.55
Area (km²)	0.14	0.36	0.35	0.32	0.43	0.42	0.41	0.49	0.49	0.34
Permafrost$_{discont}$ (%)	-0.22	-0.12	-0.46	-0.29	-0.45	-0.36	-0.49	-0.34	-0.02	-0.52
Permafrost$_{cont}$ (%)	-0.17	-0.15	-0.47	-0.21	-0.56	-0.38	-0.52	-0.37	-0.03	-0.55
Glaciation (%)	-0.12	-0.16	-0.59	-0.27	-0.64	-0.42	-0.63	-0.54	-0.20	-0.61
Unconsolidated rock (%)	-0.20	-0.16	-0.01	0.23	0.00	-0.03	0.08	-0.13	0.09	0.10
Limestone (%)	0.02	0.00	0.24	0.34	0.18	0.17	0.28	0.10	-0.14	0.18
Magmatic rock (%)	-0.01	-0.25	-0.04	-0.09	-0.28	-0.26	-0.20	-0.08	0.05	-0.17
Metamorphic rock (%)	0.09	0.29	-0.03	-0.11	0.19	0.19	0.06	0.10	-0.05	0.05
Aspect flat (%)	0.15	0.15	0.53	0.49	0.29	0.32	0.45	0.38	0.28	0.42
Aspect N (%)	0.51	0.31	0.68	0.67	0.35	0.46	0.51	0.54	0.19	0.51
Aspect NO (%)	0.35	0.32	0.13	0.21	-0.06	0.09	-0.09	0.24	0.00	-0.16
Aspect O (%)	-0.35	-0.16	-0.56	-0.45	-0.31	-0.37	-0.47	-0.37	-0.26	-0.60
Aspect SO (%)	-0.48	-0.44	-0.37	-0.42	-0.20	-0.34	-0.21	-0.34	-0.19	-0.26
Aspect S (%)	-0.46	-0.36	-0.25	-0.21	0.00	-0.24	-0.06	-0.25	0.02	0.13
Aspect SW (%)	-0.38	-0.16	-0.58	-0.57	-0.19	-0.37	-0.44	-0.49	-0.23	-0.31
Aspect W (%)	0.37	0.37	0.08	-0.01	-0.02	0.24	0.00	0.10	0.18	-0.06
Aspect NW (%)	0.45	0.23	0.54	0.45	0.19	0.40	0.41	0.38	0.22	0.34
Slope 0-1 (°)	0.14	0.15	0.53	0.60	0.38	0.41	0.55	0.40	0.29	0.48
Slope 1-2 (°)	0.01	0.09	0.09	0.35	-0.06	0.09	0.07	0.18	0.39	0.06
Slope 2-3 (°)	-0.18	-0.11	-0.22	-0.02	-0.17	-0.20	-0.20	-0.05	0.17	-0.16
Slope 3-4 (°)	-0.28	-0.33	-0.37	-0.40	-0.20	-0.37	-0.30	-0.34	-0.22	-0.29
Slope 4-5 (°)	-0.10	-0.18	-0.19	-0.38	-0.05	-0.19	-0.15	-0.31	-0.49	-0.16
Slope 5-6 (°)	0.02	-0.04	-0.20	-0.43	-0.09	-0.14	-0.21	-0.25	-0.38	-0.19
Slope >6 (°)	0.12	0.10	-0.21	-0.43	-0.13	-0.10	-0.27	-0.18	-0.27	-0.22
Runoff rate (mm/a)	-0.10	-0.13	-0.24	-0.39	-0.19	-0.23	-0.26	-0.31	0.15	-0.11

The data indicate a close correlation between the chemical composition of the waters in the sub-basins and their proportion of permafrost or glaciation as well as the prevailing slope orientations as given in more detail below. Correlation coefficients around r = -0.50 show that the waters in areas with large permafrost areas and glacier covers have comparably low mean ion concentrations, especially in concentrations of sodium, magnesium and bicarbonate. In addition, there is a similar correlation between permafrost cover and glaciation

with mean pH values. Furthermore, the same linear relationship between the mentioned parameters and the mean heights of the catchment areas can be observed. The different slope orientations are also related to different ion concentrations. Catchments with many flat areas obviously have higher sodium, potassium and bicarbonate concentrations (r = 0.53, r = 0.60 and r = 0.55, respectively). Areas with predominantly north-facing slopes show higher concentrations of calcium, sodium, potassium, chloride and bicarbonate, at the same time the conductivity of the water and the water temperature are higher. In areas with predominantly east and south-east oriented slopes the waters show lower chloride, sulphate, sodium, potassium and bicarbonate concentrations, in those with predominantly south-west oriented slopes lower sodium, potassium and bicarbonate concentrations as well as lower conductivities. Significant linear correlations between the lithological units and the ion concentrations cannot be demonstrated.

5.2   Discussion of hydrochemical parameters

Generally, the hydrochemical composition of the river water samples of the Gunt catchment show major ion concentrations that are typical for high altitude regions (Jenkins et al. 1995; Żelazny et al. 2011; Li et al. 2018) meaning a general very low total dissolved ion content (here EC ≤ 400 µS/cm). Li and Zhang (2008) also cite particularly low ion concentrations as an indication of a lack of anthropogenic influence from e.g. agricultural activities and the presence of predominantly crystalline rock.

The cation and anion concentrations of the Gunt catchment reflect values that are typical for silicate and crystalline rocks (Mason et al. 1985; Merkel and Sperling (1996); Sigg and Stumm 1996). Additionally, the major ion concentrations are in line with findings of Jenkins et al. (1995)´who investigated rivers of the Himalaya and Huang et al. (2009) who also analysed river waters of the Tibetan Highlands.

According to Li and Zhang (2008) and Huang et al. (2009), the chemical composition of water in the Himalayas is predominantly characterized by chemical and physical weathering processes of the rocks, whereby according to Sigg and Stumm (1996) the physical weathering clearly predominates in general and above all in plateau areas. Gibbs (1970) names the geological subsoil, precipitation and evaporation effects as the main factors influencing the chemical composition of the water. According to his explanations, the ion composition of waters with dominant calcium and bicarbonate concentrations has its origin predominantly in the chemical weathering of rocks.

The descriptive analysis of all hydrochemical parameters shows a very inhomogeneous data distribution. Especially the fluctuations in Ca and HCO_3 as well as SO_4 concentrations reflect spatial and seasonal variations. The multi-modal distribution of some parameters indicates an overlap of various distribution types. This is a result of spatial and temporal variations in ion concentrations. The right skewed distribution of K and Cl (Figure 30 und Figure 34) concentrations is an indication for generally low ion concentrations in the waters and the occasional occurrence of higher mineralisation. Nevertheless, the composition of major ions in

the study area are less varying, which is an indication of very continuous entries, due to continuous weathering or dissolution of the mineral phases like feldspars, micas (e.g. biotite) or amphibolites (e.g. hornblende) in the occurring rock.

The electrical conductivities of the waters in the catchment area of the Gunt vary between 100 µS/cm and 200 µS/cm, respectively, and are representative of high mountain regions. Huang et al. (2009) and Jenkins et al. (1995) show similar values for rivers in the Himalaya. The distribution of the electrical conductivities shows that especially the northern tributaries are less enriched compared to the main stream. This is due to the fact that these northern areas are characterised by pronounced glacier cover and high relief. The low mineralisation shows that the receiving waters are mainly fed by melt water and surface runoff. The small fluctuations of the tributary values are an indication that relatively constant processes take place. The higher enrichment of the main stream is due to the fact that it i) is characterised by the high mineralised water from the lake Yashilkul and ii) represents a kind of mixed sample from all catchment areas. The large fluctuations in its values in turn provide indications of the spatial and/or temporal variability of the inflows.

According to Furtak and Langguth (1967), the mean values of the main ions can be differentiated in seven water types, or chemical facies. When presenting hydrochemical data according to Piper (1944) (Figure 40) using water types according to Furtak and Langguth (1967)or Kralik et al. (2005), most of the data is plotted for the alkaline earth-carbonate water type (type 1). According to Kralik et al. (2005), this is typical for a fast turnover when considering groundwater and frequently occurs in crystalline mountains and in areas with increased flow velocities, which makes the results plausible. In addition, tendencies towards the groundwater type 2 (alkaline earth carbonate-sulphatic) can be detected for some river waters of the southern tributaries. Type 2 is characteristic for slower circulations and thus more exchange processes. Some river waters also show tendencies towards groundwater type 4 (alkaline earth – alkaline – carbonate water). It is typical in flowing waters from crystalline areas and is caused by a relatively frequent shift from water type 1 and 2 to water type 4, which occurs in the low-mineralized crystalline waters through the addition of little sodium and potassium. Usually the addition of sodium and potassium is explained by human activities or the admixture of alkaline waters from water type 7, e.g. NaCl-rich alkaline-choridic waters. In the Gunt catchment there are also some hot springs, e.g. the hot springs in Djelondi. The hydrochemical analysis of the waters from the hot springs showed that they are higher mineralized (EC~477 µS/cm) and belong to water type 7 with a higher SO_4 component (alkaline-sulphatic water type). Therefore, it can be concluded that the southern tributaries tending to water type 4 might be influenced by waters emerging from hot-springs.
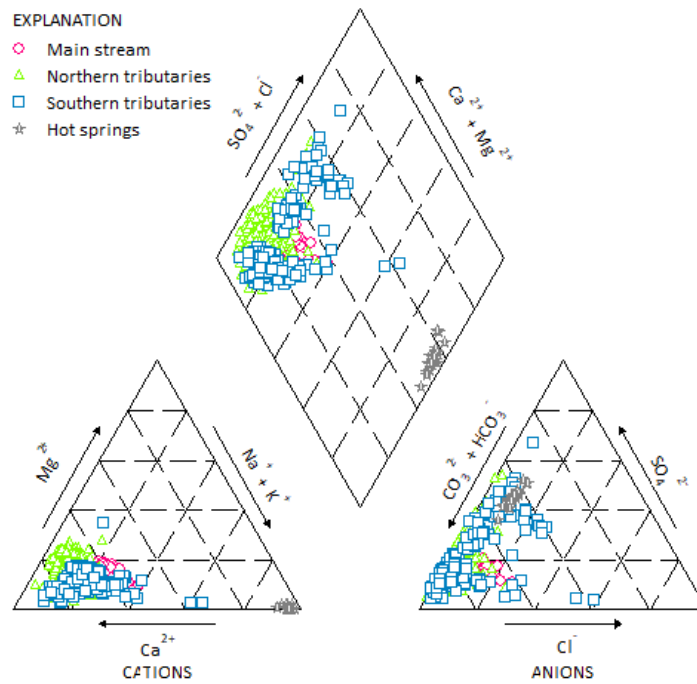
Figure 40: Piper Plot of all water samples.

Summarizing, the main stream does not show strong variations in the hydrochemical composition along its flow path (Figure 41). The tributaries neither show very distinctive major ion compositions in their waters.
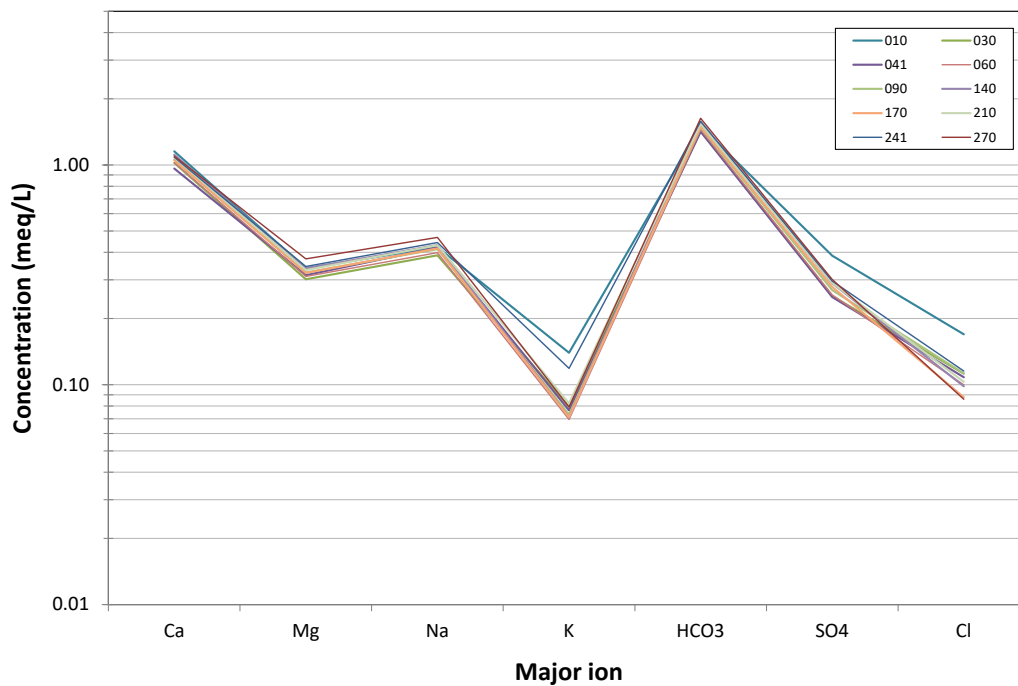
Figure 41: Schöller plot representing the major ion distribution of all sampling locations at the main stream.

Therefore, the catchment is obviously characterised by a relatively homogeneous geogenic composition, which is reflected in the river waters. Abundant mineral phases of the ingenious and magmatic rocks in the investigation area like mainly quartz, mica, and feldspars are characterized by low dissolubility (low solubility products). The spatial differences between between northern and southern tributaries and the main stream can be seen only in the grade of minerlisation. The main stream shows higher ion loads that the tributaries (Figure 42).
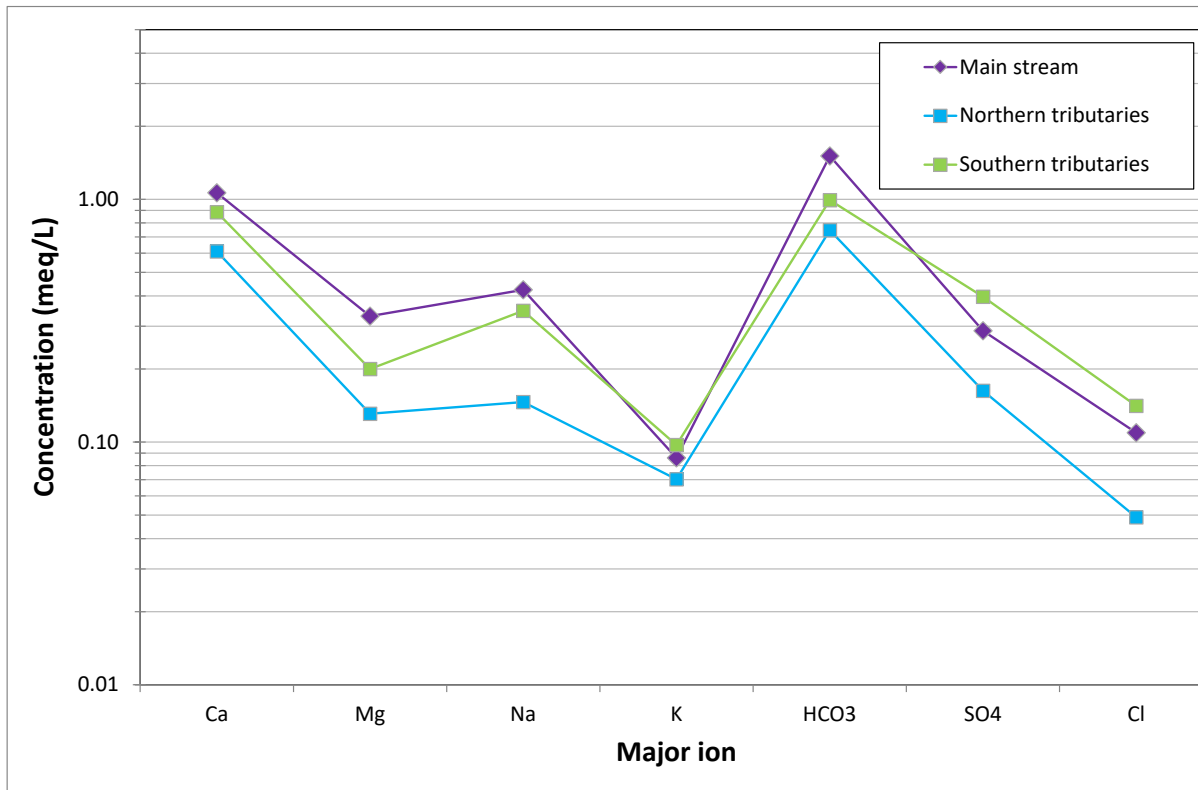
Figure 42: Schöller plot representing the mean major ion distribution of the main stream, the northern and southern tributaries, respectively.

The correlation analysis between the major ions highlights strong relationships between the dominant ions in the stream water. This is an indication that the major source of cations to surface waters is from chemical weathering. The strong correlations between bicarbonate and calcium and magnesium are a clear indication that these originate from the weathering of carbonates. The correlation between calcium and chloride ions, respectively, and sulfate ions indicates evaporite weathering, the correlation between sodium and bicarbonate indicates silicate weathering (Li and Zhang 2008; Zhu et al. 2012; Varol et al. 2013).

Correlation analyses (Table 4) have shown a negative linear correlation between the glacier coverage of a catchment area and the ion concentrations of its waters. This shows that the receiving waters in areas with significant glacier occurrence are predominantly fed by little mineralized meltwater.

Since a large part of the areas in the study area are affected by permafrost, it is supposed that the occurrence of permafrost has an impact on the mineralization of river water in the Gunt catchment. Permafrost should limit water-rock-interaction processes and lead to lower

mineralisations. Therefore, this correlation is important with regard to identify areas of possibly high interactions between groundwater and rock. The fact that there is a negative linear relationship between the permafrost cover of a catchment area and the ion concentrations of its waters shows that such a strong water-rock-interaction does not occur. On the other hand, it is an indication for the rivers in this area are primarily fed by little mineralized meltwater or precipitation water. Hayashi et al. (2004) also show that in areas with continuous permafrost no infiltration into the soil or the rock can take place, precipitation and meltwater therefore enter the receiving waters as surface runoff. Areas with discontinuous permafrost are of particular importance for indications of water-rock-interactions, because there are areas that are not frozen and are therefore theoretically available for infiltration processes. However, the statistical analyses did not provide clear evidence for a major influence of discontinuous permafrost on the hydrochemical footprint, since the parameters of continuous and discontinuous permafrost basically showed the same relationships to all other properties.

If it is assumed that the chemical composition of the water is mainly influenced by the geological formations through which it flows, catchment areas with high limestone deposits or predominantly metamorphic rock should also show correspondingly different major ion concentrations in the water. Thus, differences should occur in the chemistry of the eastern areas, which have larger upcoming limestone and marble deposits, and the hydrochemical composition of the western areas with particularly high metamorphic proportions. However, the correlation analyses showed no correlation between the chemical composition of the waters and the geological units of the areas. This is a clear indication that in the studied catchment areas are only little exchange processes with the bedrock, that there is high flow energy and that the rivers are mainly fed by surface runoff from precipitation and melt water. The fact that the waters in the entire catchment area of the Gunt are dominated by calcium and bicarbonate is due to the "simpler" structures of the sedimentary rocks in the eastern area compared to the crystalline rocks in the west. Zhu et al. (2012) also note that due to different weathering resistances in crystalline areas water may occur, which is characterized by carbonate weathering. The hydrochemical composition of the hot spring waters in Djelondi can be explained by their, in comparison to the surface waters, longer transit time (see Table 6) and higher water temperatures, which intensify water-rock-interaction and support dilution of silicate minerals.

In general, temporal variations in the concentrations of major ions of the surface waters could be detected (Figure 43). The monthly fluctuations in ion concentrations at all sites are very similar over the course of the year. This shows that there are no clear regional influencing factors. Strong and suddenly decreasing ion concentrations from April onwards can be associated with the onset of snowmelt, which leads to corresponding dilution effects. The fact that this continuous depletion continues until its peak in July is due to the fact that the glacier melts after the snow melts. A further reason is the fact that with increasing temperatures, higher and higher areas are affected by the melting process. According to Huang et al. (2009), exactly this depletion in the first part of the dry period is also evidence that the ions dissolved in the water originate primarily from rock weathering. According to Zhu et al.

(2012), the fact that precipitation favors chemical weathering also explains lower ion concentrations and fewer fluctuations during the dry period.
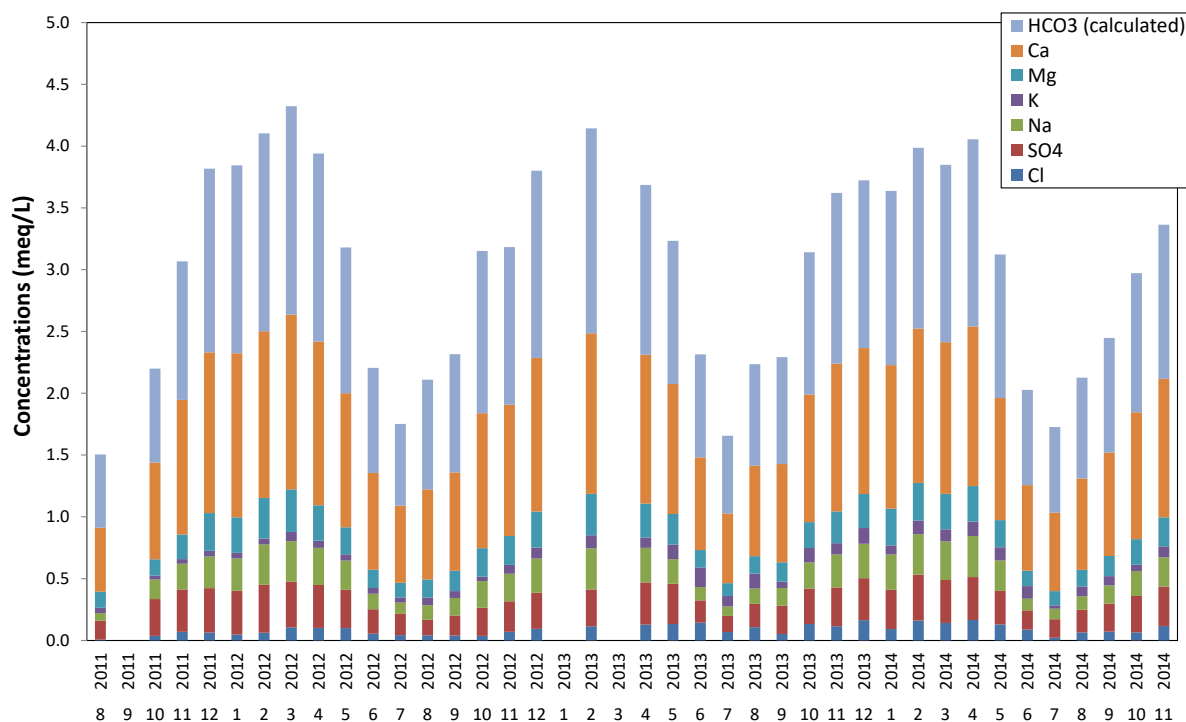
Figure 43: Temporal evolution of mean major ion concentrations in the Gunt catchment. Sample set was too small for statistically robust evaluation for 09/2011, 01/2013, 03/2013.

From August onwards the concentrations gradually increase again, which is due to arid conditions combined with appropriate enrichment. If one assumes that the upper soil layers of the permafrost areas, in particular the discontinuous areas are now also available for infiltration processes, the increase in concentration can also be explained by corresponding groundwater inflows. Since, apart from the extreme west, the precipitation in the study area is relatively low and falls due to decreasing temperatures primarily as snow. Therefore, the increase in ion concentrations continues until next spring. Due to the high intensity and continuous increase of this effect and considering the fact that homogeneous permafrost areas are present again after a certain time, a further theory is applied: Bagard et al. (2011) and Beylich and Laute (2012) describe a circulation of higher mineralized deep groundwater in areas with high permafrost or glacier occurrence in winter, which infiltrates into the receiving waters in areas below the permafrost boundary and accordingly explains the higher concentrations in winter. However, the occurrence of deeper groundwater reservoirs is not yet investigated.

5.3   Conclusions to the evaluation of hydrochemical parameters in river water

Hydrochemical parameters showed that there is a geogenic basic composition of water in the entire catchment area, which is hardly influenced regionally, but rather seasonally by various factors. The temporal variations can be explained by time-dependent variations in

runoff relevant parameters. The Gunt catchment is dominated in summer by snow and glacier melt, which is characterized by low major ion concentrations. In contrast, in winter high mineralized water from the subsurface feeds the rivers.

The classification using a Piper diagram showed that the less mineralized waters all correspond to the same watertype, the calcium carbonate type. In addition to the dominant watertype, evaporitically and silicatically enriched waters occur in form of hot springs.

6   Water-rock interactions in the Gunt catchment area[3]

The hydrochemical system of a catchment is usually described by analyzing the distribution of major ions all over the catchment area as it was presented in chapter 7. But also, minor elements or trace minerals can be used to describe processes having an influence on the hydrogeochemical design of a river catchment. Lithium (Li) is a rare metal that is naturally part of biological systems and geological cycles. It plays an important role in lots of different fields: medicine, pharmacology, energy, nuclear science, ecology, but lithium is also used as tracer in geo- and cosmochemical studies. The radius of Li^+ is small (0.78A) and similar to that of Mg^{2+} (0.72A) (Huh et al. 1998). This leads to a different behavior than that of other large alkali ions (K, Rb, and Cs) with larger ionic radius (Tang et al. 2007) so that lithium can substitute Mg in secondary clays formed by weathering (Froelich and Misra 2014). However, in geoscientific studies the focus is more on lithium isotopes than on the element lithium itself. Lithium has two stable isotopes: Li^6 and Li^7 with natural abundances of 7.5 % and 92.5 % respectively (Millot and Négrel 2007; Tang et al. 2007). This large relative mass difference causes large isotopic fractionations during (hydro)geochemical processes, especially in rock-water-systems (Tomascak 2004; Millot and Négrel 2007; Tang et al. 2007). Li isotopic ratios span different ranges in geological reservoirs and aquatic systems (Figure 44). Due to that, lithium isotopes have recently been introduced as innovative tool for geo- and hydrosciences. They are often used in environmental sciences to describe continental weathering processes (Huh et al. 1998, 2001; Millot et al. 2010b; Wanner et al. 2014; Pogge von Strandmann et al. 2017), for detecting geothermal and thermo-mineral water resources (Fouillac and Michard 1981; Chan et al. 1993; Millot and Négrel 2007), and in geological studies focusing on crust-mantle cycling (Seitz and Woodland 2000; Woodland et al. 2004; Elliott et al. 2004; Elliott et al. 2006; Tomascak et al. 2016). Lithium isotopes have been confirmed as a good tracer of water-rock-interactions (Négrel et al. 2010; Lemarchand et al. 2010; Henchiri et al. 2014). However, studies using lithium isotopes to describe water flow paths or to link the isotopic signature to water transit times, are rare (Pogge von Strandmann et al. 2014; Liu et al. 2015b; Wanner et al. 2017).

---

[3] Parts of this work were published as Meier et al. 2017.
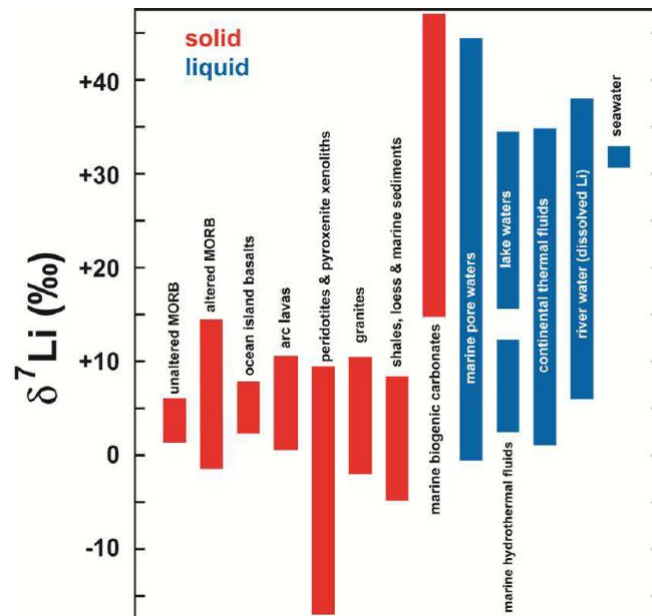
Figure 44: Lithium isotopic signatures of different reservoirs (Millot 2013).

In contrast to other geochemical and isotopic signatures (e.g. $^{87}Sr/^{86}Sr$), the lithium isotopic composition (δ^7Li) of surface and groundwater in river basins is not only controlled by mixing of lithology and input signatures like e.g. from precipitation (Huh et al. 2001; Penniston-Dorland et al. 2017). The lithium concentrations and δ^7Li values of water samples are a consequence of dissolution of lithium during weathering and the incorporation of lithium into secondary minerals (Huh et al. 1998; Tomascak 2004; Tang et al. 2007). During weathering, the heavier isotope ^7Li is preferred to go into solution whilst the lighter isotope ^6Li remains in the solid phase (Huh et al. 1998; Rudnick et al. 2004; Tang et al. 2007). Taylor and Urey (1938) already investigated the greater affinity of ^6Li to the stationary phase. Huh et al. explained this process as follows: "Bonds containing the lighter isotope have higher vibrational energy and during a chemical reaction (e.g. weathering), molecules bearing the lighter isotopes will react more readily, enriching the reaction product in the lighter isotope." (Huh et al. (2001, p. 196)). The dissolution of basalt rocks takes place without any fractionation (Huh et al. 2001; Kısakűrek et al. 2005; Pogge von Strandmann et al. 2006; Pogge von Strandmann et al. 2014), while dissolution of granitic rocks can cause fractionation (Pistiner and Henderson 2003; Millot et al. 2010b). The occurrence and extent of fractionation due to the precipitation of secondary minerals has been confirmed in several laboratory experiments (Pistiner and Henderson 2003; Wunder et al. 2006; Millot et al. 2010a). At the catchment level, however, the hydrological conditions and flow processes that control the enriched lithium isotope signatures observed in many catchment areas are still insufficiently known. The highest Li isotopic fractionation between river water and rock was found in in topographically high, recently glaciated and relatively less weathered regions, e.g. Himalaya (Bohlin and Bickle 2019), Andes (Teng et al. 2017) or Rocky and Mackenzie Mountains (Millot et al. 2010b).

This chapter focusses on lithium isotope systematics on a large scale by studying the processes of lithium isotope fractionation and linking these processes with flow paths and transit times. Figure 45 gives an overview over the locations of the water samples that were

used for lithium isotope analysis. All lithium and strontium data of water samples is reported in (Table 5).
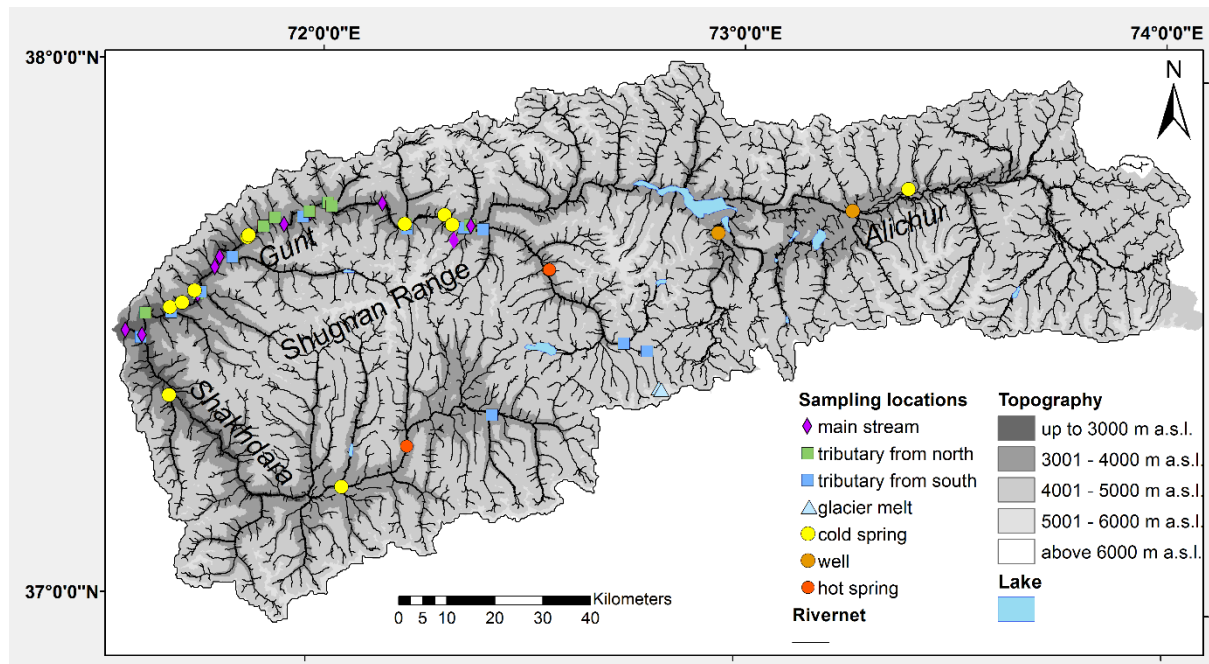
Figure 45: Locations of sampling stations for lithium isotope analysis.

6.1   Results of lithium isotopes

A wide range of δ^7Li values in water (from +4.3 ‰ in thermal water to + 28.2 ‰ in glacial and +36.4 ‰ in surface runoff) was found (Figure 47). The δ^7Li values are in the range of the global average for river waters of 23 ‰ (Huh et al. 1998; Misra and Froelich 2012). In general, the δ^7Li values are similar to values reported from alpine rivers, e.g. in the Himalayan (from +10.2 ‰ to +25.0 ‰) (Kısakűrek et al. 2005) and the Mackenzie Basin in Canada (from +9.3 ‰ to 29.0 ‰) (Millot et al. 2010b) and a granitic catchment in the Vosges Mountains in France (from +5.3 ‰ to +19.6 ‰) (Lemarchand et al. 2010).

The lithium concentrations are in the range of 0.08 µmol/L to 32.42 µmol/L (n = 69). The Gunt river samples are in the range of 0.31 µmol/L to 4.30 µmol/L (n = 11), the northern tributaries 0.31 µmol/Ll to 4.28 µmol/L (n = 15), the southern tributaries 0.29 µmol/L to 6.15 µmol/L (n = 14), the cold springs 0.18 µmol/L to 9.34 µmol/L (n = 13), wells 1.64 µmol/L to 2.74 µmol/L (n = 2), hot springs 3.46 µmol/L to 32.42 µmol/L (n = 7) and lake water 2.63 µmol/L (n = 1).

Lithium isotopic compositions of the rivers flowing from the northern edge into the main stream range from +7.6 ‰ to +36.4 ‰ (n = 15), the rivers of the southern sub-basins vary between +5.6 ‰ and +22.2 ‰ (n = 15), the Gunt River has a range from +9.4 ‰ to +14.0 ‰ (n = 11). The lowest δ^7Li values are represented by thermal water samples (+4.3 ‰ to +8.4 ‰, n = 7). The wide range of δ^7Li values (+6.2 ‰ to +27.0 ‰, n = 13) of cold springs can be divided into two groups, the first group is defined by samples with high δ^7Li values (+19.8 ‰ to +27.0 ‰) and very low Li concentrations, the second group shows medium to low δ^7Li values (+6.2 ‰ to +10.9 ‰) and higher Li mineralization.

Table 5: Hydrochemical and isotope data for water samples in the Gunt River catchment.

Water type	Sample ID	Date (MM/YYYY)	Latitude (°dec N)	Longitude (°dec E)	Altitude (m a.s.l.)	δ⁷Li (‰)	1σ	⁸⁷Sr/⁸⁶Sr	2σ	Li (μmol/L)	Na(μmol/L)	Sr (μmol/L)	fLi	transit time (years)
Cold Spring	08/13-FT-043	08/2013	37.53677	71.65669	2447	22.8	0.1	0.71253	0.000014	0.6	177.5	0.8	0.5	0.3
Cold Spring	08/13-FT-044	08/2013	37.54603	71.68494	2430	19.8	0.7	0.71277	0.000017	0.2	149.2	1.0	0.2	1.0
Cold Spring	08/13-FT-045	08/2013	37.67589	71.83632	2580	8.6	0.9	0.71573	0.000019	7.1	487.2	1.6	2.0	16.5
Cold Spring	08/13-FT-231	08/2013	37.70640	72.20388	3024	26.9	0.6	0.71456	0.000014	0.7	111.4	1.0	0.9	
Cold Spring	08/13-FT-244	08/2013	37.72536	72.29706	3241	20.04	1.82	0.71475	0.000018	0.27	42.24	1.0	0.9	0.1
Cold Spring	08/13-FT-246	08/2013	37.70785	72.31588	3095	6.2	0.1	0.71286	0.000018	2.3	182.3	1.1	1.7	1.3
Cold Spring	09/13-FT-021	09/2013	37.37196	71.66192	2597	9.2	0.4	0.71189	0.000019	3.9	179.6	2.7	3.0	0.9
Cold Spring	09/13-FT-022	09/2013	37.21067	72.07327	2980	10.88	2.58	0.71237	0.000019	7.92	761.20	4.9	1.4	
Cold Spring	09/13-FT-051	09/2013	37.56946	71.71330	2577	21.9	0.3	0.71262	0.000018	0.3	72.6	0.6	0.5	
Cold Spring	08/13-FT-382	08/2013	37.79355	73.39228	3900	6.17	1.10	0.71099	0.000017	4.61	556.76	2.4	1.1	
Cold Spring	10/11-110	10/2011	37.67256	71.83347	2564	8.31	0.36	0.71560	0.000018	7.35	340.71	1.3	3.0	7.5
Cold Spring	03/13-110	03/2013	37.67256	71.83347	2564	8.11	0.01			9.34				7.5
Cold Spring	09-14-FT-382	09/2014	37.79355	73.39228	3900	9.54	0.21			5.26	565.46		1.28	
Main stream	10/11-010	10/2011	37.48900	71.52244	2086	12.03	1.41	0.71430	0.00001	3.76	242.06	1.1	2.1	
Main stream	10/11-030	10/2011	37.48312	71.59300	2102	10.77	0.05	0.71347	0.000013	2.87	219.75	1.0	1.8	
Main stream	10/11-060	10/2011	37.56253	71.72122	2347	9.39	0.15	0.71341	0.000009	3.08	212.48	1.0	2.0	
Main stream	10/11-080	10/2011	37.61490	71.75914	2467			0.71337	0.000016			1.0		
Main stream	10/11-090	10/2011	37.63383	71.76953	2479	11.07	1.13	0.71337	0.000017	2.59	239.71	1.0	1.5	
Main stream	10/11-140	10/2011	37.69903	71.91923	2648	9.64	0.08	0.71297	0.000018	2.45	252.72	1.1	1.3	
Main stream	10/11-170	10/2011	37.72297	71.98008	2729			0.71278	0.000008		231.06	1.0	0.0	
Main stream	10/11-210	10/2011	37.74389	72.14961	2934	10.91	0.71	0.71263	0.00001	3.05	268.51	1.1	1.6	
Main stream	10/11-240	10/2011	37.71667	72.29867	3083			0.71200	0.000009		276.95	1.1	0.0	
Main stream	10/11-270	10/2011	37.70639	72.35984	3131	13.53	0.11	0.71198	0.000007	1.24	294.00	1.2	0.6	
Main stream	03/13-010	03/2013	37.48900	71.52244	2086	10.14	0.12			4.28	434.97		1.36	
Main stream	06/12-210	06/2012	37.74389	72.14961	2934	10.47	0.08			1.65	189.65		1.20	
Main stream	06/12-241	06/2012	37.71667	72.29867	3083	14.00	0.17			0.31	168.33		0.26	
Main stream	06/12-270	06/2012	37.70639	72.35984	3131	12.94	0.11			1.29	201.39		0.88	
Glacier melt	09/13-FT-305	09/2013	37.40882	72.81888	4716	17.44	0.66	0.71101	0.000017	0.14	4.35	0.3	4.6	
Glacier melt	09/13-FT-306	09/2013	37.41198	72.81287	4594	28.18	1.63	0.71130	0.000011	0.78	25.84	0.7	4.2	
Well	08/13-FT-351	08/2013	37.70458	72.94510	3760	14.25	1.55	0.71075	0.000019	2.74	900.39	2.9	0.4	
Well	08/13-FT-381	08/2013	37.75088	73.26127	3892	16.67	0.28	0.71142	0.000016	1.64	548.06	2.6	0.4	0.2
Hot Spring	08/13-FT-290	08/2013	37.62829	72.54729	3512	4.50	0.92	0.71332	0.000016	23.05	4019.14	1.0	0.8	19.0
Hot Spring	08/13-FT-300	08/2013	37.62769	72.54786	3506	4.34	0.40	0.71330	0.000013	23.05	3958.24	1.0	0.8	50.0
Hot Spring	09/13-FT-023	09/2013	37.29031	72.22307	3184	6.41	0.88	0.71472	0.000018	3.46	1879.08	4.7	0.3	
Hot Spring	10/11-290	10/2011	37.62816	72.54681	3512	5.86	0.13	0.71339	0.000088	25.52	3958.98	0.9	0.9	
Hot Spring	10/11-300	10/2011	37.62812	72.54597	3506	8.39	0.22	0.71287	0.000009	32.42	4046.76	0.7	1.1	
Hot Spring	03/13-290	03/2013	37.62816	72.54681	3512	6.26	0.01			31.55				
Hot Spring	03/13-300	03/2013	37.62812	72.54597	3506	6.60	0.15			23.01				
Northern tributary	08/13-FT-031	08/2013	37.52499	71.59907	2281	21.67	0.72	0.71142	0.000018	0.55	79.16	0.4	1.0	2.8
Northern tributary	09/13-FT-301	09/2013	37.49365	72.72764	3938	36.35	0.87	0.71165	0.000019	0.13	40.50	0.5	0.4	
Northern tributary	10/11-050	10/2011	37.56416	71.72075	2368	18.11	0.08	0.71282	0.000012	0.27	41.10	0.3	0.9	
Northern tributary	10/11-120	10/2011	37.69503	71.87072	2632	22.16	0.88	0.71850	0.000022	0.23	31.40	0.4	1.0	
Northern tributary	10/11-130	10/2011	37.71169	71.89626	2654	18.90	0.51	0.71678	0.000015	0.14	35.80	0.6	0.5	
Northern tributary	10/11-180	10/2011	37.72443	71.97808	2734	19.96	0.17	0.71727	0.000015	0.18	40.71	0.6	0.6	
Northern tributary	10/11-190	10/2011	37.74238	72.02067	2787	15.42	0.30	0.71542	0.000017	0.13	42.67	0.6	0.4	
Northern tributary	10/11-200	10/2011	37.73610	72.02978	2793	36.21	0.59	0.71184	0.00001	0.10	47.32	0.3	0.3	
Northern tributary	10/11-230	10/2011	37.70762	72.20615	3020	20.10	0.61	0.71342	0.000018	0.30	64.55	0.3	0.6	
Northern tributary	10/11-260	10/2011	37.70803	72.35799	3169	18.93	0.02	0.71231	0.000008	0.27	64.20	0.5	0.6	
Northern tributary	06/12-120	06/2012	37.69503	71.87072	2632	7.63	0.11			0.08	39.58		0.28	
Northern tributary	06/12-190	06/2012	37.74238	72.02067	2787	16.78	0.08			0.12	42.19		0.40	
Northern tributary	06/12-200	06/2012	37.73610	72.02978	2793	9.04	0.50			0.15	46.98		0.43	
Northern tributary	06/12-230	06/2012	37.70762	72.20615	3020	20.22	0.05			0.29	58.72		0.68	
Northern tributary	06/12-260	06/2012	37.70803	72.35799	3169	15.44	0.07			0.22	60.03		0.51	
Southern tributary	09/13-FT-028	09/2013	37.35390	72.42151	3418	22.22	0.82	0.71313	0.000014	0.75	110.92	0.9	0.9	
Southern tributary	09/13-FT-302	09/2013	37.48068	72.78277	4274	15.15	0.48	0.71122	0.000014	0.66	28.23	0.6	3.2	
Southern tributary	10/11-020	10/2011	37.47910	71.59096	2119	9.64	1.38	0.71605	0.000011	3.14	275.73	1.4	1.6	
Southern tributary	10/11-040	10/2011	37.52754	71.65921	2291	10.13	0.45	0.71730	0.000017	1.47	108.05	0.5	1.9	
Southern tributary	10/11-070	10/2011	37.56765	71.72877	2359	11.47	0.06	0.71336	0.000017	1.50	91.04	0.6	2.3	
Southern tributary	10/11-100	10/2011	37.63468	71.79994	2570	11.54	0.43	0.71327	0.000017	0.88	70.81	0.3	1.7	
Southern tributary	10/11-220	10/2011	37.69837	72.20995	3013	18.47	0.38	0.71402	0.000013	0.29	77.29	0.4	0.5	
Southern tributary	10/11-250	10/2011	37.70237	72.34425	3142	12.57	0.40	0.71136	0.00001	0.59	53.07	0.4	1.5	
Southern tributary	10/11-280	10/2011	37.70084	72.38910	3155	17.71	0.53	0.71201	0.000017	1.19	287.21	0.9	0.6	
Southern tributary	03/13-020	03/2013	37.47910	71.59096	2119	8.18	0.16			6.15	495.87		1.71	
Southern tributary	06/12-250	06/2012	37.70237	72.34425	3142	14.64	0.10			1.02	37.41		3.77	
Southern tributary	06/12-280	06/2012	37.70084	72.38910	3155	15.19	0.02			0.71	135.28		0.72	
Southern tributary	09/14-FT-302	09/2014	37.48068	72.78277	4274	5.63	0.11			0.85	52.20		2.23	
Southern tributary	09-14-FT-024	09/2014	37.30929	72.22173	3197	16.62	0.09			1.29	204.44		0.87	
Lake	09/14-FT-310	09/2014	37.791286	72.743397	3727	12.17	0.01			2.63	543.71		0.67	

The waters display systematically heavier lithium isotopic compositions relative to the bedrock and the suspended particulate matter (SPM). All lithium data of bedrock and SPM samples is reported in (Table 6).

Table 6: Lithium isotope data of bedrock and suspended particulate matter in the Gunt catchment.

Sample type	Sample ID	Date (MM/YYYY)	Latitude (°dec N)	Longitude (°dec E)	Altitude (m a.s.l.)	δ^7Li (‰)	1σ	Li (ppm)	Na(ppm)	Description
bedrock	0909 A2		37.82425	73.43569	4018	-6.5	0.3	25.6		bt-granite gneiss
	4726 A1		37.63427	73.0796	3876	-7.2	0.4	23.6	11350.4	Kfs-orthogneiss
	4726 C1		37.48713	72.74987	4206	-10.9	0.4	33.6	11610.1	bt-granite
	4726 H1		37.71780	72.234	3037	-1.7	0.6	29.2		pegmatitic gneiss
	4727 A1		37.71080	71.96935	2728	1.5	0.3	4.5	10089.3	pegmatite
	4727 B1		37.70180	71.88482	2625	-2.1	0.6	31.5	8457.2	two-mica orthogneiss
	6827 A2		37.39782	71.64978	2383	-2.5	0.2	134.9		granite
	6901 A2		37.36733	72.36718	3376	-1.4	0.7	11.5	10571.5	post-migmatitic leucogranites
	6901 B1		37.34290	72.56252	3702	-5.3	0.1	36.8	14540.4	rt-sil-gneiss intruded by granitoids and pegmatites
	6903 C1		37.73187	72.40135	2241	-7.1	0.01	33.5	10093.0	kfs-granite
	6904 E1		37.71355	71.78952	4194	-0.6	0.2	13.4	16098.3	granite
	6904 F1		37.70583	71.7888	3827	-14.1	0.3	10.2	12418.7	foliated granite
	6904 H1		37.67800	71.8028		-5.5	1.0	4.0		well-foliated quartzite
	6904 P2		37.63996	71.74479	3544	-11.8	0.4	18.6	10682.8	granite-gneiss
	9917 A1		37.78044	72.87642	3781	-3.9	0.1	42.4	9199.1	hbl-granodiorite
sediment	SPM 03 G	03/2013	37.48900	71.52244	2086	-2.9	0.2	37.5		Gunt
	SPM 03 P	03/2014	37.70762	72.20615	3020	0.3	0.0	17.8		Patkhur
	SPM 03 S	03/2015	37.47910	71.59096	2119	-3.3	0.2	41.1		Shakhdara
	SPM 04 G	04/2013	37.48900	71.52244	2086	-0.3	0.0	25.9		Gunt
	SPM 04 P	04/2014	37.70762	72.20615	3020	-0.6	0.1	24.2		Patkhur
	SPM 04 S	04/2015	37.47910	71.59096	2119	-3.0	0.0	36.0		Shakhdara
	SPM 05 G	05/2013	37.48900	71.52244	2086	-1.5	0.2	40.5		Gunt
	SPM 05 P	05/2014	37.70762	72.20615	3020	-1.6	0.0	23.9		Patkhur
	SPM 05 S	05/2015	37.47910	71.59096	2119	-9.6	0.1	36.7		Shakhdara

The range of lithium isotope ratios from water analyses is higher and the water samples are also more enriched in ^{7}Li than it is found in analysed SPM samples (from -9.6 ‰ to +0.3 ‰). The δ^7Li from SPM is not significantly different from the δ^7Li of bedrock (from -14.1 ‰ to +1.5 ‰).

In contrast to the water samples, the majority of the analytical values of δ^7Li from the geological environment (n = 15) showed negative values ($_{mean}\delta^7$Li$_{bedrock}$ = -5.5 ‰, n=14; $_{mean}\delta^7$Li$_{SPM}$ = -2.5 ‰, n=8). Only one bedrock sample and one SPM sample show positive δ^7Li values ($_{max}\delta^7$Li$_{bedrock}$ = 1.5 ‰, $_{max}\delta^7$Li$_{SPM}$ = 0.3 ‰). The δ^7Li values of bedrock and SPM are well in line with data published for granitic and granitoid environments (Huh et al. 1998, 2001; Teng et al. 2009; Froelich and Misra 2014).

Lithium concentrations in SPM range between 17.8 ppm and 41.1 ppm, which is also in line with data published for suspended loads, e.g. Huh et al. (2001).

Bedrock samples display Li contents ranging between 4 ppm and 134 ppm. These values are also typical for granitic and granitoid environments (Shearer et al. 1987).

6.2 Discussion of lithium isotopes

6.2.1.1.1 Distribution of lithium isotopes in the Gunt catchment

The Li isotopic composition of seawater is very homogenous and quite heavy with a global average of δ^7Li = +31.6±1.6‰ (Lui-Heung and Edmond 1988). In contrast, river waters

weathering of the continental crust show a large range of δ^7Li (from +6 ‰ to +42 ‰) in water due to the fractionation between dissolution and secondary minerals during weathering processes (Pogge von Strandmann et al. 2014). As shown in a lab experiment by Millot et al. (2010a), the dissolution of lithium from rock material in water leads to a fractionation. The ^7Li is preferably leached in comparison to ^6Li. During weathering preferentially the heavy ^7Li migrates into waters and the lighter ^6Li is left in the solid weathered residual (Tang et al. 2007; Misra and Froelich 2012). In tectonically active regions weathering may become larger because weathering is rapid in these regions (Huh et al. 2001; Tang et al. 2007; Froelich and Misra 2014). The Li isotopic composition of continental granites and their metamorphic equivalents range between -6 ‰ and +14 ‰ (Tomascak et al. 2016).

In the presented sample set, the SPM samples show δ^7Li values similar to the bedrock (Figure 46) indicating the SPM is a result of physical weathering of the bedrock.
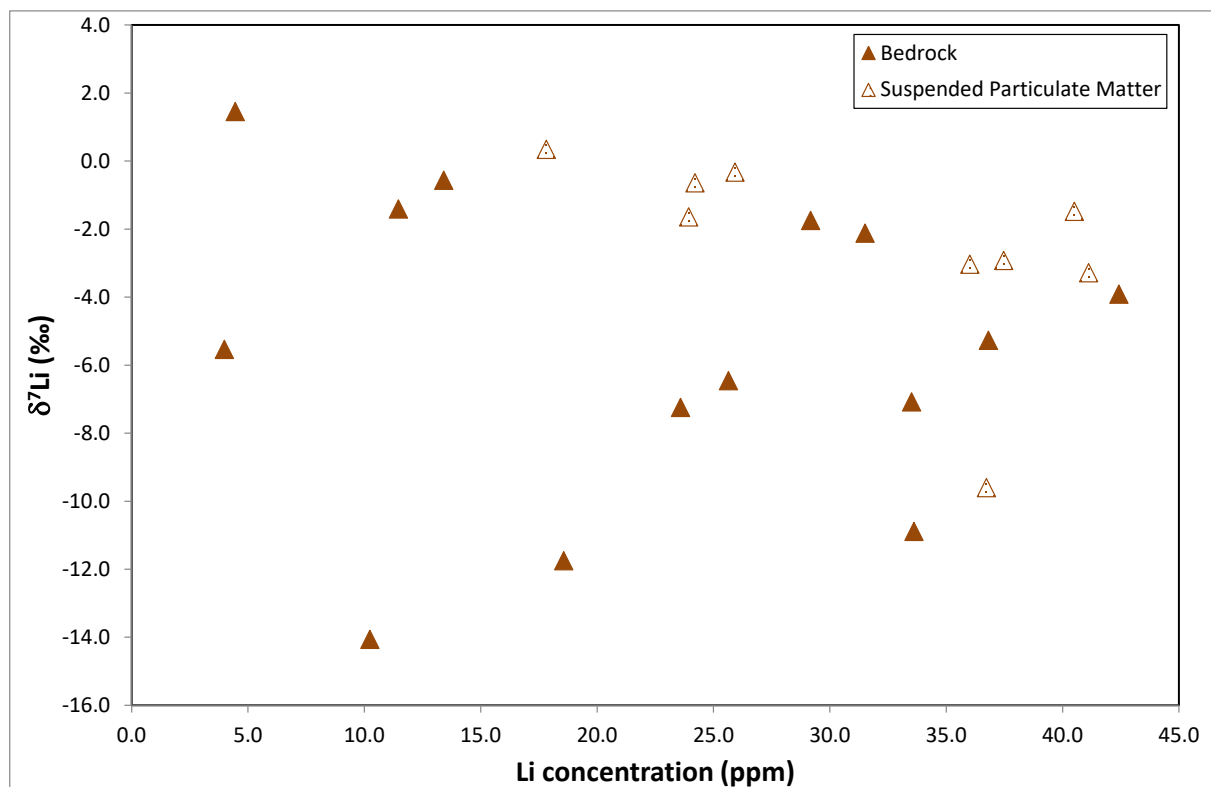
Figure 46: δ^7Li in rock samples and Suspended Particulate Matter.

The SPM samples were taken at three different locations: from the drain of the most glaciated catchment Patkhur, the biggest Gunt-tributary Shakhdara and from the Gunt river itself. In Froelich and Misra (2014), lithium isotopic composition of SPM depends on the source of the SPM and the duration of dilution. That means, the longer the SPM is in contact with water, the lighter the isotopic composition of SPM is and the heavier the isotopic signature of the liquid. The three SPM sampling points support this theory. The shortest river Patkhur shows the heaviest lithium isotopic composition in SPM (mean δ^7Li = -0.65 ‰). The Gunt river itself, which is the longest river in the catchment, shows medium isotopic ratios in SPM (mean δ^7Li = -1.58 ‰). Its longest tributary Shakhdara instead shows the lightest isotope ratios (mean δ^7Li = -5.31 ‰). This phenomenon is a result of the hydromorphological set-

ting in the catchment. The Gunt river has lots of small tributaries that contribute to the run-off and which might show lithium isotopic signatures as heavy as the Patkhur. By mixing the heavy δ^7Lisignature in SPM of the small tributaries with the light δ^7Li signature in SPM of the Shakhdara, the result is a medium δ^7Li signature in SPM. To strengthen these hypotheses, more lithium-analyses of SPM-samples are necessary.

Generally there is a negative relationship between dissolved Li concentrations and δ^7Li in the water samples in Figure 47. The river water samples (main stream and some tributaries) show a pattern in their δ^7Li values with higher values in tributaries from the North and medium enriched δ^7Li values in the Southern tributaries. The lowest δ^7Li values can be detected in the hot spring samples.

Subsurface water samples from cold springs can be divided into two groups, one group (group I) with high δ^7Li values and low Li concentrations and the other group (group II) with low δ^7Li values and high Li concentrations, respectively. Group (I) sampling points are mainly located in the northern sub-basin area, while Group (II) samples were taken in the southern part of the Gunt catchment area or nearby the Gunt river (Figure 47).
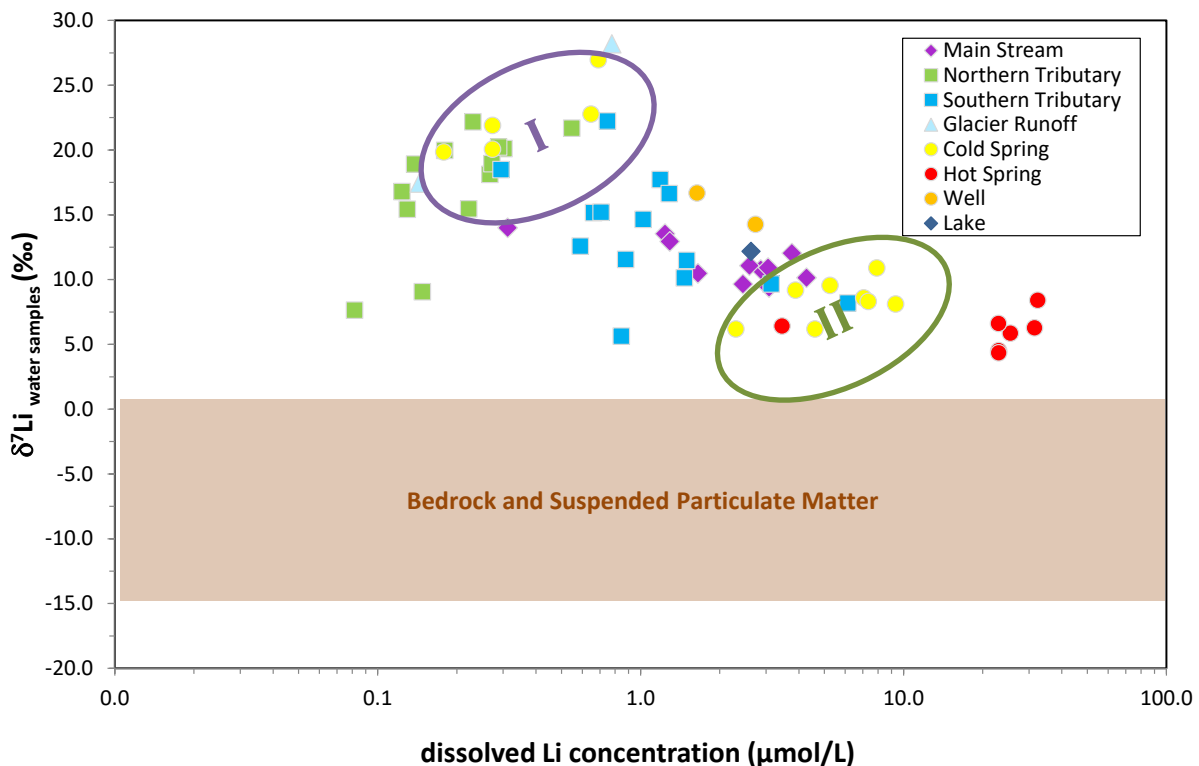
Figure 47: Evolvement of δ^7Li in water in respect to bedrock and suspended particulate matter.

It can be supposed that the differences in the δ^7Li values between the northern and southern tributaries are due to different mean catchment area sizes, flow length (Appendix Figure 2) and thus different transit times in the catchment as well as different weathering properties. The subcatchments at the northern border with higher δ^7Li values are related to smaller catchment areas (area$_{mean}$=26 km^2) and shorter flow paths (flow length$_{mean}$=17 km) with at the same time shorter flow times. Southern subcatchments show contradictory characteristics (area$_{mean}$=104 km^2; flow length$_{mean}$=55 km) (Appendix Figure 2). They, instead, show

lower δ⁷Li values than the northern tributaries and have higher Li concentrations. There-
fore, it is concluded, that the southern tributaries are characterized by longer transit times
than the northern tributaries. However, the Li concentration in the southern catchments is
lower than the concentration of the Gunt river itself and obviously lower than the Li concen-
tration of the hot springs. Further, the δ⁷Li values of the Gunt river and the hot springs are
lower than the δ⁷Li values of the tributaries. Consequently, it indicates that, as expected, the
transit times of the Gunt river is longer than the transit times of the tributaries and the
transit times of the hot springs are the longest. Measurements of ³H in the water samples
support this interpretation. Water samples of the hot springs show ³H values below 0.5 TU
while river water samples show higher ³H values indicating longer transit times or higher
mean residence times for the hot springs than for the river water.

The Li isotope pattern of the subcatchments includes additional information: the higher the
degree of glaciation in the catchment, the higher is the δ⁷Li value. Already major ion evalua-
tion showed the positive relationship between the percentage of glaciation of a catchment
and the level of mineralization. The subcatchments at the northern border with higher δ⁷Li
values show a mean area of glaciation of 10.6 km², the southern subcatchments 5.4km², re-
spectively (Appendix Figure 2). This can be explained by (i) the finger print of the glacial
meltwater, which shows high δ⁷Li values and low Li concentrations and by (ii) the smaller
rate of water rock interaction (WRI) related to shorter flow path of the river.

The same interpretation of the lithium isotope values of the tributaries is applicable to the
cold springs as well. Due to the geomorphological situation in the Gunt catchment it can be
assumed that the hydrogeological catchments have a similar course to the hydrological
catchments. Therefore, the catchment areas of Group (I) should be significantly smaller than
those of Group (II). Smaller catchment areas with the same morphology and porosity should
have shorter transit times, so that lower water-rock interaction can be assumed for smaller
catchment areas. This becomes apparent in comparing the transit times of the springs: cold
springs at the northern flank of the catchment are characterized by small RTs and springs in
the southern part show higher RTs.

6.2.1.1.2   Reactive transport modelling using lithium isotopes

For assessing the controls on evolution of Li isotope ratios along a flow path a model can be
used. That model should incorporate simple formulations of the main processes. In this
study we modified and then applied a reactive transport model after Pogge von Strandmann
et al. (2014) (Equation 17) by integration estimated RT (τ) (Equation 18 and Equation 19).
In the model of Pogge von Strandmann et al. (2014) the following processes have a major in-
fluence on the lithium isotopic composition in water:

- Advective transport
- The dissolution rate of rocks, where ions are dissolved from the rock and released
  into the water. The weathering rate is mineral-specific and can be described in a
  first-order rate constant.
- The precipitation rate of lithium, where lithium is removed from the water according
  to a first order rate constant. This value depends on the phase in which the element
  will be incorporated.

Adsorption and desorption. Each is also controlled by first order rate constants.

$$\left(\frac{^7Li}{^6Li}\right) = \frac{[^6Li]_w^{SS}}{[^6Li]_w}\left[\frac{^{7}/_{6}\alpha_{weath}\left(^{7Li}/_{6Li}\right)_r}{^{7}/_{6}\alpha_{precip}}\right]\left(1 - e^{\frac{-^6Q*^{7}/_{6}\alpha_{precip}}{v}x}\right)$$

$$+ \frac{^i[^6Li]_w^0}{[^6Li]_w}\left(\frac{^7Li}{^6Li}\right)_w^0 e^{\frac{-^6Q*^{S7}/_{6}\alpha_{precip}}{v}x}$$

Equation 17: Evolution of ^7Li/^6Li along the flow path according to Pogge von Strandmann et al. (2014). α_{weath}= fractionation during weathering, α_{precip}=fractionation during precipitation of secondary minerals, r=index for rock, Q=precipitation rate, x=distance, v=flow velocity, SS=index for steaty state, w=index for water, 0=index for initial.

Where x can be substituted by the RT (τ) in years:

$$\left(\frac{^7Li}{^6Li}\right) = \frac{[^6Li]_w^{SS}}{[^6Li]_w}\left[\frac{^{7}/_{6}\alpha_{weath}\left(^{7Li}/_{6Li}\right)_r}{^{7}/_{6}\alpha_{precip}}\right]\left(1 - e^{\frac{-^6Q*^{7}/_{6}\alpha_{precip}}{v}\tau}\right)$$

$$+ \frac{^i[^6Li]_w^0}{[^6Li]_w}\left(\frac{^7Li}{^6Li}\right)_w^0 e^{\frac{-^6Q*^{S7}/_{6}\alpha_{precip}}{v}\tau}$$

Equation 18: Adaptation of Equation 17 by consideration of RT (Equation 19).

Where (τ) is given by:

$$\tau = \frac{x}{v}$$

Equation 19: Simple estimation of RT.

The derivation of these values and the implementation into the final equation are published in Pogge von Strandmann et al. (2014), the values used for modeling the lithium isotopic signature of water samples in the Gunt catchment are presented in Appendix Table 9.

The model calculates the development of the lithium isotope signatures and the lithium concentrations along the flow path of groundwater or river water, respectively. Therefore, the δ^7Li and the Li concentration are dependent on the distance a water package has covered from its entrance to the water body up to the sampling point. The length of the flow path or distance can be substituted by the transit time of a water package if the flow velocity is known.

The advective velocity is supposed to be fast ($1*10^{-4}$ m/s) depending on the coarse material (sand to gravel) the water has to pass through. This is in line with the findings presented in Pohl et al. (2015).

Assuming steady state conditions in the (ground)water the lithium isotopic composition in the water will only be affected by the bedrock the water is flowing through. If the physico-chemical conditions in the water change, the concentration of lithium changes exponentially (Pogge von Strandmann et al. 2014).

The model, therefore, requests two input parameters that have to be generated from field samples: the lithium isotope ratio and the lithium concentration of each of the water source and the bedrock the water is flowing through.

As input values representing the water source the measured-values of glacier ice and precipitation are used, because it is assumed that nearby precipitation one main contributor to the hydrological system is glacier melt water (Appendix Table 9).

Table 7: Isotope ratios for bedrock samples in the Gunt River basin, and their Li concentrations used in the reactive transport model. Class 1 represents the minimum δ^7Li value of bedrock, class 2 the maximum, class 3 the mean value and class 4 represents the special location Djelondi (bedrock sample ID 4726-C1), where the hot springs emerge.

Class	ID	δ^7Li (‰)	C_{Li} (ppm)
Class 1	Min	-14.1	10.2
Class 2	Max	1.5	4.5
Class 3	Mean	-5.5	22.7
Class 4	4726-C1	-10.9	33.6

Due to the fact that the large Gunt River catchment is characterized by about four to five lithological types (Brehme 2014; Pohl et al. 2015) a variety of 15 rock samples throughout the catchment were selected for lithium (isotope) analysis (Table 6). Out of these 15 isotopic signatures four model inputs were chosen: the minimum value, the maximum value, the mean value and an isotopic signature representing the surrounding bedrock of the particular case of the hot springs in Djelondi (Table 7).

In Figure 48 the modelled curves for the four assumed lithological classes are plotted. The highest δ^7Li values for each lithological class can be found up to the time point of around 2 years. After an expected transit time of 2 years, the δ^7Li values decrease (class 2) or tend to reach stable status (classes 1, 3 and 4). It is obvious that at the time point of around 10 years in all classes a steady state is reached.

At nine sampling locations transit times of different water samples are determined (Table 5). The estimated transit time vs. δ^7Li -values of the mentioned samples (n = 9) is added. All the observed-values are in the range of the modelled curves. Therefore, it can be assumed that the input parameters of the model are in the correct range. As Figure 48 shows, the sample set can be distinguished into two groups (A) and (B). Group A is characterized by short transit times and high δ^7Li values of more than +15 ‰. The best model fit for group (A) can be found by using the highest δ^7Li value of bedrock (+1.5 ‰). Group (B) shows lower δ^7Li values (<+10 ‰) and represents the classes of the lithological δ^7Li$_{Class\_3}$ value of -5.5 ‰ and of the δ^7Li$_{Class\_4}$ value of -10 ‰. For group (A) transit times of ≤2 years and for group (B) transit times of ≥10 years up to at least 50 years can be postulated.
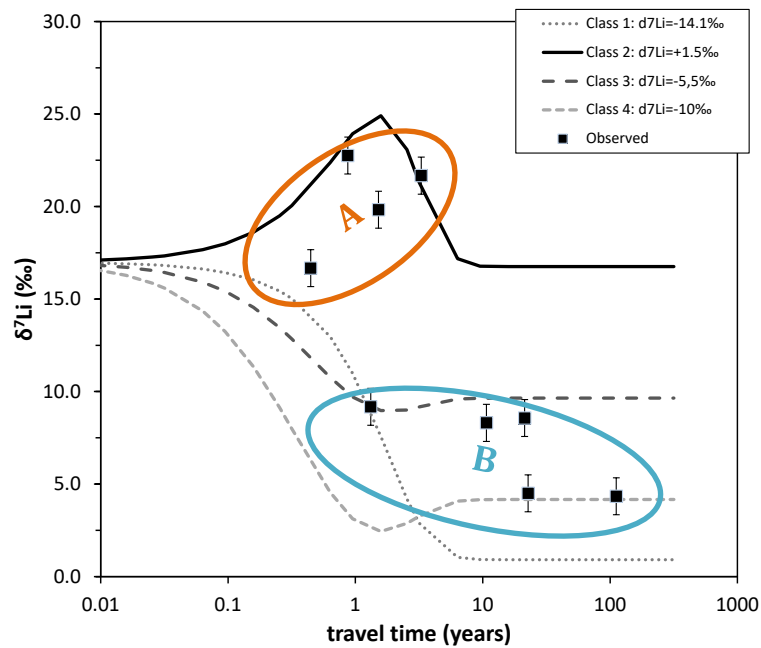
Figure 48: δ^7Li ratios as a function of flow distance overlain by model results for four modelled classes. The classes represent the range of lithium isotopic signatures of the bedrock. Class 1 = minimum, class 2 = maximum, class 3 = mean, class 4 = special value of location 4726-C1 (hot springs Djelondi).

The results of the reactive transport modelling show, that water samples with high Li concentration and low δ^7Li (≤+8 ‰) values must have reached a chemical and isotopic equilibrium state in accordance with local geochemical conditions due to comparably long transit times and persistent water-rock interactions in the subsurface. That means hot spring-samples and the Gunt river samples are at steady-state. If the presented lithium isotope values are set in relation to the transit time, it can be found that steady state conditions are reached at a time point of around ten years and is not influenced by the lithological class. The steady state of the Li concentration and Li isotopic ratio depends on W/Q ratios, the porosity (n) and the fractionation factor (α).

Enriched δ^7Li signatures are caused by flow paths with relatively short transit times far below ten years. The high δ^7Li values are a result of combination of high weathering-precipitation-rates (W/Q) of primary minerals (bedrock) with low weathering-precipitation-rates of secondary minerals sections. The isotopic process that takes places during weathering and precipitation of minerals can be described in an exponential relation, also called Rayleigh fractionation, resulting in an increase in δ^7Li values. Additionally, a huge variety in lithium isotopes in dissolved lithium is found indicating weathering as highly dynamic process. The high δ^7Li values and low Li concentrations of the northern catchments are well in the range of reported data by Kısakűrek et al. (2005), Millot et al. (2010a), Pogge von Strandmann et al. (2014), which linked their findings to strong silicate weathering.

By interpreting the lithium isotope data, final conclusions comprises the following facts: (I) the northern subcatchments are characterized by short transit times (RT) of ≤2 years; (II) the Gunt river and hot springs show RT ≥10 years and (III) most of the southern tributaries range between 2 years and 10 years RT. Due to the fact that the cold springs are behaving

like the tributaries and any contribution of an unknown groundwater source was not detectable, it can be constituted that (IV) no unknown groundwater source plays any important role in generation of runoff in the Gunt catchment.

A combination of lithium isotopes and strontium isotopes (Figure 49) in the water samples does not show any correlation. Where strontium is an indicator for carbonate weathering and rock dissolution processes without fractionation (Faure 1986), the water analyses of the tributaries, Gunt, springs and glacier range between 0.710 and 0.719 of $^{87}Sr/^{86}Sr$ without any systematically pattern related to their origin.

Consequently, most riverine Li derives from silicate lithologies of the Precambrian metamorphites and Mesozoic and palaeogenic granite intrusions and there is no carbonate weathering control on the Li isotopic composition (Huh et al. 1998; Kısakűrek et al. 2005; Millot et al. 2010b). So, the concentration of Li in the dissolved load of the rivers is controlled by silicate weathering.
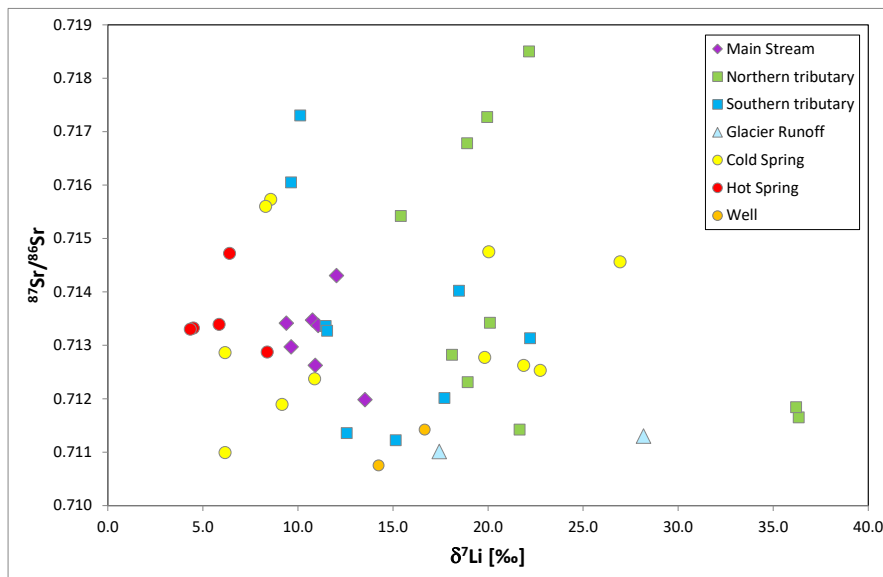
Figure 49: Sr-isotopic signature vs. Li-isotopic signature of water samples.
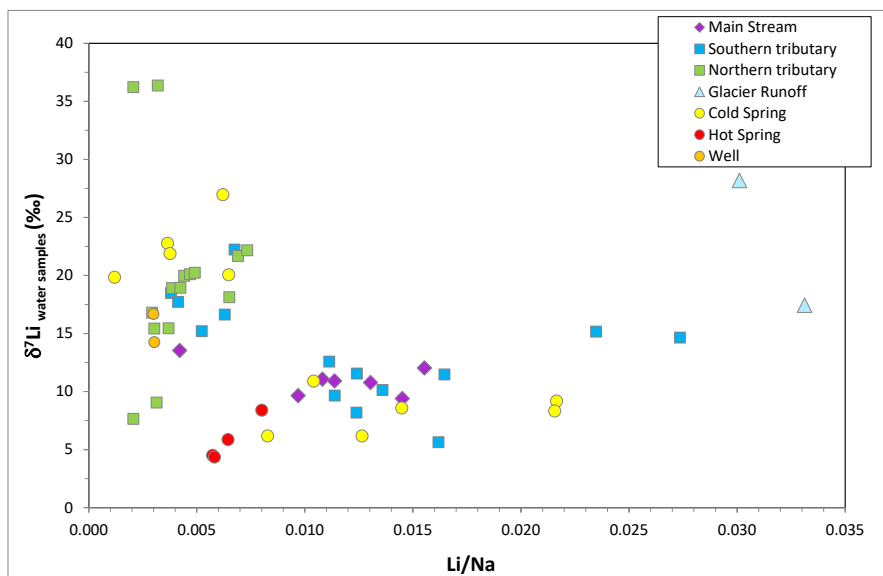
Figure 50: Li-isotopic composition in the water samples as a function of Li/Na ratio.

Liu et al. (2015b) discussed a negative correlation between δ^7Li und molar Li/Na-ratio as an indicator for high chemical weathering. Na and Li are alkali metals that are mobile during water rock interaction. Na stays mobile after dissolution while Li is likely to be incorporated into secondary minerals. Since there is no clear correlation of the whole dataset when combining molar Li/Na ratio with δ^7Li (Figure 50), it can be concluded that not the whole catchment is characterized by strong chemical weathering but rather by dissolution of primary minerals of the igneous rocks. Looking instead only on the southern tributaries, the Gunt river and the hot spring samples, these samples tend to show a negative relationship between δ^7Li and the Li/Na ratio. Therefore, for these samples it can be assumed that chemical weathering takes place. Additionally the Li/Na ratio can be used as an index of Li mobility (Millot et al. 2010b). The fraction of Li remaining in solution relative to Na can be defined after Millot et al. (2010b) as follows:

$$f_{Li} = \frac{(Li/Na)_{dissolved}}{(Li/Na)_{bedrock}}$$

Equation 20

By comparing the Li/Na ratio of the dissolved load to the Li/Na-ratio of the bedrock the result shows, if chemical weathering is congruent (f_{Li} = 1) or if dissolution, which is thought to be incongruent, ($f_{Li}\neq$1) plays the main role (Table 5). The reincorporation of Li into secondary phases leads to Li/Na-ratios<1, f_{Li}>1 instead shows a preferential leaching of Li compared to Na. The calculated mean f_{Li} in the Gunt catchment (Li/Na$_{dissolved\_mean\ water}$: Li/Na$_{bedrock\_mean\ bedrockvalue}$) is 1.3. This indicates that the reincorporation of Li into secondary minerals is not the most important process in the whole Gunt catchment, but also cannot be excluded. The Gunt catchment is dominated by physical weathering and mineral dissolution with preferential leaching of Li. By combining the isotopic composition of dissolved lithium with the f_{Li} (Figure 51), the data shows two clusters (a) and (b). In cluster (b) a remarkably correlation (r^2 = 0.61) is detectable. This correlation can be explained by two endmembers. Endmember 1 is characterized by high δ^7Li values and a high f_{Li}, which represents low or no incorporation of Li in secondary minerals. This is fully comprehensible, because this endmember consists of samples from juvenile glacier melt water. End-member 2 is characterized by low δ^7Li values and a low f_{Li}, represented by the hot springs' samples. The f_{Li} below 1 is an indication for proceeding weathering, where Li is incorporated into e.g. secondary minerals. However, e.g. Froelich and Misra (2014) showed that the lighter ^{6}Li is preferred to be incorporated. So finally, when Li is incorporated into secondary minerals, the clay shows lower δ^7Li signatures and the remaining water shows higher δ^7Li values. Therefore, integration of lithium into secondary minerals cannot explain the isotopic signature of end-member 2. Evidently the Li isotopic signature of endmember 2 is a result of dissolution of lithium from the bedrock material. During dissolution, the Li concentration in the solution is rising and the Li isotopic signature of the dissolved lithium is declining (Millot et al. 2010a).
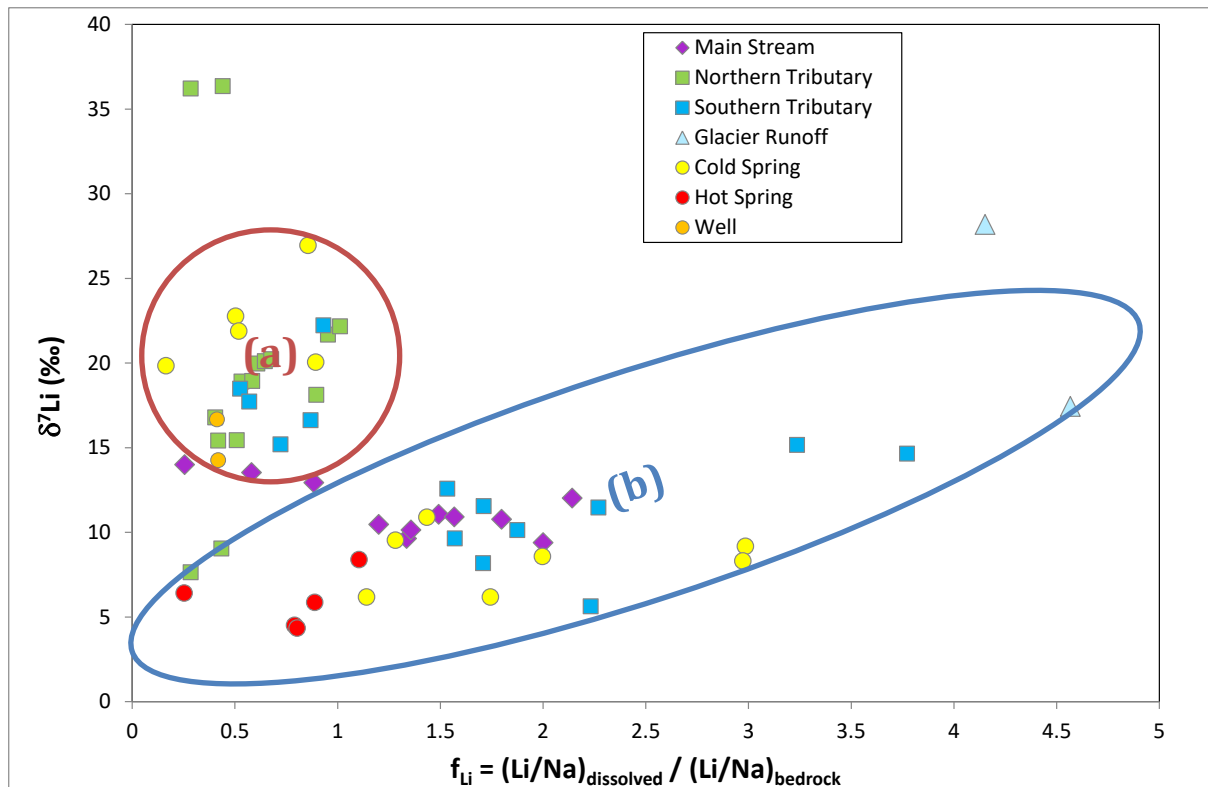
Figure 51: Lithium isotopic composition in the dissolved load as a function of f_{Li}.

Cluster (a) instead comprises low Li concentrations and high δ^7Li. This can be explained either by mineral dissolution or the incorporation of ^6Li on Fe-oxyhydroxide surfaces, typical arising from weathering of Fe-minerals from the ingenious rocks and metamorphic rocks (e.g. amphibolite, biotite, garnet) (Wimpenny et al. 2010). Mn and Fe deposits are often found in the river bedloads in the Gunt catchment, e.g. at the surfaces of rocks and boulders. By application of PHREEQC (Parkhurst and Appelo 1999; Merkel et al. 2005), saturation indices (SI) were calculated for the weathering products goethite (clay mineral group) and hematite (Appendix Table 6). All water samples are oversaturated in those two mineral species, which is not correlated with the δ^7Li in all water samples. This confirms the assumption, that δ^7Li is not controlled by mineral-specific fractionation.

6.3   Conclusions to lithium isotopes and water-rock-interaction

Lithium and its isotopes are usually used as proxies for silicate weathering and only in a few case studies the connection between the lithium isotope system and transit times was investigated. However, the main causes for the behavior of lithium isotopes in natural environments are not fully known. Lithium concentrations and lithium isotope compositions in various water reservoirs (rivers, groundwater, thermal water, lakes), in solid rocks and suspended solids (SPM) were analyzed. High lithium isotope signatures in the water samples and low lithium isotope values for the solid rock and the SPM were measured. The most important mechanism for producing ^7Li-enriched waters is leaching of silicate rocks along the flow path of the groundwater and surface water in the catchment area. The dissolution of lithium leads to higher lithium concentrations in the water phase whereas $\delta^7Li_{dissolved}$ decreases.

A relationship between the Li isotope composition and the residence time (RT) of water samples in the exemplary catchment area was found. With increasing flow length and therefore increasing RT an increasing water-rock interaction (WRI) is supported. This is characterized by lithium isotope fractionation, which takes place during the chemical weathering and dissolution of lithium of the bedrock material. Therefore, samples with low lithium concentration and high δ^7Li values have small RT with low WRI, samples with high Li concentrations and low δ^7Li values have higher RT and higher WRI. The δ^7Li signatures of the water samples depend on the δ^7Li signature of the bed rock material. A steady state is reached between dissolution of bedrock and precipitation of secondary minerals at least for the main stream and the hot springs.

To get more robust information on linking lithium isotopes with transit time estimation, more research on the potential of using lithium isotopes for age dating is necessary. For that, a combination of multiple age tracers is suggested.

7 Summary

The Pamir Mountains in Tajikistan are part of a semi- to cold-arid mountain region in Central Asia. Its snow and glacier deposits are the source of one of the largest Central Asian rivers - the Amu Darya. The development of the further availability of this important fresh water resource depending on factors such as climate change is in the focus of water management discussions. For this, the actual hydrological condition of the high-alpine catchment of the Gunt river is defined exemplary for the Pamir. By application of hydrochemical tracers (major ions and physico-chemical parameters) and isotope hydrological methods (δ^2H, ^{3}H, δ^{18}O, δ^7Li, ^{87}Sr/^{86}Sr, noble gases), basic hydrological processes are identified and described.

The following emphases build the framework of the dissertation:

▶ Subproject 1 - Characterization of precipitation and river water by using oxygen and hydrogen isotopes

The origin of precipitation and evolution of river water have been investigated with oxygen and hydrogen isotopes in those waters.

The investigation of the stable isotope composition of the river waters shows very low δ^{18}O and δ^2H values that means that they are strongly depleted with respect to ^{18}O and ^{2}H. Such values are typical for high mountain regions. However regional inhomogeneity in the catchment causes also a wide range of isotope ratios: due to increasing distance from the source of precipitation and the increasing height of the catchment area towards the west, waters with heavier isotope signatures are more likely in the western part of the catchment area and towards east a further decrease of δ^{18}O and δ^2H values is detectable. The northern catchments show higher δ^{18}O and δ^2H values than the southern catchments, which is mainly reasoned by the distribution of precipitation in the catchment area: the northern subcatchments are on the windward side of the mountains, that means the side facing the weather of the mountains, and thus receive more precipitation than the southern subcatchments. Consequently, more enriched rainwater remains in the northern catchment areas than in the southern catchment areas. Furthermore, the isotopic composition of the main stream is primarily characterized by the isotopy of Lake Yashilkul, which contains enriched water due to strong evaporation. With increasing flow length of the Gunt, the enriched water mixes with the isotopically depleted water of the subcatchments. As the flow length of the main stream increases, its isotope ratios become smaller. In addition to the regional effects in the water isotopes, seasonal effects are also important: In winter the water is characterized by particularly low δ^{18}O and δ^2H isotope values. These values increase in the course of the year and reach their maximum in summer. The low values come from the base runoff, which is characterized by low δ^{18}O and δ^2H values and must be therefore generated at a high altitude. In spring and summer, water more enriched with heavier isotopes is added to the runoff, caused by the melting of snowfields and glaciers. In addition to those higher δ^{18}O and δ^2H values, these meltwaters are also characterized by a comparatively higher d-excess, which is typical for precipitation coming from arid regions and thus indicates re-evaporation effects. Furthermore, the high d-excess values in the river waters and in the precipitation also indicate that the precipitation is mainly transported into the catchment area by sources where

re-evaporation plays an important role like south-westerly winds. The sources of precipitation lie in the Atlantic Ocean, the Mediterranean Sea, the Caspian Sea and the Persian Gulf. This is confirmed by a backtracking model (HYSPLIT) based on the modelling of air mass flows. The monsoonal influence could neither be confirmed nor denied by the stable isotopes. In order to better understand its influence, more detailed studies are necessary.

▶ Subproject 2 - Assessment of the hydrochemical system using descriptive statistical analysis methods

To describe the hydrochemical system in the Gunt catchment, water samples were analyzed for their major ion concentrations and physicochemical parameters (pH, T, EC). To evaluate the analytical results, descriptive statistical analysis methods were applied, e.g. frequency distribution, box plots, correlations.

The hydrochemical investigation of the river waters shows that the basic composition is mainly caused by the local geology. Calcium bicarbonate waters dominate the catchment area. In the course of the year, fluctuations occur in the strength of the mineralization of the waters, whereby the basic chemical composition remains constant and the river waters show highest dissolved contents in winter month. With the onset of snow and of glacier melting, less mineralized water is added to the comparably high mineralized water, so that the outflow increases but the mineralization decreases. There are additional local entries of evaporitic and silicate waters, mostly from hot springs.

Correlation analyses have shown that the strength of the mineralization of the water is clearly related to increased permafrost and glacier cover. In addition, the size of the subcatchments plays a role in the level of mineralization, meaning that catchments with a larger area show also higher concentrations of major anions and cations. Higher elevated catchments also have a higher permafrost and glacier cover, which delays the interaction of surface water with the bedrock and can therefore cause higher mineral concentrations at low altitudes.

Northern and southern subcatchments are clearly distinguishable in grades of mineralization in the river waters on the basis of different characteristics of catchments: generally, the northern subbasins have lower mineralization grades than the southern ones. In comparison with the northern subcatchments, southern ones comprise (i) a larger area and thus allow a stronger interaction between water and rock on a longer flow path, (ii) are flatter and cause a slower flow velocity of the rivers and also allow a stronger water-rock-interaction, (iii) are less glaciated than the northern catchment areas, which has a positive effect on the mineralization of river waters in this case.

The highest ion concentrations are found in the river Gunt itself, because it receives already higher mineralized water from the lake Yashilkul. Additionally, higher mineralization in the Gunt is caused by more intensive water rock interaction in comparison to its tributaries due to its bigger size, higher water input and flow length.

▶ Subproject 3 - Characterization of water-rock interactions with lithium isotopes with respect to residence times (RT)

Shallow groundwater resources and water-rock interactions are investigated by using lithium isotopes. The lithium isotope ratios are set into relation to transit times by modification and application of the reactive transport model of Pogge von Strandmann et al. (2014).

The lithium isotope ratios of water are primarily influenced by the geological conditions in the catchment area. The most important mechanism in the Gunt river waters to obtain [7]Li enriched water is to dissolve the silicate rock along the flow path rather than the process of incorporation of [6]Li in secondary minerals.

The transit time of the water has an influence on the evolution of the lithium isotopic composition in water. The longer the transit time, the lower the δ^7Li values. The RT of the tributaries in our catchment area is determined in particular by the size of the subcatchments. This is reasoned by the comparatively homogeneous geological and geomorphological basic conditions of the subcatchments and the coarse superficial material. By using a reactive transport model it is shown that the lithium isotopy in our exemplary catchment area appears to depend on the transit time of the water and that approximate estimates of the transit times can be made by knowing the δ^7Li values in water and rock.

This multi-tracer approach allows to get a detailed picture on the flow regime and chemical evolution of the river water of two to three circles of season and gives the important fact that chemical weathering is not that strong as physical weathering is. This leads to the conclusion that the catchment area of the Gunt is a geomorphologically young catchment area, which reacts quickly due to its climatically, geological and geomorphological conditions. There are clear regional and seasonal variations in all investigated parameters. Due to the hydrochemical and isotopic analysis of river water and the geomorphological characteristics the catchment area can be clearly subdivided into northern catchment areas, southern catchment areas and the eastern plateau, which is mainly characterized by the lake Yashilkul and the main river Gunt collecting all signals. In the δ^{18}O and δ^2H values and in the major anions and major cations, a clear annual cycle is recognizable. This shows that snow melting and glacier melting are the dominant processes for runoff formation and that runoff is less strongly fed by large groundwater deposits. Mean transit times of <2 years at exemplary cold springs and in wells in the steep northern subcatchments result in high δ^7Li values. The southern subbasins and the Gunt river itself show lower δ^7Li values which can be explained by the longer transit time between 2 and 10 years. The hot spring samples showed the lowest δ^7Li signature and ^{3}H values <0.5 TU indicating long transit times of up to 50 years. The calculated results reflect the natural conditions of the above-mentioned influence of permafrost and slope gradient and therefore low retention of meltwater in deeper aquifers.

The glaciers in the catchment area of the Gunt are also affected by strong melting processes. This in turn would mean that the investigated catchment is very sensitive to any changes of water input from the available current glacier decreases and the current meteorological circulations containing poor precipitation from the Atlantic, the Mediterranean, the Caspian Sea and the Persian Gulf and it also would be affected by increasing water scarcity in the next decades.

8 Outlook

This study gives an overview about the general hydrological situation and hydrochemical processes that take place in the Gunt catchment as part of the Pamir Mountains. For further understanding of short term and long-term changes through impact of climate change and human activities in the Pamir Mountains or even the whole Third Pole Environment, continuative investigations based on the following research questions are necessary:

▶ The influence of the Indian summer monsoon in the Pamir is still under discussion and needs to be further investigated. This could be carried out by high resolution isotope measurements of precipitation at diverse meteorological stations on various altitudes in the Pamirs based on the assumption that precipitation transported via monsoonal drifts can be distinguished by enriched $\delta^{18}O$ and δ^2H isotope ratios.

▶ The influence of the different wind systems on the whole Pamir region is not completely understood. Will climate change have an impact on the meteorological circulations and therefore on the availability of precipitation in the Pamir mountains? The information generated for the Gunt catchment must be extended to the whole Pamir Mountains. This can be done by collecting and analyzing precipitation and the application of remote sensing data and modelling instruments.

▶ The amount of annual groundwater recharge in the Pamirs and the occurrence of deeper groundwater reservoirs in the Eastern Pamir Mountains is unknown. Is glacier melt or snow melt the dominant contributor to runoff? If glaciers are the most important inputs for groundwater recharge, what are the future consequences of this melt for the region's water system? Does melting permafrost end up in groundwater recharge?

▶ The evolution and transit times of thermal water and the vulnerability of this resource is an open question. What are the sources of thermal water – infiltrating melt water from snow, glaciers or melting permafrost? Are there links between the occurrence of hot springs and tectonic processes? Groundwater age dating and hydrochemical methods would provide information about the flow path.

▶ The application of lithium isotopes for derivation of the strength of water-rock interaction and rough transit time estimation needs much further and deeper investigation, especially in multi lithology regions. Therefore, it is necessary to apply lithium isotope measurements in further catchments. Additionally, it is indispensable to use "conventional" age dating parameters to estimate mean residence times (MRT).

9 References

Aemisegger, F.; Pfahl, S.; Sodemann, H.; Lehner, I.; Seneviratne, S. I.; Wernli, H. (2014): Deuterium excess as a proxy for continental moisture recycling and plant transpiration. In Atmospheric Chemistry and Physics 14 (8), pp. 4029–4054. DOI: 10.5194/acp-14-4029-2014.

Aeschbach-Hertig, Werner; Solomon, D. Kip (2013): Noble Gas Thermometry in Groundwater Hydrology. In Pete Burnard (Ed.): The noble gases as geochemical tracers. Heidelberg, New York: Springer (Advances in isotope geochemistry), pp. 81–122.

Aizen, Vladimir B.; Aizen, Elena M.; Melack, John M. (1995): Climate, snow cover, glaciers, and runoff in the Tien Shan, Central Asia. In J Am Water Resources Assoc 31 (6), pp. 1113–1129. DOI: 10.1111/j.1752-1688.1995.tb03426.x.

Aizen, Vladimir B.; Aizen, Elena M.; Melack, John M.; Martma, Tonu (1996): Isotopic measurements of precipitation on central Asian glaciers (Southeastern Tibet, northern Himalayas, central Tien Shan). In Journal of Geophysical Research 101 (D4), pp. 9185–9198. DOI: 10.1029/96JD00061.

Aizen, Vladimir B.; Mayevski, Paul A.; Aizen, Elena M.; Joswiak, Daniel R.; Surazakov, Arzhan B.; Kaspari, Susan et al. (2009): Stable-isotope and trace element time series from Fedchenko glacier (Pamirs) snow/firn cores. In Journal of Glaciology 55 (190), pp. 275–291, checked on 11/9/2012.

Al Charideh, Abdul Rahman; Abou Zakhem, Boulos (2010): Distribution of tritium and stable isotopes in precipitation in Syria. In Hydrological sciences journal 55 (5), pp. 832–843. DOI: 10.1080/02626667.2010.487977.

Ali, Kamal K.; Al-Kubaisi, Qusai Y.; Al-Paruany, Kamal B. (2015): Isotopic study of water resources in a semi-arid region, western Iraq. In Environmental Earth Sciences 74 (2), pp. 1671–1686. DOI: 10.1007/s12665-015-4172-6.

Alyamani, Mahmoud S. (2001): Isotopic composition of rainfall and ground-water recharge in the western province of Saudi Arabia. In Journal of Arid Environments 49 (4), pp. 751–760. DOI: 10.1006/jare.2001.0815.

Araguás-Araguás, Luis J.; Froehlich, Klaus; Rozanski, Kazimierz (1998): Stable isotope composition of precipitation over southeast Asia. In J. Geophys. Res. 103 (D22), pp. 28721–28742. DOI: 10.1029/98JD02582.

Bagard, Marie-Laure; Chabaux, François; Pokrovsky, Oleg S.; Viers, Jérome; Prokushkin, Anatoly S.; Stille, Peter et al. (2011): Seasonal variability of element fluxes in two Central Siberian rivers draining high latitude permafrost dominated areas. In Geochimica et Cosmochimica Acta 75 (12), pp. 3335–3357. DOI: 10.1016/j.gca.2011.03.024.

Baidulloeva, Jamila (2011): Runofff source Gunt river catchment to Christiane Meier. Dushanbe, August 2011.

Bajjali, William (2012): Spatial variability of environmental isotope and chemical content of precipitation in Jordan and evidence of slight change in climate. In Applied Water Science 2 (4), pp. 271–283. DOI: 10.1007/s13201-012-0046-1.

Barlow, Mathew A.; Tippett, Michael K. (2008): Variability and Predictability of Central Asia River Flows: Antecedent Winter Precipitation and Large-Scale Teleconnections. In J. Hydrometeor 9 (6), pp. 1334–1349. DOI: 10.1175/2008JHM976.1.

Bershaw, John; Penny, Sandra M.; Garzione, Carmala N. (2012): Stable isotopes of modern water across the Himalaya and eastern Tibetan Plateau: Implications for estimates of paleoelevation and paleoclimate. In J. Geophys. Res. 117 (D2), n/a-n/a. DOI: 10.1029/2011JD016132.

Beylich, Achim A.; Laute, Katja (2012): Seasonal and annual variations of surface water chemistry, solute fluxes and chemical denudation in a steep and glacier-fed mountain catchment in western Norway (Erdalen, Nordfjord). In CATENA 96, pp. 12–27. DOI: 10.1016/j.catena.2012.04.004.

Bill, Sonja; Schreiber, Dagmar (2010): Tadschikistan. Zwischen Dušanbe und dem Dach der Welt. 1st ed. (Reiseführer (Trescher)).

Bohlin, Madeleine S.; Bickle, Mike J. (2019): The reactive transport of Li as a monitor of weathering processes in kinetically limited weathering regimes. In Earth and Planetary Science Letters 511, pp. 233–243. DOI: 10.1016/j.epsl.2019.01.034.

Bottyán, Emese; Czuppon, György; Weidinger, Tamás; Haszpra, László; Kármán, Krisztina (2017): Moisture source diagnostics and isotope characteristics for precipitation in east Hungary: implications for their relationship. In Hydrological sciences journal 62 (12), pp. 2049–2060. DOI: 10.1080/02626667.2017.1358450.

Bowen, Gabriel J.; Revenaugh, Justin (2003): Interpolating the isotopic composition of modern meteoric precipitation. In Water Resour. Res 39 (10), p. 23. DOI: 10.1029/2003WR002086.

Brehme, Maria (2014): Statistische Auswertung der Flusswasserzusammensetzung im Einzugsgebiet des Gunt (Pamir-Gebirge) im Hinblick auf ihre räumliche und zeitliche Variabilität. Master thesis. Martin-Luther-Universität Halle-Wittenberg, Halle (Saale). Institut für Geowissenschaften und Geographie, Hydro- und Umweltgeologie.

Brockhaus (1928): Der Große Brockhaus in 20 vols. 15th ed. Leipzig (4).

Burtman, Valentin Semenovich; Molnar, Peter Hale (Eds.) (1993): Geological and geophysical evidence for deep subduction of continental crust beneath the Pamir. Boulder: The Geological Society of America (Special paper / Geological society of America, 0281).

Chan, Lui-Heung; Edmond, John M.; Thompson, Geoffrey (1993): A lithium isotope study of hot springs and metabasalts from Mid-Ocean Ridge Hydrothermal Systems. In J. Geophys. Res 98 (B6), p. 9653. DOI: 10.1029/92JB00840.

Clark, Ian D.; Fritz, Peter (1997): Environmental Isotopes in Hydrogeology. New York: CRC Press. Available online at http://www.amazon.co.uk/Environmental-Isotopes-Hydrogeology-Ian-Clark/dp/1566702496.

Craig, Harmon (1961): Isotopic Variations in Meteoric Waters. In Science (New York, N.Y.) 133 (3465), pp. 1702–1703. DOI: 10.1126/science.133.3465.1702.

Craig, Harmon; Gordon, Louis Irwin (Eds.) (1965): Deuterium and oxygen 18 variations in the ocean and the marine atmosphere. With assistance of Harmon Craig, Louis Irwin Gordon. Conference on Stable Isotopes in Oceanographic Studies and Paleotemperatures. Pisa: Consiglio nazionale delle richerche Laboratorio de geologia nucleare. Available online at http://worldcatlibraries.org/wcpa/oclc/8019537.

Dalai, Tarun K.; Bhattacharya, S. K.; Krishnaswami, S. (2002): Stable isotopes in the source waters of the Yamuna and its tributaries: seasonal and altitudinal variations and relation to major cations. In Hydrol. Process. 16 (17), pp. 3345–3364. DOI: 10.1002/hyp.1104.

Dansgaard, W. (1964): Stable isotopes in precipitation. In Tellus XVI, pp. 436–468.

Dimri, A. P.; Chevuturi, Amulya (2016): Western Disturbances - An Indian Meteorological Perspective. 1st ed. 2016. Cham: Springer International Publishing. Available online at http://gbv.eblib.com/patron/FullRecord.aspx?p=4403221.

Dimri, A. P.; d. Niyogi; Barros, Ana P.; Ridley, J.; Mohanty, U. C.; Yasunari, T.; Sikka, D. R. (2015): Western Disturbances: A review. In Reviews of Geophysics 53 (2), pp. 225–246. DOI: 10.1002/2014RG000460.

Dongmann, G.; Nürnberg, H. W.; Förstel, H.; Wagener, K. (1974): On the enrichment of H2 18O in the leaves of transpiring plants. In Radiat Environ Biophys 11 (1), pp. 41–52. DOI: 10.1007/BF01323099.

Elliott, Tim; Jeffcoate, Alistair B.; Bouman, Claudia (2004): The terrestrial Li isotope cycle: light-weight constraints on mantle convection. In Earth and Planetary Science Letters 220 (3), pp. 231–245. DOI: 10.1016/S0012-821X(04)00096-2.

Elliott, Tim; Thomas, Alex; Jeffcoate, Alistair B.; Niu, Yaoling (2006): Lithium isotope evidence for subduction-enriched mantle in the source of mid-ocean-ridge basalts. In Nature 443 (7111), p. 565. DOI: 10.1038/nature05144.

Faure, Gunter (1986): Principles of isotope geology. 2.ed. New York: Wiley.

Flesch, G. D.; Anderson, A. R.; Svec, H. J. (1973): A secondary isotopic standard for 6Li/7Li determinations. In International Journal of Mass Spectrometry and Ion Physics 12 (3), pp. 265–272. DOI: 10.1016/0020-7381(73)80043-9.

Food and agriculture organization of the United Nation (2017): Drought Characteristics and Management in Central Asia and Turkey. Rome: FAO.

Fouillac, C.; Michard, G. (1981): Sodium/lithium ratio in water applied to geothermometry of geothermal reservoirs. In Geothermics 10 (1), pp. 55–70. DOI: 10.1016/0375-6505(81)90025-0.

Friedman, Irving; Machta, Lester; Soller, Ralph (1962): Water-vapor exchange between a water droplet and its environment. In J. Geophys. Res 67 (7), pp. 2761–2766. DOI: 10.1029/JZ067i007p02761.

Friedman, Irving; Smith, George I. (1970): Deuterium content of snow cores from Sierra Nevada area. In Science (New York, N.Y.) 169 (3944), pp. 467–470. Available online at http://www.ncbi.nlm.nih.gov/pubmed/5424790.

Froehlich, Klaus; Gibson, John J.; Aggarwal, Pradeep K. (2002): Deuterium excess in precipitation and its climatological significance. In International Atomic Energy Agency (IAEA) (Ed.): Study of Environmental Change Using Isotope Techniques. International conference held in Vienna, 23-27 April 2001 : proceedings. Vienna: International Atomic Energy Agency (C&S papers series, 13), pp. 54–66.

Froehlich, Klaus; Kralik, Martin; Papesch, Wolfgang; Rank, Dieter; Scheifinger, Helfried; Stich-ler, Willibald (2008): Deuterium excess in precipitation of Alpine regions - moisture recyc-ling. In Isotopes in environmental and health studies 44 (1), pp. 61–70. DOI: 10.1080/10256010801887208.

Froelich, Philip N.; Misra, Sambuddha (2014): Was the Late Paleocene-Early Eocene Hot Because Earth Was Flat? An Ocean Lithium Isotope View of Mountain Building, Continental Weathering, Carbon Dioxide, and Earth's Cenozoic Clima. In oceanog 27 (1), pp. 36–49. DOI: 10.5670/oceanog.2014.06.

Fuchs, Margret C.; Gloaguen, Richard; Pohl, Eric (2013): Tectonic and climatic forcing on the Panj river system during the Quaternary. In Int J Earth Sci (Geol Rundsch) 102 (7), pp. 1985–2003. DOI: 10.1007/s00531-013-0916-2.

Furtak, H.; Langguth, H.-R. (Eds.) (1967): Zur hydrochemischen Kennzeichnung von Grund-wässern und Grundwassertypen mittels Kennzahlen. Mem. IAH Congress. Hannover, 1965. 7 volumes.

Galewsky, Joseph; Steen-Larsen, Hans Christian; Field, Robert D.; Worden, John; Risi, Camille; Schneider, Matthias (2016): Stable isotopes in atmospheric water vapor and applications to the hydrologic cycle. In Reviews of Geophysics 54 (4), pp. 809–865. DOI: 10.1002/2015RG000512.

Gat, Joel R. (2000): Atmospheric water balance?the isotopic perspective. In Hydrol. Process 14 (8), pp. 1357–1369. DOI: 10.1002/1099-1085(20000615)14:8<1357::AID-HYP986>3.0.CO;2-7.

Gat, Joel R.; Carmi, I. (1970): Evolution of the isotopic composition of atmospheric waters in the Mediterranean Sea area. In J. Geophys. Res 75 (15), pp. 3039–3048. DOI: 10.1029/JC075i015p03039.

Gat, Joel R.; Klein, B.; Kushnir, Y.; Roether, W.; Wernli, H.; Yam, R.; Shemesh, Aldo (2003): Isotope composition of air moisture over the Mediterranean Sea: an index of the air–sea in-teraction pattern. In Tellus 55B (5), pp. 953–965. Available online at http://online-library.wiley.com/doi/10.1034/j.1600-0889.2003.00081.x/full.

Gat, Joel R.; Shemesh, Aldo; Tziperman, Eli; Hecht, Artur; Georgopoulos, Dimitri; Basturk, Ozden (1996): The stable isotope composition of waters of the eastern Mediterranean Sea. In J. Geophys. Res. 101 (C3), pp. 6441–6451. DOI: 10.1029/95JC02829.

Gibbs, R. J. (1970): Mechanisms controlling world water chemistry. In Science 170 (3962), pp. 1088–1090. DOI: 10.1126/science.170.3962.1088.

Gibson, John J.; Birks, S. J.; Yi, Y. (2016): Stable isotope mass balance of lakes: a contemporary perspective. In Quaternary Science Reviews 131 (Part B), pp. 316–328. DOI: 10.1016/j.quascirev.2015.04.013.

Gorbunov, A. P. (1990): Permafrost in the arid mountains of middle asia—the eastern pamirs, USSR. In Permafrost and Periglacial Processes 1, pp. 309–312.

Greifenhagen, Götz (2000): Untersuchungen zur Hydrogeologie des Stadtgebietes Darmstadt mit Hilfe eines Grundwasserinformationssystems: unter Verwendung von einer Datenbank, Datenmodellierung und ausgewählten statistischen Methoden. Dissertation. TU Darmstadt, Darmstadt.

Gröning, Manfred; Duren, Michael van; Andreescu, Liliana (2010): Metrological Characteristics of the Conventional Measurement Scales for Hydrogen and Oxygen Stable Isotope Amount Ratios: The δ-Scales. In A. Fajgelj, Maria Belli, Umberto Sansone (Eds.): Combining and reporting analytical results. Cambridge: RSC Pub (Special publication, no. 307), pp. 62–72.

Guan, Huade; Zhang, Xinping; Skrzypek, Grzegorz; Sun, Zhian; Xu, Xiang (2013): Deuterium excess variations of rainfall events in a coastal area of South Australia and its relationship with synoptic weather systems and atmospheric moisture sources. In Journal of Geophysical Research: Atmospheres 118 (2), pp. 1123–1138. DOI: 10.1002/jgrd.50137.

Hamamin, Dara Faeq; Ali, Salahalddin Saeed (2013): Hydrodynamic study of karstic and intergranular aquifers using isotope geochemistry in Basara basin, Sulaimani, North-Eastern Iraq. In Arabian Journal of Geosciences 6 (8), pp. 2933–2940. DOI: 10.1007/s12517-012-0572-z.

Hayashi, Masaki; Quinton, William L.; Pietroniro, Alain; Gibson, John J. (2004): Hydrologic functions of wetlands in a discontinuous permafrost basin indicated by isotopic and chemical signatures. In Journal of Hydrology 296 (1), pp. 81–97. DOI: 10.1016/j.jhydrol.2004.03.020.

Helliker, Brent R.; Ehleringer, James R. (2000): Establishing a grassland signature in veins: 18O in the leaf water of C3 and C4 grasses. In Proceedings of the National Academy of Sciences of the United States of America 97 (14), pp. 7894–7898.

Henchiri, S.; Clergue, C.; Dellinger, Mathieu; Gaillardet, Jérôme; Louvat, Pascale; Bouchez, Julien (2014): The Influence of Hydrothermal Activity on the Li Isotopic Signature of Rivers Draining Volcanic Areas. In Procedia Earth and Planetary Science 10, pp. 223–230. DOI: 10.1016/j.proeps.2014.08.026.

Huang, Xiang; Sillanpää, Mika; Gjessing, Egil T.; Vogt, Rolf D. (2009): Water quality in the Tibetan Plateau: Major ions and trace elements in the headwaters of four major Asian rivers. In Science of The Total Environment 407 (24), pp. 6242–6254. DOI: 10.1016/j.scitotenv.2009.09.001.

Huh, Youngsook; Chan, Lui-Heung; Edmond, John M. (1998): Lithium and its isotopes in major world rivers: Implications for weathering and the oceanic budget. In Geochimica et Cosmochimica Acta 62 (12), pp. 2039–2051, checked on 7/15/2015.

Huh, Youngsook; Chan, Lui-Heung; Edmond, John M. (2001): Lithium isotopes as a probe of weathering processes: Orinoco River. In Earth and Planetary Science Letters 194, pp. 189–199, checked on 7/15/2015.

Hussain, Shakir; Xianfang, Song; Hussain, Iqtidar; Jianrong, Liu; Dong Mei, Han; Li Hu, Yang; Huang, Wei (2015): Controlling Factors of the Stable Isotope Composition in the Precipitation of Islamabad, Pakistan. In Advances in Meteorology 2015 (1–4), pp. 1–11. DOI: 10.1155/2015/817513.

International Atomic Energy Agency (IAEA) (2005): Isotopic composition of precipitation in the Mediterranean Basin in relation to air circulation patterns and climate. Final report of a coordinated research project, 2000-2004. Vienna: International Atomic Energy Agency (IAEA-TECDOC, 1453).

International Atomic Energy Agency (IAEA) (2018): Global Network of Isotopes in Precipitation. The GNIP Database. International Atomic Energy Agency (IAEA). Wien.

Jeelani, Ghulam; Deshpande, Rajendrakumar D.; Shah, Rouf A.; Hassan, Wasim (2017): Influence of southwest monsoons in the Kashmir Valley, western Himalayas. In Isotopes in environmental and health studies 53 (4), pp. 400–412. DOI: 10.1080/10256016.2016.1273224.

Jeelani, Ghulam; Saravana Kumar, U.; Kumar, Bhishm (2013): Variation of $\delta 18O$ and δD in precipitation and stream waters across the Kashmir Himalaya (India) to distinguish and estimate the seasonal sources of stream flow. In Journal of Hydrology 481, pp. 157–165. DOI: 10.1016/j.jhydrol.2012.12.035.

Jenkins, Alan; Sloan, William T.; Cosby, B.Jack (1995): Stream chemistry in the middle hills and high mountains of the Himalayas, Nepal. In Journal of Hydrology 166 (1), pp. 61–79. DOI: 10.1016/0022-1694(94)02600-G.

Johnsen, S. J.; Dansgaard, W.; White, James W. C. (1989): The origin of Arctic precipitation under present and glacial conditions. In Tellus B 41B (4), pp. 452–468. DOI: 10.1111/j.1600-0889.1989.tb00321.x.

Joussaume, Sylvie; Sadourny, Robert; Jouzel, Jean (1984): A general circulation model of water isotope cycles in the atmosphere. In Nature 311 (5981), p. 24. DOI: 10.1038/311024a0.

Jouzel, Jean; Merlivat, Liliane (1984): Deuterium and Oxygen 18 in Precipitation: Modeling of the Isotopic Effects During Snow Formation. In Journal of Geophysical Research 89 (D7), pp. 11749–11757. DOI: 10.1029/JD089iD07p11749.

Jouzel, Jean; Merlivat, Liliane; Lorius, Claude (1982): Deuterium excess in an East Antarctic ice core suggests higher relative humidity at the oceanic surface during the last glacial maximum. In Nature 299 (5885), p. 688. DOI: 10.1038/299688a0.

Juhlke, Tobias R.; Meier, Christiane; Geldern, Robert van; Vanselow, Kim A.; Wernicke, Jakob; Baidulloeva, Jamila et al. (2019): Assessing moisture sources of precipitation in the Western Pamir Mountains (Tajikistan, Central Asia) using deuterium excess. In Tellus B: Chemical and Physical Meteorology 71 (1), pp. 1–16. DOI: 10.1080/16000889.2019.1601987.

Kalnay, E.; Kanamitsu, M.; Kistler, R.; Collins, W.; d. Deaven; Gandin, L. et al. (1996): The NCEP/NCAR 40-Year Reanalysis Project. In Bull. Amer. Meteor. Soc. 77 (3), pp. 437–471. DOI: 10.1175/1520-0477(1996)077<0437:TNYRP>2.0.CO;2.

Kang, Shichang; Kreutz, Karl J.; Mayevski, Paul A.; Qin, Dahe; Yao, Tandong (2002): Stable-isotopic composition of precipitation over the northern slope of the central Himalaya. In Journal of Glaciology 48 (163), pp. 519–526. Available online at http://www.ingenta-connect.com/content/igsoc/jog/2002/00000048/00000163/art00004.

Karim, Ajaz; Veizer, Jan (2002): Water balance of the Indus River Basin and moisture source in the Karakoram and western Himalayas: Implications from hydrogen and oxygen isotopes in river water. In Journal of Geophysical Research: Atmospheres 107 (D18), ACH 9-1-ACH 9-12. DOI: 10.1029/2000JD000253.

Kattan, Z. (1997): Chemical and environmental isotope study of precipitation in Syria. In Journal of Arid Environments 35 (4), pp. 601–615. DOI: 10.1006/jare.1996.0228.

Kısakűrek, Başak; James, Rachael H.; Harris, Nigel B.W (2005): Li and $\delta7Li$ in Himalayan rivers: Proxies for silicate weathering? In Earth and Planetary Science Letters 237 (3-4), pp. 387–401. DOI: 10.1016/j.epsl.2005.07.019.

Knoche, Malte; Merz, Ralf; Lindner, Martin; Weise, Stephan M. (2017): Bridging Glaciological and Hydrological Trends in the Pamir Mountains, Central Asia. In Water 9 (6), p. 422. DOI: 10.3390/w9060422.

Koeniger, Paul; Leibundgut, Christian; Stichler, Willibald (2009): Spatial and temporal characterisation of stable isotopes in river water as indicators of groundwater contribution and confirmation of modelling results; a study of the Weser river, Germany. In Isotopes in Environmental and Health Studies 45 (4), pp. 289–302. DOI: 10.1080/10256010903356953.

Kralik, Martin; Zieritz, Irene; Grath, Johannes; Vincze, Gabriele; Philippitsch, Rudolph; Pavlik, Heinrich (2005): HYDROCHEMISCHE KARTE ÖSTERREICHS HYDROCHEMICAL MAP OF AUSTRIA. Oberflächennaher Grundwasserkörper und Fließgewässer. Mittelwerte von Wassergüteerhebungsdaten. umweltbundesamt. Wien, checked on 2/1/2019.

Kreutz, Karl J.; Wake, Cameron P.; Aizen, Vladimir B.; DeWayne, Cecil L. (2003): Seasonal deuterium excess in a Tien Shan ice core: Influence of moisture transport and recycling in Central Asia. In Geophys. Res. Lett 30 (18). DOI: 10.1029/2003GL017896.

Lachniet, Matthew S.; Patterson, William P. (2009): Oxygen isotope values of precipitation and surface waters in northern Central America (Belize and Guatemala) are dominated by temperature and amount effects. In Earth and Planetary Science Letters 284 (3-4), pp. 435–446. DOI: 10.1016/j.epsl.2009.05.010.

Lamb, Kara D.; Clouser, Benjamin W.; Bolot, Maximilien; Sarkozy, Laszlo; Ebert, Volker; Saathoff, Harald et al. (2017): Laboratory measurements of HDO/H2O isotopic fractionation during ice deposition in simulated cirrus clouds. In Proceedings of the National Academy of Sciences of the United States of America 114 (22), pp. 5612–5617. DOI: 10.1073/pnas.1618374114.

Lang, Timothy J.; Barros, Ana P. (2004): Winter Storms in the Central Himalayas. In JMSJ 82 (3), pp. 829–844. DOI: 10.2151/jmsj.2004.829.

Lee, Jung-Eun; Fung, Inez (2008): "Amount effect" of water isotopes and quantitative analysis of post-condensation processes. In Hydrol. Process 22 (1), pp. 1–8. DOI: 10.1002/hyp.6637.

Lemarchand, Emmanuel; Chabaux, François; Vigier, Nathalie; Millot, Romain; Pierret, Marie-Claire (2010): Lithium isotope systematics in a forested granitic catchment (Strengbach, Vosges Mountains, France). In Geochimica et Cosmochimica Acta 74 (16), pp. 4612–4628. DOI: 10.1016/j.gca.2010.04.057.

Leonov, M. G.; Rybin, A. K.; Batalev, V. Yu.; Matyukov, V. E.; Shchelochkov, G. G. (2017): Tectonic structure and evolution of the Hissar–Alay Mountain Domain and the Pamirs. In Geotecton. 51 (6), pp. 566–583. DOI: 10.1134/S001685211706005X.

Li, Qianyu; Wu, Jinglu; Shen, Beibei; Zeng, Haiao; Li, Yanhong (2018): Water Chemistry and Stable Isotopes of Different Water Types in Tajikistan. In Environ. Process. 5 (S1), pp. 127–137. DOI: 10.1007/s40710-018-0312-9.

Li, Siyue; Zhang, Quanfa (2008): Geochemistry of the upper Han River basin, China, 1: Spatial distribution of major ion compositions and their controlling factors. In Applied Geochemistry 23 (12), pp. 3535–3544. DOI: 10.1016/j.apgeochem.2008.08.012.

Lindner, Martin (2014): Rezente Gletscheranderung im Einzugsgebiet des Gunts, Tadschikistan. Norderstedt: GRIN Publishing.

Liotta, Marcello; Favara, Rocco; Valenza, Mariano (2006): Isotopic composition of the precipitations in the central Mediterranean: Origin marks and orographic precipitation effects. In J. Geophys. Res 111 (D19), p. 1341. DOI: 10.1029/2005JD006818.

Liu, Q.; Tian, L.D; Wang, J.L; Wen, Rong; Weng, YongBiao; Shen, Yongping et al. (2015a): A study of longitudinal and altitudinal variations in surface water stable isotopes in West Pamir, Tajikistan. In Atmospheric Research 153, pp. 10–18. DOI: 10.1016/j.atmosres.2014.07.029.

Liu, Xiao-Ming; Wanner, Christoph; Rudnick, Roberta L.; McDonough, William F. (2015b): Processes controlling δ7Li in rivers illuminated by study of streams and groundwaters draining basalts. In Earth and Planetary Science Letters 409, pp. 212–224. DOI: 10.1016/j.epsl.2014.10.032.

Lui-Heung, Chan; Edmond, John M. (1988): Variation of lithium isotope composition in the marine environment: A preliminary report. In Geochimica et Cosmochimica Acta 52 (6), pp. 1711–1717. DOI: 10.1016/0016-7037(88)90239-6.

Mason, Brian; Moore, Carleton B.; Hintermaier-Erhard, Gerd (1985): Grundzüge der Geochemie. Mit 66 Tabellen. Stuttgart: Enke.

Maussion, Fabien; Scherer, Dieter; Mölg, Thomas; Collier, Emily; Curio, Julia; Finkelnburg, Roman (2014): Precipitation Seasonality and Variability over the Tibetan Plateau as Re-

solved by the High Asia Reanalysis*. In J. Climate 27 (5), pp. 1910–1927. DOI: 10.1175/JCLI-D-13-00282.1.

Meier, Christiane; Knoche, Malte; Merz, Ralf; Weise, Stephan M. (2013): Stable isotopes in river waters in the Tajik Pamirs: regional and temporal characteristics. In Isotopes in environmental and health studies 49 (4), pp. 542–554. DOI: 10.1080/10256016.2013.835809.

Meier, Christiane; Knoche, Malte; Merz, Ralf; Weise, Stephan M. (2015a): Monitoring of stable isotopes in river water and precipitation in the Tajik Pamirs. In Proceedings of the International Symposium on Isotope Hydrology: Revisiting Foundations and Exploring Frontiers.

Meier, Christiane; Knoche, Malte; Merz, Ralf; Weise, Stephan M. (2015b): Single or multiple source(s) of precipitation in the Western Pamirs, Tajikistan? In EGU General Assembly 2015.

Meier, Christiane; Osenbrück, Karsten; Seitz, Hans-Michael; Weise, Stephan M. (2017): First Lithium Isotope Data from Rivers and Subsurface Water in the Pamirs. In Procedia Earth and Planetary Science 17, pp. 574–577. DOI: 10.1016/j.proeps.2016.12.147.

Merkel, Broder J.; Planer-Friedrich, Britta; Nordstrom, Darrell Kirk (Eds.) (2005): Groundwater geochemistry. A practical guide to modeling of natural and contaminated aquatic systems ; with … a CD-ROM. Berlin: Springer. Available online at http://www.loc.gov/catdir/enhancements/fy0662/2004117858-d.html.

Merkel, Broder J.; Sperling, Barbara ((1996)): Hydrogeochemische Stoffsysteme. Bonn: Wirtschafts- und Verl.-Ges. Gas und Wasser (Schriftenreihe des Deutschen Verbandes für Wasserwirtschaft und Kulturbau, 110).

Merlivat, Liliane; Jouzel, Jean (1979): Global climatic interpretation of the deuterium-oxygen 18 relationship for precipitation. In Journal of Geophysical Research: Oceans 84 (C8), pp. 5029–5033. DOI: 10.1029/JC084iC08p05029.

Meybeck, Michel (1987): Global chemical weathering of surficial rocks estimated from river dissolved loads. In American Journal of Science 287 (5), pp. 401–428. DOI: 10.2475/ajs.287.5.401.

Meybeck, Michel; Green, Pamela; Vörösmarty, Charles (2001): A New Typology for Mountains and Other Relief Classes: An Application to Global Continental Water Resources and Population Distribution. In Mountain Research and Development - MT RES DEV 21, pp. 34–45.

Michelsen, Nils; Geldern, Robert van; Roßmann, Yasmin; Bauer, Ingo; Schulz, Stephan; Barth, Johannes A.C.; Schüth, Christoph (2018): Comparison of precipitation collectors used in isotope hydrology. In Chemical Geology 488, pp. 171–179. DOI: 10.1016/j.chemgeo.2018.04.032.

Michelsen, Nils; Reshid, Mustefa; Siebert, Christian; Schulz, Stephan; Knöller, Kay; Weise, Stephan M. et al. (2015): Isotopic and chemical composition of precipitation in Riyadh, Saudi Arabia. In Chemical Geology 413, pp. 51–62. DOI: 10.1016/j.chemgeo.2015.08.001.

Millot, Romain (2013): Les isotopes du lithium: exemples d'applications en géochimie. Habili-tation. Université d'Orléans, Orléans.

Millot, Romain; Négrel, Philippe (2007): Multi-isotopic tracing ($\delta 7$Li, $\delta 11$B, 87Sr/86Sr) and chemical geothermometry: evidence from hydro-geothermal systems in France. In Chemical Geology 244 (3-4), pp. 664–678. DOI: 10.1016/j.chemgeo.2007.07.015.

Millot, Romain; Scaillet, Bruno; Sanjuan, Bernard (2010a): Lithium isotopes in island arc geo-thermal systems: Guadeloupe, Martinique (French West Indies) and experimental approach. In Geochimica et Cosmochimica Acta 74 (6), pp. 1852–1871. DOI: 10.1016/j.gca.2009.12.007.

Millot, Romain; Vigier, Nathalie; Gaillardet, Jérôme (2010b): Behaviour of lithium and its isotopes during weathering in the Mackenzie Basin, Canada. In Geochimica et Cosmochimica Acta 74 (14), pp. 3897–3912. DOI: 10.1016/j.gca.2010.04.025.

Misra, Sambuddha; Froelich, Philip N. (2012): Lithium Isotope History of Cenozoic Seawater: Changes in Silicate Weathering and Reverse Weathering. In Science 335 (6070), pp. 818–823. DOI: 10.1126/science.1214697.

Mook, Willem G. (2005): Introduction to Isotope Hydrology. Stable and Radioactive Isotopes of Hydrogen, Carbon, and Oxygen. 1st ed.: Taylor & Francis. Available online at http://www.amazon.com/Introduction-Isotope-Hydrology-International-Contributions/dp/0415398053.

Négrel, Philippe; Millot, Romain; Brenot, Agnès; Bertin, Clotilde (2010): Lithium isotopes as tracers of groundwater circulation in a peat land. In Chemical Geology 276 (1-2), pp. 119–127. DOI: 10.1016/j.chemgeo.2010.06.008.

Niewodniczanski, Jerzy; Grabczak, Jerzy; Baranski, Leslaw; Rzepka, Jerzy (1981): The altitude effect on the isotopic composition of snow in high mountains. In Journal of Glaciology 27 (95), pp. 99–111. Available online at http://www.igsoc.org/journal.old/27/95/igs_journal_vol27_issue095_pg99-111.pdf.

NOAA (2018): Global Data Assimilation System (GDAS). Washington DC.

Ohlanders, N.; Rodriguez, M.; McPhee, J. (2012): Stable water isotope variation in a Central Andean watershed dominated by glacier- and snowmelt. In Hydrology and Earth System Sciences Discussions 9 (10), pp. 12227–12269. DOI: 10.5194/hessd-9-12227-2012.

Osati, Khaled; Koeniger, Paul; Salajegheh, Ali; Mahdavi, Mohammad; Chapi, Kamran; Malekian, Arash (2014): Spatiotemporal patterns of stable isotopes and hydrochemistry in springs and river flow of the upper Karkheh River Basin, Iran. In Isotopes in environmental and health studies 50 (2), pp. 169–183. DOI: 10.1080/10256016.2014.857317.

Pande, K.; Padia, J. T.; Ramesh, R.; Sharma, K. K. (2000): Stable isotope systematics of surface water bodies in the Himalayan and Trans-Himalayan (Kashmir) region. In Proceedings of the Indian Academy of Sciences - Earth and Planetary Sciences 109 (1), pp. 109–115. Available online at http://www.springerlink.com/index/aj6mx11xp93h3t33.pdf.

Pang, H.; Hou, S.; Kaspari, Susan; Mayevski, Paul A. (2014): Influence of regional precipitation patterns on stable isotopes in ice cores from the central Himalayas. In The Cryosphere 8 (1), pp. 289–301. DOI: 10.5194/tc-8-289-2014.

Parizi, Hassan Sahraei; Samani, Nozar (2014): Environmental Isotope Investigation of Groundwater in the Sarcheshmeh Copper Mine Area, Iran. In Mine Water and the Environment 33 (2), pp. 97–109. DOI: 10.1007/s10230-014-0277-5.

Parkes, Stephen d.; McCabe, Matthew F.; Griffiths, Alan d.; Wang, Lixin; Chambers, Scott; Ershadi, Ali et al. (2017): Response of water vapour D-excess to land–atmosphere interactions in a semi-arid environment. In Hydrol. Earth Syst. Sci 21 (1), pp. 533–548. DOI: 10.5194/hess-21-533-2017.

Parkhurst, David L.; Appelo, C. A. J. (1999): User's guide to PHREEQC (Version 2) : a computer program for speciation, batch-reaction, one-dimensional transport, and inverse geochemical calculations. U.S. Geological Survey.

Peel, M. C.; Finlayson, B. L.; McMahon, T. A. (2007): Updated world map of the Köppen-Geiger climate classification. In Hydrology and Earth System Sciences 11, pp. 1633–1644.

Peng, Haidong; Mayer, Bernhard; Norman, Ann-Lise; Krouse, H. Roy (2005): Modelling of hydrogen and oxygen isotope compositions for local precipitation. In Tellus B: Chemical and Physical Meteorology 57 (4), pp. 273–282. DOI: 10.3402/tellusb.v57i4.16545.

Penniston-Dorland, Sarah; Liu, Xiao-Ming; Rudnick, Roberta L. (2017): Lithium Isotope Geochemistry. In Fang-Zhen Teng, James Watkins, Nicolas Dauphas (Eds.): Non-traditional stable isotopes. [Berlin]: De Gruyter.

Pfahl, S.; Sodemann, H. (2014): What controls deuterium excess in global precipitation? In Clim. Past 10 (2), pp. 771–781. DOI: 10.5194/cp-10-771-2014.

Piper, Arthur M. (1944): A graphic procedure in the geochemical interpretation of water-analyses. In Trans. AGU 25 (6), p. 914. DOI: 10.1029/TR025i006p00914.

Pistiner, Janna S.; Henderson, Gideon M. (2003): Lithium-isotope fractionation during continental weathering processes. In Earth and Planetary Science Letters 214 (1), pp. 327–339. DOI: 10.1016/S0012-821X(03)00348-0.

Pogge von Strandmann, Philip A.E.; Burton, Kevin W.; James, Rachael H.; Calsteren, Peter van; Gíslason, Sigurður R.; Mokadem, Fatima (2006): Riverine behaviour of uranium and lithium isotopes in an actively glaciated basaltic terrain. In Earth and Planetary Science Letters 251 (1-2), pp. 134–147. DOI: 10.1016/j.epsl.2006.09.001.

Pogge von Strandmann, Philip A.E.; Frings, Patrick J.; Murphy, Melissa J. (2017): Lithium isotope behaviour during weathering in the Ganges Alluvial Plain. In Geochimica et Cosmo-chimica Acta 198, pp. 17–31. DOI: 10.1016/j.gca.2016.11.017.

Pogge von Strandmann, Philip A.E.; Porcelli, Don; James, Rachael H.; Calsteren, Peter van; Schaefer, Bruce; Cartwright, Ian et al. (2014): Chemical weathering processes in the Great Artesian Basin: Evidence from lithium and silicon isotopes. In Earth and Planetary Science Letters 406, pp. 24–36. DOI: 10.1016/j.epsl.2014.09.014.

Pohl, Eric; Knoche, Malte; Gloaguen, Richard; Andermann, Christoff; Krause, P. (2015): Sensitivity analysis and implications for surface processes from a hydrological modelling ap-

proach in the Gunt catchment, high Pamir Mountains. In Earth Surf. Dynam. 3 (3), pp. 333–362. DOI: 10.5194/esurf-3-333-2015.

Ramesh, R.; Sarin, M. M. (1992): Stable isotope study of the Ganga (Ganges) river system. In Journal of Hydrology 139, pp. 49–62. Available online at http://www.sciencedirect.com/science/article/pii/002216949290194Z.

Ricketts, Richard D.; Johnson, Thomas C.; Brown, Erik T.; Rasmussen, Kenneth a.; Romanovsky, Vladimir V. (2001): The Holocene paleolimnology of Lake Issyk-Kul, Kyrgyzstan: trace element and stable isotope composition of ostracodes. In Palaeogeography, Palaeoclimatology, Palaeoecology 176 (1-4), pp. 207–227. DOI: 10.1016/S0031-0182(01)00339-X.

Rindsberger, M.; Magaritz, M.; Carmi, I.; d. Gilad (1983): The relation between air mass trajectories and the water isotope composition of rain in the Mediterranean Sea area. In Geophys. Res. Lett 10 (1), pp. 43–46. DOI: 10.1029/GL010i001p00043.

Rizk, Zein S.; Alsharhan, Abdulrahman S. (2003): Water resources in the United Arab Emirates. In Abdulrahman S. Alsharhan, Warren W. Wood (Eds.): Developments in Water Science : Water Resources Perspectives: Evaluation, Management and Policy, vol. 50: Elsevier, pp. 245–264. Available online at http://www.sciencedirect.com/science/article/pii/S0167564803800229.

Robinson, Alexander C.; an Yin; Manning, Craig E.; Harrison, T. Mark; Zhang, Shuan-Hong; Wang, Xiao-Feng (2004): Tectonic evolution of the northeastern Pamir: Constraints from the northern portion of the Cenozoic Kongur Shan extensional system, western China. In Geol Soc America Bull 116 (7), p. 953. DOI: 10.1130/B25375.1.

Rolph, Glenn; Stein, Ariel F.; Stunder, Barbara J. B. (2017): Real-time Environmental Applications and Display sYstem: READY. In Environmental Modelling & Software 95, pp. 210–228. DOI: 10.1016/j.envsoft.2017.06.025.

Rozanski, Kazimierz; Araguás-Araguás, Luis J.; Gonfiantini, Roberto (1993): Isotopic Patterns in Modern Global Precipitation. In P. K. Swart, K. C. Lohmann, Jeffrey M. Mckenzie, S. Savin (Eds.): Climate Change in Continental Records, vol. 78. Washington DC, pp. 1–36. Available online at http://www.agu.org/books/gm/v078/GM078p0001/GM078p0001.shtml.

Rudnick, Roberta L.; Tomascak, Paul B.; Njo, Heather B.; Gardner, L. Robert (2004): Extreme lithium isotopic fractionation during continental weathering revealed in saprolites from South Carolina. In Chemical Geology 212 (1), pp. 45–57. DOI: 10.1016/j.chemgeo.2004.08.008.

Schneider, Petra; Neitzel, Peter L.; Schaffrath, Martin; Schlumprecht, Helmut (2003): Leitbildorientierte physikalisch-chemische Gewässerbewertung – Referenzbedingungen und Qualitätsziele. Edited by umweltbundesamt. Berlin (UBA Texte, 15/03).

Schwab, Martina; Ratschbacher, Lothar; Siebel, Wolfgang; McWilliams, Michael; Minaev, Vladislav; Lutkov, Valery et al. (2004): Assembly of the Pamirs: Age and origin of magmatic belts from the southern Tien Shan to the southern Pamirs and their relation to Tibet. In Tectonics 23 (4), n/a-n/a. DOI: 10.1029/2003TC001583.

Seitz, Hans-Michael; Brey, Gerhard P.; Lahaye, Yann; Durali, Soodabeh; Weyer, Stefan (2004): Lithium isotopic signatures of peridotite xenoliths and isotopic fractionation at high temperature between olivine and pyroxenes. In Chemical Geology 212 (1-2), pp. 163–177. DOI: 10.1016/j.chemgeo.2004.08.009.

Seitz, Hans-Michael; Woodland, Alan B. (2000): The distribution of lithium in peridotitic and pyroxenitic mantle lithologies — an indicator of magmatic and metasomatic processes. In Chemical Geology 166 (1), pp. 47–64. DOI: 10.1016/S0009-2541(99)00184-9.

Shearer, C.K; Papike, J.J; Laul, J.C (1987): Mineralogical and chemical evolution of a rare-element granite-pegmatite system: Harney Peak Granite, Black Hills, South Dakota. In Geochimica et Cosmochimica Acta 51 (3), pp. 473–486. DOI: 10.1016/0016-7037(87)90062-7.

Sigg, Laura; Stumm, Werner (1996): Aquatische Chemie. Eine Einführung in die Chemie wässriger Lösungen und natürlicher Gewässer. 4., durchges. Aufl. Zürich: vdf.

Steffensen, Jørgen Peder; Andersen, Katrine K.; Bigler, Matthias; Clausen, Henrik B.; Dahl-Jensen, Dorthe; Fischer, Hubertus et al. (2008): High-resolution Greenland ice core data show abrupt climate change happens in few years. In Science (New York, N.Y.) 321 (5889), pp. 680–684. DOI: 10.1126/science.1157707.

Stein, Ariel F.; Draxler, R. R.; Rolph, Glenn; Stunder, Barbara J. B.; Cohen, M. d.; Ngan, F. (2015): NOAA's HYSPLIT Atmospheric Transport and Dispersion Modeling System. In Bull. Amer. Meteor. Soc. 96 (12), pp. 2059–2077. DOI: 10.1175/BAMS-D-14-00110.1.

Stern, Libby A.; Blisniuk, Peter M. (2002): Stable isotope composition of precipitation across the southern Patagonian Andes. In Journal of Geophysical Research 107 (D23), ACL 3-1-ACL 3-14. DOI: 10.1029/2002JD002509.

Stewart, Michael K. (1975): Stable isotope fractionation due to evaporation and isotopic exchange of falling waterdrops: Applications to atmospheric processes and evaporation of lakes. In J. Geophys. Res 80 (9), pp. 1133–1146. DOI: 10.1029/JC080i009p01133.

Stichler, Willibald; Herrmann, A.; Rau, R. G. (1986): Modelling snowmelt runoff using environmental isotope and conventional methods. In E. M. Morris (Ed.): Modelling Snowmelt-Induced Processes: IAHS Press, pp. 231–244.

Stumpp, C.; Klaus, J.; Stichler, Willibald (2014): Analysis of long-term stable isotopic composition in German precipitation. In Journal of Hydrology 517, pp. 351–361. DOI: 10.1016/j.jhydrol.2014.05.034.

Tang, Yan-Jie; Zhang, Hong-Fu; Ying, Ji-Feng (2007): Review of the Lithium Isotope System as a Geochemical Tracer. In International Geology Review 49, pp. 374–388, checked on 7/15/2015.

Taylor, Susan; Feng, Xiahong; Kirchner, James W.; Osterhuber, Randall; Klaue, Björn; Renshaw, Carl E. (2001): Isotopic evolution of a seasonal snowpack and its melt. In Water Resources Research 37 (3), pp. 759–769. DOI: 10.1029/2000WR900341.

Taylor, Susan; Feng, Xiahong; Williams, Mark; McNamara, James (2002): How isotopic fractionation of snowmelt affects hydrograph separation. In Hydrological Processes 16 (18), pp. 3683–3690. DOI: 10.1002/hyp.1232.

Taylor, Thomas Ivan; Urey, Harold C. (1938): Fractionation of the Lithium and Potassium Isotopes by Chemical Exchange with Zeolites. In The Journal of Chemical Physics 6 (8), pp. 429–438. DOI: 10.1063/1.1750288.

Teng, Fang-Zhen; Rudnick, Roberta L.; McDonough, William F.; Wu, Fu-Yuan (2009): Lithium isotopic systematics of A-type granites and their mafic enclaves: Further constraints on the Li isotopic composition of the continental crust. In Chemical Geology 262 (3), pp. 370–379. DOI: 10.1016/j.chemgeo.2009.02.009.

Teng, Fang-Zhen; Watkins, James; Dauphas, Nicolas (Eds.) (2017): Non-traditional stable isotopes. [Berlin]: De Gruyter.

Terzer, S.; Wassenaar, L. I.; Araguás-Araguás, Luis J.; Aggarwal, Pradeep K. (2013): Global isoscapes for $\delta18O$ and $\delta2H$ in precipitation: improved prediction using regionalized climatic regression models. In Hydrol. Earth Syst. Sci 17 (11), pp. 4713–4728. DOI: 10.5194/hess-17-4713-2013.

Tian, Lide; Yao, Tandong; MacClune, Kenneth; White, James W. C.; Schilla, A.; Vaughn, B. et al. (2007): Stable isotopic variations in west China: A consideration of moisture sources. In Journal of Geophysical Research 112 (D10), 1-12. DOI: 10.1029/2006JD007718.

Tichomirowa, M.; Heidel, C.; Junghans, M.; Haubrich, F.; Matschullat, J. (2010): Sulfate and strontium water source identification by O, S and Sr isotopes and their temporal changes (1997–2008) in the region of Freiberg, central-eastern Germany. In Chemical Geology 276 (1), pp. 104–118. DOI: 10.1016/j.chemgeo.2010.06.004.

Tomascak, Paul B. (2004): Developments in the Understanding and Application of Lithium Isotopes in the Earth and Planetary Sciences. In Reviews in Mineralogy and Geochemistry 55 (1), pp. 153–195. DOI: 10.2138/gsrmg.55.1.153.

Tomascak, Paul B.; Magna, Tomáš; Dohmen, Ralf (2016): Advances in Lithium isotope geochemistry. Cham, Heidelberg, New York, Dordrecht, London: Springer (Advances in isotope geochemistry).

U.S. Geological Survey (2015): GW Chart. Version 1.29.0.0: U.S. Geological Survey. Available online at https://water.usgs.gov/water-resources/software/GW-CHART/, checked on 7/2/2019.

Uemura, Ryu; Matsui, Yohei; Yoshida, Naohiro; Abe, Osamu; Mochizuki, Shigeto (2005): Isotopic fractionation of water during snow formation: Experimental evidence of kinetic effect. In Polar Meteorol. Glaciol. 19, pp. 1–14.

Varol, Memet; Gökot, Bülent; Bekleyen, Aysel; Şen, Bülent (2013): Geochemistry of the Tigris River basin, Turkey: Spatial and seasonal variations of major ion compositions and their con-trolling factors. In Quaternary International 304, pp. 22–32. DOI: 10.1016/j.quaint.2012.12.043.

Viviroli, Daniel; Weingartner, Rolf (2004): The hydrological significance of mountains: from regional to global scale. In Hydrol. Earth Syst. Sci 8 (6), pp. 1017–1030. DOI: 10.5194/hess-8-1017-2004.

Viviroli, Daniel; Weingartner, Rolf; Messerli, Bruno (2003): Assessing the Hydrological Significance of the World's Mountains. In Mountain Research and Development 23 (1), pp. 32–40. DOI: 10.1659/0276-4741(2003)023[0032:ATHSOT]2.0.CO;2.

Wang, Xiaoyan; LI, Zhongqin; Tayier, Ruozihan; Wang, Shengjie (2015): Characteristics of atmospheric precipitation isotopes and isotopic evidence for the moisture origin in Yushugou River basin, Eastern Tianshan Mountains, China. In Quaternary International 380-381, pp. 106–115. DOI: 10.1016/j.quaint.2014.12.023.

Wanner, Christoph; Bucher, Kurt; Pogge von Strandmann, Philip A.E.; Waber, H. Niklaus; Pettke, Thomas (2017): On the use of Li isotopes as a proxy for water–rock interaction in fractured crystalline rocks: A case study from the Gotthard rail base tunnel. In Geochimica et Cosmochimica Acta 198, pp. 396–418. DOI: 10.1016/j.gca.2016.11.003.

Wanner, Christoph; Sonnenthal, Eric L.; Liu, Xiao-Ming (2014): Seawater δ7Li: A direct proxy for global CO2 consumption by continental silicate weathering? In Chemical Geology 381, pp. 154–167. DOI: 10.1016/j.chemgeo.2014.05.005.

West, Jason B.; Bowen, Gabriel J.; Dawson, Todd E.; Tu, Kevin P. (Eds.) (2009): Isoscapes: Understanding movement, pattern, and process on Earth through isotope mapping. 1st ed.: Springer. Available online at http://www.amazon.com/Isoscapes-Understanding-movement-pattern-process/dp/904813353X.

Wimpenny, Josh; James, Rachael H.; Burton, Kevin W.; Gannoun, Abdelmouhcine; Mokadem, Fatima; Gíslason, Sigurður R. (2010): Glacial effects on weathering processes: New insights from the elemental and lithium isotopic composition of West Greenland rivers. In Earth and Planetary Science Letters 290 (3-4), pp. 427–437. DOI: 10.1016/j.epsl.2009.12.042.

Woodland, Alan B.; Seitz, Hans-Michael; Yaxley, G.M (2004): Varying behaviour of Li in metasomatised spinel peridotite xenoliths from western Victoria, Australia. In Lithos 75 (1), pp. 55–66. DOI: 10.1016/j.lithos.2003.12.014.

Wunder, Bernd; Meixner, Anette; Romer, Rolf L.; Heinrich, Wilhelm (2006): Temperature-dependent isotopic fractionation of lithium between clinopyroxene and high-pressure hydrous fluids. In Contrib Mineral Petrol 151 (1), pp. 112–120. DOI: 10.1007/s00410-005-0049-0.

Yao, Tandong; Masson-Delmotte, Valérie; Gao, Jing; Yu, Wusheng; Yang, XiaoXin; Risi, Camille et al. (2013): A review of climatic controls on δ 18 O in precipitation over the Tibetan Plateau: Observations and simulations. In Reviews of Geophysics 51 (4), pp. 525–548. DOI: 10.1002/rog.20023.

Yao, Tandong; Thompson, Lonnie G.; Mosbrugger, Volker; Zhang, Fan; Ma, Yaoming; Luo, Tianxiang et al. (2012): Third Pole Environment (TPE). In Environmental Development 3, pp. 52–64. DOI: 10.1016/j.envdev.2012.04.002.

Yurtsever, Y.; Gat, Joel R. (1981): Atmospheric waters.

Zech, Roland; Abramowski, Uwe; Glaser, Bruno; Sosin, Pjotr; Kubik, Peter W.; Zech, Wolfgang (2005): Late Quaternary glacial and climate history of the Pamir Mountains derived from cosmogenic 10Be exposure ages. In Quaternary Research 64 (2), pp. 212–220. DOI: 10.1016/j.yqres.2005.06.002.

Żelazny, Mirosław; Astel, Aleksander; Wolanin, Anna; Małek, Stanisław (2011): Spatiotemporal dynamics of spring and stream water chemistry in a high-mountain area. In Environmental Pollution 159 (5), pp. 1048–1057. DOI: 10.1016/j.envpol.2010.11.021.

Zhu, Bingqi; Yu, Jingjie; Qin, Xiaoguang; Rioual, Patrick; Xiong, Heigang (2012): Climatic and geological factors contributing to the natural water chemistry in an arid environment from watersheds in northern Xinjiang, China. In Geomorphology 153-154, pp. 102–114. DOI: 10.1016/j.geomorph.2012.02.014.

This dissertation includes excerpts of the following articles:

- "Stable isotopes in river waters in the Tajik Pamirs: regional and temporal characteristics" published by Taylor & Francis in Journal "Isotopes in Environmental and Health studies" in 2013, available online: https://www.tandfonline.com/doi/abs/10.1080/10256016.2013.835809. Christiane Meier is first author of this article and has the right to include the Accepted Manuscript in this dissertation.

- "Assessing moisture sources of precipitation in the Western Pamir Mountains (Tajikistan, Central Asia) using deuterium excess" published by Taylor & Francis in Journal "Tellus B: Chemical and Physical Meteorology" in 2019, available online: https://www.tandfonline.com/doi/full/10.1080/16000889.2019.1601987. Christiane Meier is second author of this article, contributed with the first author equally to this work, and has the right to include the Accepted Manuscript in this dissertation.

- "First Lithium Isotope Data from Rivers and Subsurface Water in the Pamirs" published by Elsevier in Journal "Procedia Earth and Planetary Science" in 2017, available online: https://www.sciencedirect.com/science/article/pii/S1878522016301813?via%3Dihub. Christiane Meier is author of this article and has the right to include the Accepted Manuscript in this dissertation.

10 Appendix

Appendix Table 1: Overview about location, sampling rhythm, sampling period of all water samples that were collected in the Gunt catchment.

Location number	name	Latitude (°dec N)	Longitude (°dec E)	Altitude (m a.s.l.)	Sampling interval	Sampling period	Number of samples	Water type
010	Gunt	37.488998	71.522440	2086	monthly	fieldtrip 08/2011, 10/2011-11/2014	37	main stream
020	Shakdara	37.479097	71.590958	2119	monthly	fieldtrip 08/2011, 10/2011-11/2014	37	tributary from south
021	Tusion	37.371956	71.661920	2597	once	fieldtrip 08/2013	1	cold spring
022	Sejd	37.210668	72.073271	2980	once	fieldtrip 08/2013	1	cold spring
023	Kök	37.290308	72.223074	3184	once	fieldtrip 08/2013	1	hot spring
024	Shakhdara - 1 km downstream Nimos	37.309291	72.221727	3197	twice	fieldtrip 08/2013, 09/2014	2	tributary from south
025	Nimos	37.318953	72.223556	3232	once	fieldtrip 08/2013	1	tributary from north
026	Shoshboard	37.352598	72.279145	3256	once	fieldtrip 08/2013	1	tributary from north
027	1. northern tributary to Shakhdara	37.381183	72.349193	3410	once	fieldtrip 08/2013	1	tributary from north
028	Shakhdara - near Javshangoz	37.353898	72.421511	3418	once	fieldtrip 08/2013	1	tributary from south
029	Drumdara	37.213667	72.069617	2972	once	fieldtrip 08/2013	1	tributary from north
0210	Shakhdara - upstream from Shohirizm	37.187711	72.004561	2866	once	fieldtrip 08/2013	1	tributary from south
030	Gunt - near Pamir Energy	37.483121	71.593002	2102	monthly	fieldtrip 08/2011, 10/2011-11/2014	37	main stream
031	Bidurd	37.536774	71.656691	2281	three times	fieldtrip 03/2013, 08/2013, 09/2014	3	tributary from north
032	Outflow in gallery	37.516806	71.591597	2252	once	fieldtrip 09/2014	1	cold spring
040=510	Bogevdara	37.527538	71.659213	2291	monthly	fieldtrip 08/2011, 10/2011-11/2014	21	tributary from south
041	Gunt	37.532833	71.657444	2273	monthly	11/2011-11/2014	34	main stream
042=500	Zjemjetdara	37.531897	71.655217	2295	monthly	04/2013-11/2014	12	tributary from north
043	Bogev - debris cone	37.536774	71.656691	2447	once	fieldtrip 08/2013	1	cold spring
044	Manem	37.546034	71.684943	2430	once	fieldtrip 08/2013	1	cold spring
045	Navabad - upstream	37.675889	71.836321	2580	once	fieldtrip 08/2013	1	cold spring
050	Barsemdara	37.564161	71.720747	2368	monthly	fieldtrip 08/2011, 10/2011-11/2014	37	tributary from north
051	Barsem	37.569462	71.713297	2577	once	fieldtrip 08/2013	1	cold spring
060	Gunt	37.562528	71.721222	2347	monthly	10/2011-11/2014	36	main stream
070	Shirindara	37.567649	71.728767	2359	monthly	fieldtrip 08/2011, 10/2011-11/2014	37	tributary from south
080	Tang - Reservoir from Pamir Energy	37.614902	71.759137	2467	monthly	fieldtrip 08/2011, 10/2011-02/2013	18	main stream
090	Gunt	37.633831	71.769528	2479	monthly	10/2011-11/2014	35	main stream
091	Gunt	37.644333	71.792611	2510	once	11/2011	1	main stream
100	Rivakdara	37.634681	71.799942	2570	monthly	fieldtrip 08/2011, 10/2011-11/2014	37	tributary from south
101=520	Big Mundara	37.663778	71.820516	2580	monthly	06/2013-11/2014	9	tributary from north
102=530	Gunt	37.671211	71.832382	2577	monthly	04/2013-11/2014	19	main stream
110	Groundwater Navabad	37.672563	71.833468	2564	monthly	08/2011-11/2014, fieldtrip 08/2013	38	well
111=540	Debastadara	37.681285	71.846126	2601	monthly	fieldtrip 08/2011, 10/2011-11/2014	20	tributary from north
112=550	Gunt	37.679689	71.849369	2585	monthly	04/2013-11/2014	19	main stream
120	Vibistdara (West)	37.695025	71.870723	2632	monthly	fieldtrip 08/2011, 10/2011-11/2014	37	tributary from north
121=560	Gunt	37.701943	71.886032	2615	monthly	04/2013-11/2014	19	main stream
130	Vibistdara (East)	37.711694	71.896260	2654	monthly	fieldtrip 08/2011, 10/2011-11/2014	33	tributary from north
140	Gunt	37.699028	71.919231	2648	monthly	10/2011-11/2014	36	main stream
150	near Dehmiyona	37.697823	71.926077	2680	monthly	fieldtrip 08/2011, 10/2011-09/2014	28	tributary from south
151	x	37.713781	71.954323	2783	once	fieldtrip 08/2011	1	tributary from south
160	Vushdara	37.714678	71.963297	2716	monthly	fieldtrip 08/2011, 10/2011-11/2014	36	tributary from south
170	Gunt	37.722972	71.980083	2729	monthly	10/2011-11/2014	36	main stream
180	Shubordara	37.724433	71.978075	2734	monthly	fieldtrip 08/2011, 10/2011-11/2014	37	tributary from north
190	Shitamdara	37.742381	72.020672	2787	monthly	fieldtrip 08/2011, 10/2011-11/2014	37	tributary from north
200	Zuvordara	37.736097	72.029778	2793	monthly	fieldtrip 08/2011, 10/2011-11/2014	37	tributary from north
201	Werdara	37.736967	72.081486	2916	once	fieldtrip 08/2011	1	tributary from south
210	Gunt	37.743889	72.149611	2934	monthly	10/2011-11/2014	36	main stream
211=590	Charthemdara	37.715397	72.166028	2947	monthly	fieldtrip 08/2011, 10/2011-11/2014	20	tributary from south
212	x	37.697528	72.185992	3003	once	fieldtrip 08/2011	1	tributary from south
220	Oqmamaddara	37.698367	72.209950	3013	monthly	fieldtrip 08/2011, 10/2011-11/2014	30	tributary from south

230	Patkhurdara	37.707619	72.206150	3020	monthly	fieldtrip 08/2011, 10/2011-11/2014	37	tributary from north
231	Patkhur - swampy spring	37.706398	72.203881	3024	once	fieldtrip 08/2013	1	cold spring
232	Patkhur - spring from tube	37.706398	72.203881	3024	once	fieldtrip 08/2013	1	cold spring
240	Gunt	37.716667	72.298667	3083	once	10/2011	1	main stream
241	Gunt	37.707639	72.349750	3121	monthly	11/2011-11/2014	35	main stream
242	Sardem hillside, small creek	37.727558	72.299436	3320	once	fieldtrip 08/2013	1	tributary from north
243	Sardem hillside, small creek	37.725395	72.297411	3246	once	fieldtrip 08/2013	1	tributary from north
244	Sardem hillside	37.725357	72.297056	3241	once	fieldtrip 08/2013	1	cold spring
245	Sardem hillside, creek	37.721843	72.296623	3163	once	fieldtrip 08/2013	1	tributary from north
246	Sardem - river plain	37.707851	72.315883	3095	once	fieldtrip 08/2013	1	cold spring
250	Varshedzdara	37.702373	72.344249	3142	monthly	fieldtrip 08/2011, 10/2011-11/2014	37	tributary from south
260	Shazuddara	37.708025	72.357994	3169	monthly	fieldtrip 08/2011, 10/2011-11/2014	37	tributary from north
270	Gunt	37.706386	72.359842	3131	monthly	fieldtrip 08/2011, 10/2011-11/2014	37	main stream
280	Toguzbulok	37.700839	72.389097	3155	monthly	fieldtrip 08/2011, 10/2011-11/2014	36	tributary from south
281	Juz Okmaylok	37.640486	72.533978	3465	twice	fieldtrip 08/2011, 09/2014	2	tributary from north
282=600	Dushakdara	37.700168	72.397032	3189	monthly	04/2013-11/2014	19	tributary from south
290	Dzelondi - tube	37.628158	72.546814	3512	monthly	fieldtrip 08/2011, 10/2011-09/2014, fieldtrip 08/2013	33	hot spring
300	Dzelondi - in building	37.628119	72.545968	3506	monthly	fieldtrip 08/2011, 10/2011-09/2014, fieldtrip 08/2013	36	hot spring
301	northern tributary - Okkuldara(?)	37.493646	72.727636	3938	once	fieldtrip 08/2013	1	tributary from north
302	Koitezek-River	37.480678	72.782775	4274	twice	fieldtrip 08/2013, 09/2014	2	tributary from south
303	Glaciertour Koitezek	37.436173	72.802661	4462	once	fieldtrip 08/2013	1	tributary from south
304	Glaciertour Koitezek	37.419802	72.811128	4539	once	fieldtrip 08/2013	1	tributary from south
305	Glacier 2 - runoff	37.40882190	72.81888330	4716	once	fieldtrip 08/2013	1	glacier melt
306	Glacier 1 - mouth	37.41197840	72.81287490	4594	once	fieldtrip 08/2013	1	glacier melt
307	Glaciertour - debris cone	37.409840	72.808243	4653	once	fieldtrip 08/2013	1	cold spring
308	Glaciertour - wetland	37.420770	72.810182	4535	once	fieldtrip 08/2013	1	cold spring
310	Outflow of Yashikul	37.791286	72.743397	3727	twice	fieldtrip 08/2011, 09/2014	2	plateau area
311	Tributary to Yashikul	37.783676	72.778658	3749	once	fieldtrip 08/2011	1	plateau area
320	Tributary to Yashikul	37.782841	72.784545	3746	once	fieldtrip 08/2011	1	plateau area
330	Tributary to Yashikul	37.767294	72.836464	3805	once	fieldtrip 08/2011	1	plateau area
340	Hot spring near Yashikul	37.731056	72.890828	3791	once	fieldtrip 08/2011	1	hot spring
350	Outlet Bulunkul	37.740537	72.984063	3728	twice	fieldtrip 08/2011, 09/2014	2	plateau area
351	Well Bulunkul	37.750884	73.261271	3892	once	fieldtrip 08/2013	1	well
360	Inflow (Alichur) to Yashikul	37.770001	72.974523	3727	once	fieldtrip 08/2011	1	plateau area
370	Geysir	37.743163	73.068783	3782	once	fieldtrip 08/2011	1	hot spring
380	Alichur	37.748222	73.251724	3878	once	fieldtrip 08/2011	1	plateau area
381	Well Alichur	37.750884	73.261271	3892	twice	fieldtrip 03/2013, 08/2013	2	well
382	Akbalik	37.793546	73.392275	3900	three times	fieldtrip 03/2013, 08/2013, 09/2014	3	well
383	Well Murghab	38.168729	73.965022	3609	once	fieldtrip 03/2013	1	well
384	Gunt before Alichur	37.748222	73.251724	3878	once	fieldtrip 03/2013	1	main stream
385	Gunt near Alichur	37.748222	73.251724	3878	once	fieldtrip 03/2013	1	main stream
386	Refreezing near Alichur	37.748222	73.251724	3878	once	fieldtrip 03/2013	1	refreezing
387	Akbalik source	37.793469	73.392292	3900	once	fieldtrip 09/2014	1	cold spring
390	Narsan (Arteser)	37.197657	71.546920	2605	once	fieldtrip 08/2011	1	well
400	Garm Chashma	37.203637	71.537207	2568	once	fieldtrip 08/2011	1	hot spring
15a	muddy water	37.697596	71.926185	2680	once	fieldtrip 08/2011	1	tributary from south
A	Khorog	37.488998	71.52244	2086	monthly or event based	01/2012-10/2014	99	meteostation
B	Navabad	37.672563	71.833468	2564	monthly or event based	01/2012-10/2014	81	meteostation
C	Bulunkul	37.7045784	72.9451011	3760	monthly or event based	11/2012-09/2014	35	meteostation
D	Dzavjangoz	37.4	72.4	3438	monthly or event based	06/2013-08/2014	11	meteostation
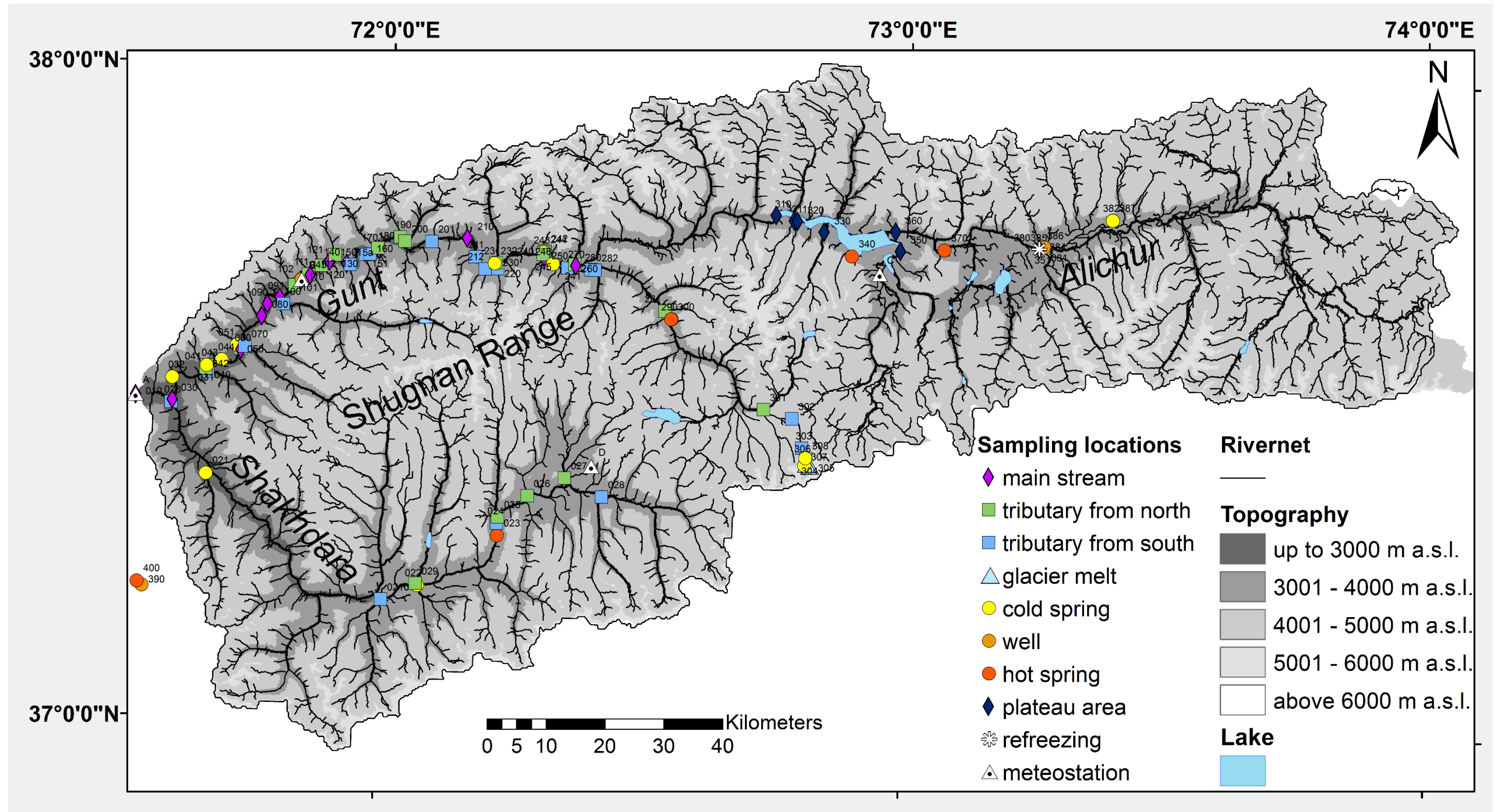
Appendix Figure 1: Map showing all sampling locations including each location number. Coordinates and sampling period are listed in appendix table 1.
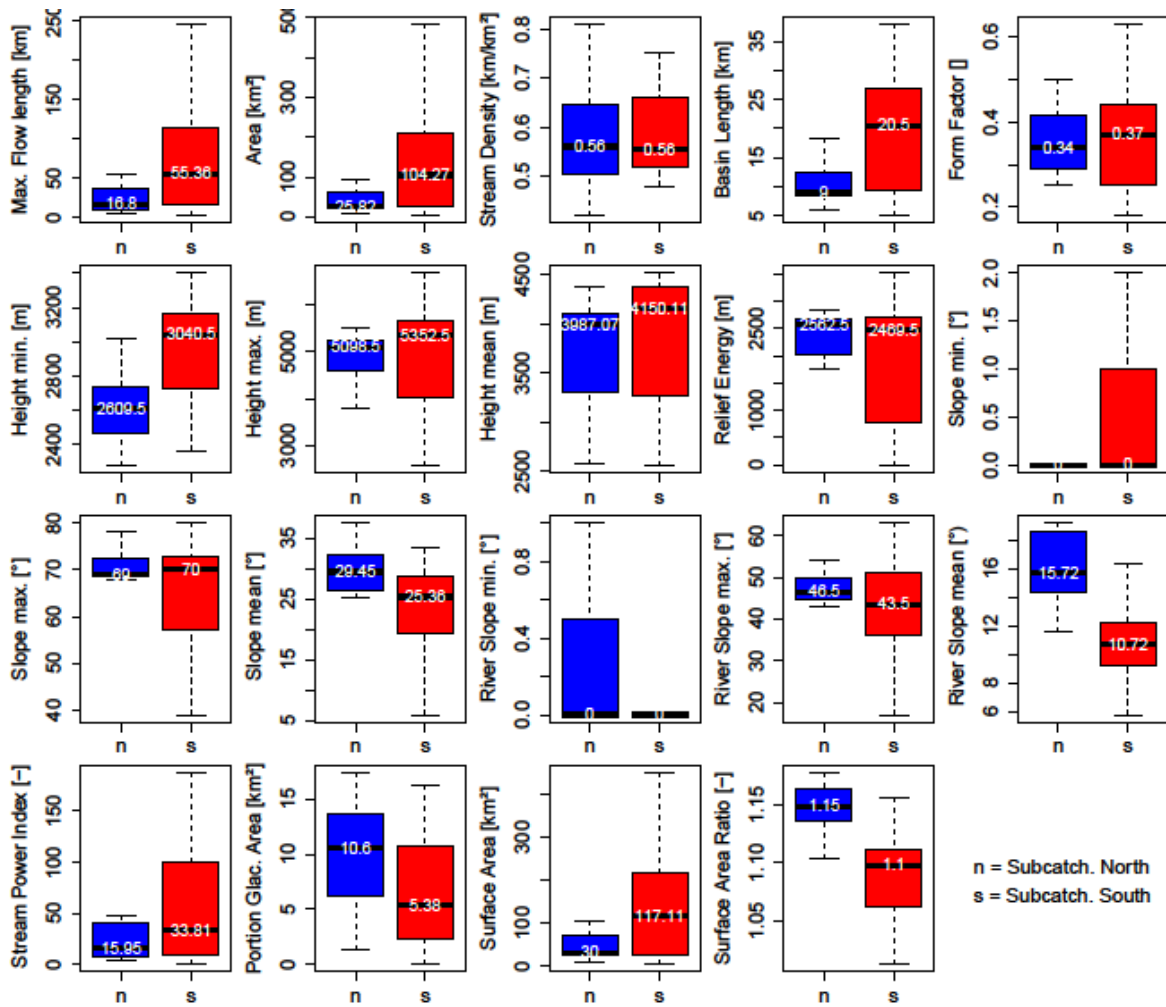
Appendix Figure 2: Comparison of catchment characteristics distinguished between northern and southern sub-catchments.

Appendix Table 2: List of monthly integrated and event-based precipitation samples and their δ^{18}O and δ^{2}H isotope values from two stations in the Western Pamir mountains. This data was also used by Meier et al. (2015a) and Meier et al. (2015b).

Annex_Table_2.pdf

only available in attached digital file

Appendix Table 3: List of GNIP stations and additional literature whose monthly isotope data was used for the calculation of averages

Annex_Table_3.pdf

only available in attached digital file

Appendix Table 4: List of surface water samples and
          their δ^{18}O and δ^2H isotope values.

Annex_Table_4.pdf

only available in attached digital file

Appendix Table 5: List of surface water samples and
          their major anion and major cation concen-
          trations.

Annex_Table_5.pdf

only available in attached digital file

Appendix Table 6: Saturation indices (SI) of surface
          water samples.

Annex_Table_6.pdf

only available in attached digital file

.

Appendix Table 7: Input parameters for correlation analysis between major ions and catchment parameters.

Location number	Water type	Altitude$_{min}$ (m a.s.l.)	Altitude$_{max}$ (m a.s.l.)	Altitude$_{mean}$ (m a.s.l.)	Area (km²)	Permafrost$_{discont}$ (%)	Permafrost$_{cont}$ (%)	Glaciation (%)	Unconsolidated rock (%)	Limestone (%)	Magmatic rock (%)	Metamorphic rock (%)	Aspect flat (%)	Aspect N (%)	Aspect NO (%)	Aspect O (%)	Aspect SO (%)	Aspect S (%)	Aspect SW (%)	Aspect W (%)	Aspect NW (%)	Slope 0-1 (°)	Slope 1-2 (°)	Slope 2-3 (°)	Slope 3-4 (°)	Slope 4-5 (°)	Slope 5-6 (°)	Slope >6 (°)	Runoff rate (mm/a)	Cl (meq/L)	SO₄ (meq/L)	Na (meq/L)	K (meq/L)	Mg (meq/L)	Ca (meq/L)	HCO₃calc (meq/L)	EC [µS/cm]	T [°C]	pH
010	main stream	2060	4300	2746.4	32.6	5.7	0.0	0.0	32.2	0.0	7.5	60.3	0.4	21.3	6.5	3.1	10.5	30.6	13.3	5.3	8.8	13.4	12.7	18.2	20.3	15.9	9.0	10.4	434.0	0.1	0.4	0.3	0.1	0.3	1.3	1.5	194.5	7.3	7.5
020	southern tributary	2092	6676	4168.0	4180.9	81.1	44.2	4.1	25.9	0.0	15.4	59.4	0.2	13.3	13.5	12.6	11.7	12.2	12.5	11.9	12.0	13.3	24.9	23.9	18.2	10.3	4.8	4.5	268.0	0.2	0.8	0.3	0.1	0.4	1.8	1.7	253.2	7.6	7.4
030	main stream	2090	5033	3784.2	272.8	60.6	27.3	1.1	23.7	0.0	45.6	30.7	0.2	16.8	15.1	9.4	10.0	13.7	14.8	10.0	9.9	7.5	16.8	23.3	23.8	15.1	7.5	6.0	434.0	0.1	0.3	0.3	0.1	0.3	1.1	1.4	173.7	7.7	7.3
041	main stream	2272	4640	3014.9	37.3	12.0	1.2	0.0	13.3	0.0	17.1	69.6	0.2	14.4	3.9	7.8	26.8	18.7	8.6	8.3	11.3	7.9	12.8	20.9	22.4	17.4	9.4	9.2	434.0	0.1	0.3	0.3	0.1	0.3	1.1	1.4	172.6	6.6	7.2
050	northern tributary	2365	4951	3932.9	28.3	66.2	36.1	4.4	13.5	0.0	24.6	61.8	0.0	9.2	18.0	16.7	17.0	22.0	14.0	2.4	0.7	4.7	12.9	18.5	20.2	16.8	12.0	14.9	434.0	0.0	0.1	0.1	0.1	0.1	0.5	0.5	148.0	6.8	6.9
060	main stream	2322	5209	3675.0	80.0	50.6	26.0	0.9	18.5	0.0	24.2	57.3	0.1	9.4	12.3	12.7	18.0	17.3	11.9	7.3	11.0	5.7	10.4	14.5	19.3	18.4	12.8	18.9	434.0	0.1	0.3	0.3	0.1	0.3	1.2	1.4	170.4	7.2	7.3
070	southern tributary	2363	5305	4075.6	188.1	76.3	41.2	3.1	28.7	0.0	57.1	14.2	0.2	19.1	12.8	5.0	6.0	17.2	19.6	10.0	10.2	7.1	17.6	23.1	23.5	15.5	7.7	5.5	516.0	0.1	0.1	0.1	0.1	0.1	0.5	0.6	130.4	6.6	7.0
090	main stream	2455	5448	4117.5	523.1	75.6	50.1	7.4	26.3	0.0	50.6	23.1	0.2	16.7	12.6	8.9	11.6	15.8	13.4	9.2	11.6	9.1	17.2	20.0	20.5	15.5	9.0	8.8	434.0	0.1	0.3	0.3	0.1	0.3	1.2	1.5	179.3	7.3	7.3
120	northern tributary	2621	5296	4076.9	24.1	72.0	38.7	10.4	31.8	0.0	13.4	54.9	0.1	5.0	13.6	17.3	15.7	17.3	20.2	7.9	2.9	2.6	9.7	17.3	22.3	19.2	12.2	16.8	434.0	0.0	0.2	0.0	0.1	0.1	0.7	0.6	119.0	5.6	7.0
130	northern tributary	2651	5027	4039.7	22.1	74.7	35.5	6.8	21.4	0.0	15.2	63.3	0.0	3.0	8.6	16.9	15.5	17.2	22.9	11.0	4.8	1.8	8.3	19.2	25.4	20.5	11.4	13.3	434.0	0.0	0.2	0.0	0.0	0.2	0.7	0.9	119.2	6.5	7.0
140	main stream	2638	5319	3546.6	50.3	39.4	16.4	3.1	22.7	0.0	24.0	53.2	0.2	19.2	11.0	10.2	10.3	10.0	7.5	13.0	18.5	8.5	8.5	12.2	20.2	19.4	13.7	17.6	434.0	0.1	0.3	0.3	0.1	0.3	1.3	1.6	177.5	7.1	7.2
160	southern tributary	2692	5406	4236.1	29.9	81.3	56.1	16.4	18.3	0.0	28.6	53.1	0.2	19.9	19.9	9.4	3.3	3.1	12.6	15.7	15.8	4.8	13.5	15.3	17.7	16.6	12.5	19.7	434.0	0.1	0.8	0.3	0.1	0.2	1.5	1.9	206.3	6.9	7.1
170	main stream	2701	5417	3804.8	135.9	54.0	29.9	3.5	27.9	0.0	17.9	53.6	0.3	17.2	12.3	7.4	12.6	17.5	9.4	8.6	14.8	10.7	13.4	16.8	20.0	17.4	10.6	11.0	434.0	0.1	0.3	0.3	0.1	0.3	1.2	1.5	170.3	7.1	7.3
180	northern tributary	2737	5332	4210.8	41.7	84.0	48.7	10.7	29.6	0.0	20.6	49.9	0.1	7.3	13.8	12.8	13.8	19.0	18.8	8.6	5.7	4.3	14.5	20.6	20.4	16.7	11.0	12.5	434.0	0.0	0.2	0.1	0.1	0.3	0.8	0.9	123.0	6.5	7.0
190	northern tributary	2797	5379	4289.8	58.0	84.9	55.8	12.2	20.4	0.0	34.6	45.0	0.1	6.7	10.7	13.5	14.4	16.1	19.9	10.3	8.2	4.6	15.0	18.8	19.7	16.1	11.0	14.7	434.0	0.0	0.2	0.0	0.0	0.2	0.8	0.9	116.3	6.7	7.1
200	northern tributary	2836	5525	4282.3	63.0	81.9	54.9	17.4	31.5	0.8	16.7	51.0	0.1	6.7	5.0	8.3	19.7	21.0	13.9	11.4	13.9	6.8	17.8	18.6	18.8	15.6	9.9	12.4	434.0	0.0	0.1	0.1	0.0	0.1	0.6	0.7	124.1	6.8	7.1
210	main stream	2900	5597	4020.0	253.7	64.2	40.1	6.9	30.5	1.3	39.1	27.8	0.3	18.4	15.6	10.5	10.2	12.1	10.3	9.3	13.4	12.5	15.2	19.3	22.0	16.4	8.4	6.2	393.0	0.1	0.3	0.3	0.1	0.3	1.2	1.5	182.0	7.5	7.3
230	northern tributary	3003	6003	4503.6	204.9	90.0	70.7	27.3	37.4	0.8	16.8	44.6	0.1	10.1	9.0	11.4	14.7	18.0	14.4	10.4	11.9	11.2	20.6	17.7	17.8	14.2	8.8	9.6	885.0	0.0	0.1	0.1	0.1	0.1	0.7	0.7	102.5	7.4	7.0
241	main stream	3097	4497	3434.6	12.1	21.8	1.6	0.0	34.6	22.4	10.5	32.5	0.8	33.9	14.0	2.1	5.1	13.9	8.1	4.5	17.7	29.9	14.1	9.0	13.6	18.7	10.3	4.4	131.0	0.1	0.3	0.3	0.1	0.3	1.3	1.6	175.6	6.3	7.3
250	southern tributary	3130	5651	4561.6	70.2	94.6	71.4	16.0	30.6	1.4	61.5	6.5	0.3	17.9	15.1	13.2	15.5	6.0	4.0	9.2	18.8	9.8	19.4	22.1	20.9	14.1	7.1	6.6	131.0	0.1	0.1	0.1	0.1	0.0	0.5	0.5	133.1	6.1	6.8
260	northern tributary	3131	5448	4508.5	95.3	94.0	71.5	15.1	31.1	4.5	23.3	41.1	0.1	7.1	12.4	14.3	14.6	16.2	17.0	11.0	7.4	9.5	20.2	21.9	21.9	14.5	6.9	5.1	131.0	0.1	0.2	0.1	0.1	0.1	0.9	0.9	120.9	6.5	6.9
270	main stream	3107	5769	4389.0	6190.3	98.5	55.6	3.3	42.9	7.9	25.5	22.9	1.2	14.3	13.2	10.9	12.4	13.4	12.2	10.4	12.0	25.7	25.5	20.7	15.3	7.9	3.1	1.9	83.0	0.1	0.3	0.3	0.1	0.3	1.3	1.6	188.1	7.8	7.3
280	southern tributary	3172	5690	4429.7	1148.0	94.5	65.8	4.1	30.7	1.4	40.0	27.6	1.0	15.0	12.5	10.2	11.4	13.2	12.5	11.1	13.0	16.2	24.0	23.3	19.3	10.8	4.3	2.1	251.0	0.1	0.2	0.3	0.1	0.1	0.9	1.1	164.5	6.9	7.2

Appendix Table 8: Correlation of major ions and catchment parameters with each other. Correlation coefficients with p<0.05 are red

	Altitude$_{min}$	Altitude$_{max}$	Altitude$_{mean}$	Area	Permafrost$_{discont}$	Permafrost$_{cont}$	Glaciation	Unconsolidated rock	Limestone	Magmatic rock	Metamorphic rock	Aspect flat	Aspect N	Aspect NO	Aspect O	Aspect SO	Aspect S	Aspect SW	Aspect W	Aspect NW	Slope 0-1	Slope 1-2	Slope 2-3	Slope 3-4	Slope 4-5	Slope 5-6	Slope >6	Cl	SO₄	Na	K	Mg	Ca	HCO₃calc	Runoff rate	EC	T	pH
Altitude$_{min}$	1.00	0.25	0.60	0.07	0.50	0.57	0.49	0.54	0.46	0.09	-0.45	0.41	0.01	0.13	0.12	-0.09	-0.38	-0.15	0.20	0.32	0.39	0.33	-0.14	-0.38	-0.21	-0.22	-0.27	-0.26	-0.31	-0.24	-0.10	-0.38	-0.29	-0.24	-0.34	-0.41	-0.27	-0.39
Altitude$_{max}$	0.25	1.00	0.75	0.53	0.75	0.72	0.45	0.28	-0.25	0.22	-0.24	0.05	-0.28	0.22	0.37	-0.05	-0.46	-0.02	0.57	0.19	0.02	0.65	0.41	-0.18	-0.61	-0.45	-0.23	0.03	0.23	-0.05	0.06	-0.03	0.10	-0.04	-0.01	0.12	0.30	-0.12
Altitude$_{mean}$	0.60	0.75	1.00	0.25	0.98	0.96	0.68	0.32	-0.10	0.40	-0.46	0.01	-0.42	0.37	0.52	-0.08	-0.46	0.25	0.47	-0.02	-0.10	0.56	0.39	-0.07	-0.46	-0.34	-0.18	-0.23	-0.16	-0.47	-0.28	-0.49	-0.38	-0.50	-0.10	-0.38	-0.09	-0.55
Area	0.07	0.53	0.25	1.00	0.32	0.20	-0.19	0.40	0.17	-0.05	-0.18	0.60	0.01	0.10	0.06	-0.08	-0.18	-0.09	0.20	0.08	0.53	0.66	0.32	-0.43	-0.79	-0.68	-0.49	0.14	0.36	0.35	0.32	0.43	0.42	0.41	-0.43	0.49	0.49	0.34
Permafrost$_{discont}$	0.50	0.75	0.98	0.32	1.00	0.95	0.62	0.29	-0.20	0.41	-0.43	0.02	-0.49	0.36	0.55	-0.07	-0.40	0.34	0.48	-0.12	-0.15	0.58	0.49	-0.01	-0.52	-0.38	-0.18	-0.22	-0.12	-0.46	-0.29	-0.45	-0.36	-0.49	-0.09	-0.34	-0.02	-0.52
Permafrost$_{cont}$	0.57	0.72	0.96	0.20	0.95	1.00	0.75	0.31	-0.22	0.41	-0.43	-0.01	-0.44	0.28	0.48	-0.02	-0.37	0.21	0.48	-0.02	-0.15	0.60	0.46	-0.05	-0.52	-0.38	-0.17	-0.17	-0.15	-0.47	-0.21	-0.56	-0.38	-0.52	-0.04	-0.37	-0.03	-0.55
Glaciation	0.49	0.45	0.68	-0.19	0.62	0.75	1.00	0.25	-0.18	0.05	-0.10	-0.34	-0.40	0.01	0.35	0.09	-0.20	0.18	0.40	0.03	-0.29	0.22	0.07	-0.08	-0.09	0.06	0.18	-0.12	-0.16	-0.59	-0.27	-0.64	-0.42	-0.63	0.34	-0.54	-0.20	-0.61
Unconsolidated rock	0.54	0.28	0.32	0.40	0.29	0.31	0.25	1.00	0.43	-0.04	-0.52	0.56	0.18	-0.06	-0.24	-0.29	0.04	-0.03	0.04	0.23	0.61	0.53	0.06	-0.39	-0.48	-0.54	-0.56	-0.20	-0.16	-0.01	0.23	0.00	-0.03	0.08	-0.22	-0.13	0.09	0.10
Limestone	0.46	-0.25	-0.10	0.17	-0.20	-0.22	-0.18	0.43	1.00	-0.22	-0.28	0.57	0.57	0.12	-0.40	-0.33	-0.12	-0.27	-0.30	0.32	0.81	0.15	-0.47	-0.63	-0.04	-0.16	-0.41	0.02	0.00	0.24	0.34	0.18	0.17	0.28	-0.52	0.10	-0.14	0.18
Magmatic rock	0.09	0.22	0.40	-0.05	0.41	0.41	0.05	-0.04	-0.22	1.00	-0.80	0.07	0.16	0.39	0.00	-0.24	-0.46	-0.12	0.20	0.23	-0.12	0.30	0.46	0.30	-0.26	-0.31	-0.29	-0.01	-0.25	-0.04	-0.09	-0.28	-0.26	-0.20	-0.08	-0.08	0.05	-0.17
Metamorphic rock	-0.45	-0.24	-0.46	-0.18	-0.43	-0.43	-0.10	-0.52	-0.28	-0.80	1.00	-0.46	-0.38	-0.35	0.22	0.42	0.42	0.20	-0.30	-0.39	-0.39	-0.53	-0.29	0.08	0.44	0.55	0.61	0.09	0.29	-0.03	-0.11	0.19	0.19	0.06	0.34	0.10	0.05	-0.17
Aspect flat	0.41	0.05	0.01	0.60	0.02	-0.01	-0.34	0.56	0.57	0.07	-0.46	1.00	0.53	0.12	-0.41	-0.36	-0.19	-0.36	-0.02	0.39	0.86	0.52	-0.01	-0.56	-0.59	-0.62	-0.63	0.15	0.15	0.53	0.49	0.29	0.32	0.45	-0.54	0.38	0.28	0.42
Aspect N	0.01	-0.28	-0.42	0.01	-0.49	-0.44	-0.40	0.18	0.57	0.16	-0.38	0.53	1.00	0.03	-0.80	-0.62	-0.26	-0.64	-0.15	0.67	0.66	0.06	-0.36	-0.45	-0.71	-0.36	-0.47	0.51	0.31	0.68	0.67	0.35	0.46	0.51	-0.27	0.54	0.19	0.51
Aspect NO	0.13	0.22	0.37	0.10	0.36	0.28	0.01	-0.06	0.12	0.39	-0.35	0.12	0.03	1.00	0.24	-0.58	-0.58	-0.08	0.02	0.01	0.04	0.10	-0.04	0.16	-0.14	0.16	0.19	0.35	0.32	0.13	0.21	-0.06	0.09	-0.09	-0.26	0.24	0.02	-0.16
Aspect O	0.12	0.37	0.52	0.06	0.55	0.48	0.35	-0.24	-0.40	0.00	0.22	-0.41	-0.80	0.24	1.00	0.41	-0.14	0.40	0.11	-0.56	-0.54	-0.08	0.24	0.33	0.04	0.14	0.32	-0.35	-0.16	-0.56	-0.45	-0.31	-0.37	-0.47	0.02	-0.37	-0.26	-0.60
Aspect SO	-0.09	-0.05	-0.08	-0.08	-0.07	-0.02	0.09	-0.29	-0.33	-0.24	0.42	-0.36	-0.62	-0.58	0.41	1.00	0.39	0.01	-0.22	-0.33	-0.35	-0.11	0.21	0.27	0.10	0.09	0.16	-0.48	-0.44	-0.37	-0.42	-0.20	-0.34	-0.21	0.12	-0.34	-0.19	-0.26
Aspect S	-0.38	-0.46	-0.46	-0.18	-0.40	-0.37	-0.20	0.04	-0.12	-0.46	0.42	-0.19	-0.26	-0.58	-0.14	0.39	1.00	0.36	-0.61	-0.57	-0.10	-0.21	0.04	0.17	0.17	0.11	0.06	-0.46	-0.36	-0.25	-0.21	0.00	-0.04	-0.06	0.32	-0.25	0.02	0.13
Aspect SW	-0.15	-0.02	0.25	-0.09	0.34	0.21	0.18	-0.03	-0.27	-0.12	0.20	-0.36	-0.64	-0.08	0.40	0.01	0.36	1.00	0.08	-0.77	-0.49	-0.13	0.27	0.43	0.15	0.13	0.19	-0.38	-0.37	-0.58	-0.57	-0.19	-0.37	-0.44	0.32	-0.49	-0.23	-0.31
Aspect W	0.20	0.57	0.47	0.20	0.48	0.48	0.40	0.04	-0.30	0.20	-0.30	-0.02	-0.15	0.02	0.11	-0.22	-0.61	0.08	1.00	0.38	-0.19	0.26	0.21	0.06	-0.24	-0.15	0.05	0.37	0.23	0.08	0.10	-0.02	0.24	0.00	0.05	0.10	0.18	-0.06
Aspect NW	0.32	0.19	-0.02	0.08	-0.12	-0.02	0.03	0.23	0.32	0.23	-0.39	0.39	0.67	0.01	-0.56	-0.33	-0.57	-0.77	0.38	1.00	0.48	0.48	-0.30	-0.45	-0.16	-0.15	0.23	0.45	0.15	0.54	0.45	0.19	0.40	0.41	-0.22	0.38	0.22	0.34
Slope 0-1	0.39	0.02	-0.10	0.53	-0.15	-0.15	-0.29	0.61	0.81	-0.12	-0.39	0.86	0.66	0.04	-0.54	-0.35	-0.10	-0.49	-0.19	0.48	1.00	0.49	-0.20	-0.71	-0.48	-0.55	-0.67	0.14	0.15	0.53	0.60	0.38	0.41	0.55	-0.52	0.40	0.29	0.48
Slope 1-2	0.33	0.65	0.56	0.66	0.58	0.60	0.22	0.53	0.15	0.30	-0.53	0.52	0.06	0.10	-0.08	-0.11	-0.21	-0.13	0.26	0.48	0.49	1.00	0.49	-0.20	-0.95	-0.91	-0.77	0.01	0.09	0.09	-0.05	-0.06	-0.04	0.07	-0.10	0.18	0.39	0.06
Slope 2-3	-0.14	0.41	0.39	0.32	0.49	0.46	0.07	0.06	-0.47	0.46	-0.29	-0.01	-0.36	-0.04	0.24	0.21	0.04	0.27	0.21	-0.30	-0.20	0.49	1.00	0.47	-0.60	-0.69	-0.52	-0.18	-0.11	-0.22	-0.02	-0.17	-0.20	-0.20	-0.10	-0.05	0.17	-0.16
Slope 3-4	-0.38	-0.18	-0.07	-0.43	-0.01	-0.05	-0.08	-0.39	-0.63	0.30	0.08	-0.56	-0.45	0.16	0.33	0.27	0.17	0.43	0.06	-0.45	-0.71	-0.20	0.47	1.00	0.37	0.14	0.12	-0.28	-0.33	-0.37	-0.40	-0.20	-0.37	-0.30	0.26	-0.34	-0.22	-0.29
Slope 4-5	-0.21	-0.61	-0.46	-0.79	-0.52	-0.52	-0.09	-0.48	-0.04	-0.26	0.44	-0.59	-0.71	-0.14	0.04	0.10	0.17	0.15	-0.24	-0.16	-0.48	-0.95	-0.60	0.37	1.00	0.90	0.68	-0.10	-0.18	-0.19	-0.38	-0.05	-0.19	-0.15	0.35	-0.31	-0.49	-0.16
Slope 5-6	-0.22	-0.45	-0.34	-0.68	-0.38	-0.38	0.06	-0.54	-0.16	-0.31	0.55	-0.62	-0.36	0.16	0.14	0.09	0.11	0.13	-0.15	-0.15	-0.55	-0.91	-0.69	0.14	0.90	1.00	0.91	0.02	-0.04	-0.20	-0.37	-0.09	-0.14	-0.21	0.44	-0.25	-0.38	-0.19
Slope >6	-0.27	-0.23	-0.18	-0.49	-0.18	-0.17	0.18	-0.56	-0.41	-0.29	0.61	-0.63	-0.47	0.19	0.32	0.16	0.06	0.19	0.05	0.23	-0.67	-0.77	-0.52	0.12	0.68	0.91	1.00	0.12	0.10	-0.21	-0.43	-0.13	-0.27	-0.27	0.47	-0.18	-0.27	-0.22
Cl	-0.26	0.03	-0.23	0.14	-0.22	-0.17	-0.12	-0.20	0.02	-0.01	0.09	0.15	0.51	0.35	-0.35	-0.48	-0.46	-0.38	0.37	0.45	0.14	0.01	-0.18	-0.28	-0.10	0.02	0.12	1.00	0.87	0.70	0.67	0.38	0.74	0.44	-0.10	0.76	0.34	0.44
SO₄	-0.31	0.23	-0.16	0.36	-0.12	-0.15	-0.16	-0.16	0.00	-0.25	0.29	0.15	0.31	0.32	-0.16	-0.44	-0.36	-0.37	0.23	0.15	0.15	0.09	-0.11	-0.33	-0.18	-0.04	0.10	0.87	1.00	0.63	0.62	0.57	0.83	0.50	-0.13	0.81	0.34	0.49
Na	-0.24	-0.05	-0.47	0.35	-0.46	-0.47	-0.59	-0.01	0.24	-0.04	-0.03	0.53	0.68	0.13	-0.56	-0.37	-0.25	-0.58	0.08	0.54	0.53	0.09	-0.22	-0.37	-0.19	-0.20	-0.21	0.70	0.63	1.00	0.69	0.74	0.90	0.54	-0.24	0.88	0.59	0.85
K	-0.10	0.06	-0.28	0.32	-0.29	-0.21	-0.27	0.23	0.34	-0.09	-0.11	0.49	0.67	0.21	-0.45	-0.42	-0.21	-0.57	0.10	0.45	0.60	-0.05	-0.02	-0.40	-0.38	-0.37	-0.43	0.67	0.62	0.69	1.00	0.39	0.74	0.54	-0.39	0.76	0.49	0.85
Mg	-0.38	-0.03	-0.49	0.43	-0.45	-0.56	-0.64	0.00	0.18	-0.28	0.19	0.29	0.35	-0.06	-0.31	-0.20	0.00	-0.19	-0.02	0.19	0.38	-0.06	-0.17	-0.20	-0.05	-0.09	-0.13	0.38	0.57	0.74	0.39	1.00	0.84	0.91	0.39	0.72	0.49	0.85
Ca	-0.29	0.10	-0.38	0.42	-0.36	-0.38	-0.42	-0.03	0.17	-0.26	0.19	0.32	0.46	0.09	-0.37	-0.34	-0.04	-0.37	0.24	0.40	0.41	-0.04	-0.20	-0.37	-0.19	-0.14	-0.27	0.74	0.83	0.90	0.74	0.84	1.00	0.89	-0.23	0.89	0.57	0.82
HCO₃calc	-0.24	-0.04	-0.50	0.41	-0.49	-0.52	-0.63	0.08	0.28	-0.20	0.06	0.45	0.51	-0.09	-0.47	-0.21	-0.06	-0.44	0.00	0.41	0.55	0.07	-0.20	-0.30	-0.15	-0.21	-0.27	0.44	0.50	0.90	0.54	0.91	0.89	1.00	-0.26	0.77	0.61	0.91
Runoff rate	-0.34	-0.01	-0.10	-0.43	-0.09	-0.04	0.34	-0.22	-0.52	-0.12	0.34	-0.54	-0.27	-0.26	0.02	0.12	0.32	0.32	0.05	-0.22	-0.52	-0.10	-0.10	0.26	0.35	0.44	0.47	-0.10	-0.13	-0.24	-0.39	0.39	-0.23	-0.26	1.00	-0.31	-0.15	-0.11
EC	-0.41	0.12	-0.38	0.49	-0.34	-0.37	-0.54	-0.13	0.10	-0.08	0.10	0.38	0.54	0.24	-0.37	-0.34	-0.25	-0.49	0.10	0.38	0.40	0.18	-0.05	-0.34	-0.31	-0.25	-0.18	0.76	0.81	0.88	0.76	0.72	0.89	0.77	-0.31	1.00	0.57	0.74
T	-0.27	0.30	-0.09	0.49	-0.02	-0.03	-0.20	0.09	-0.14	0.05	0.05	0.28	0.19	0.02	-0.26	-0.19	0.02	-0.23	0.18	0.22	0.29	0.39	0.17	-0.22	-0.49	-0.38	-0.27	0.34	0.34	0.59	0.49	0.49	0.57	0.61	-0.15	0.57	1.00	0.65
pH	-0.39	-0.12	-0.55	0.34	-0.52	-0.55	-0.61	0.10	0.18	-0.17	0.05	0.42	0.51	-0.16	-0.60	-0.26	0.13	-0.31	-0.06	0.34	0.48	0.06	-0.16	-0.29	-0.16	-0.19	-0.22	0.44	0.49	0.85	0.85	0.85	0.82	0.91	-0.11	0.74	0.65	1.00

Appendix Table 9: Input values used in the reactive transport model after Pogge von Strandmann et al. (2014); initial Li concentrations and Li isotope values are from this study

Input parameters for the model	
Porosity (n)	0.2
Density rock (ρ_r)	2700 kg/m^3
Density water (ρ_w)	1000 kg/m^3
Advective flow velocity (v)	$1.0 \cdot 10^{-4}$ m/s
Li concentration in rock ($\left[^6Li\right]_r$)	Depending on lithological class
δ^7Li rock ($\left(\frac{^7Li}{^6Li}\right)_r$)	Depending on lithological class
Precipitation rate ^{6}Li (^{6}Q)*	1 1/yr
Weathering rate ^{6}Li (^{6}W)**	$6.0 \cdot 10^{-6}$ 1/yr
W^{6}Li/Q^{6}Li	$6.0 \cdot 10^{-6}$
Steady state 6Li water [^{6}Li^{ss}]*	Depending on lithological class
Fractionation factor during precipitation (α_{precip})	0.985
Fractionation factor during weathering (α_{weath})	1
Measured Li concentration in glacier ice ($\left[^6Li\right]_w^0$)	0.01 µmol/L
Measured δ^7Li glacier ice ($\left(\frac{^7Li}{^6Li}\right)_w^0$)	17‰

* values are calculated according to the equation in Pogge von Strandmann et al. (2014)

** estimated from Li loads in the main stream

Appendix Table 10: Input parameters for residence time (RT) estimation.

Sampling location	^{4}He			^{3}He/^{4}He			Ne	Altitude	Recharge temperature	^{3}He-T	^{3}He-T			Tritium			Tritium-^{3}He Age		
	(Nml/g)						(Nml/g)	(m a.s.l.)	(°C)	(Nml/g)	(TU)			(TU)			(years)		
031	4He+B:J	±	3.0E-10	1.47E-06	±	1.5E-08	1.68E-07	2500	4.7	3.97E-15	1.6	±	0.1	9.3	±	1.0	2.8	±	0.5
043	3.54E-08	±	2.8E-10	1.32E-06	±	1.3E-08	1.52E-07	2650	3.9	3.53E-16	0.1	±	0.0	8.9	±	0.9	0.3	±	0.1
110	3.02E-07	±	1.1E-08	2.70E-07	±	2.7E-09	1.70E-07	2750	4.0	1.44E-14	5.8	±	0.6	11.2	±	1.0	7.5	±	1.2
044	4.42E-08	±	3.4E-10	1.36E-06	±	1.4E-08	1.81E-07	2650	4.2	1.52E-15	0.6	±	0.0	10.3	±	1.1	1.0	±	0.2
045	7.85E-07	±	6.0E-08	1.69E-07	±	1.7E-09	1.65E-07	2800	4.5	4.33E-14	17.4	±	2.4	11.5	±	1.3	16.5	±	2.8
244	3.59E-08	±	2.8E-10	1.39E-06	±	1.4E-08	1.59E-07	3450	3.0	2.50E-16	0.1	±	0.0	12.1	±	1.4	0.1	±	0.1
246	4.17E-08	±	3.2E-10	1.21E-06	±	1.2E-08	1.52E-07	3300	4.4	2.32E-15	0.9	±	0.1	12.1	±	1.2	1.3	±	0.2
300	2.80E-06	±	2.9E-07	1.74E-07	±	1.7E-09	1.05E-07	4000	2.5	3.19E-13	128.4	±	20.9	0.3	±	0.3	> 50		
290	5.41E-08	±	4.2E-10	1.02E-06	±	1.0E-08	1.60E-07	3750	4.2	2.80E-15	1.1	±	0.1	0.6	±	0.3	19.0	±	9.9
381	3.50E-08	±	2.8E-10	1.38E-06	±	1.4E-08	1.51E-07	4100	2.0	3.68E-16	0.1	±	0.0	14.0	±	1.4	0.2	±	0.0
021	3.88E-08	±	3.0E-10	1.38E-06	±	1.4E-08	1.64E-07	2800	5.0	1.31E-15	0.5	±	0.0	10.6	±	0.3	0.9	±	0.1

For separation of the He-components 3He/4He = 5e-8 was assumed for radiogenic helium.

Eidesstattliche Erklärung */ Declaration under Oath*

Ich erkläre an Eides statt, dass ich die Arbeit selbstständig und ohne fremde Hilfe verfasst, keine anderen als die von mir angegebenen Quellen und Hilfsmittel benutzt und die den benutzten Werken wörtlich oder inhaltlich entnommenen Stellen als solche kenntlich gemacht habe.

I declare under penalty of perjury that this thesis is my own work entirely and has been written without any help from other people. I used only the sources mentioned and included all the citations correctly both in word or content.

05.07.2019

Datum/*Date*	Unterschrift des Antragstellers */ Signature of the applicant*

Erklärung über bestehende Vorstrafen und anhängige Ermittlungsverfahren */ Declaration concerning Criminal Record and Pending Investigations*

Ich erkläre hiermit, dass ich weder vorbestraft bin noch dass gegen mich Ermittlungsverfahren anhängig sind.

I hereby declare that I have no criminal record and that no preliminary investigations are pending against me.

05.07.2019

Datum/*Date*	Unterschrift des Antragstellers */ Signature of the applicant*

Lebenslauf / Curriculum Vitae

Zu meiner Person

Dipl. Geogr. Christiane Meier

Karl-Liebknecht-Str. 19

06114 Halle (Saale)

Tel.: (+49) 1573 1145307

E-Mail: meier.christiane(at)gmx.net

Geboren am 25.12.1983 in Rodewisch

Familienstand: verheiratet, 2 Kinder

Beruflicher Werdegang

Seit 02/2016	Wissenschaftliche Mitarbeiterin
	Umweltbundesamt Fachgebiet IV 1.2 „Biozide" Exposition, Abbau, Risikominderung, Gesamtbewertung Materialschutz
10/2011-01/2016	Doktorandin und wissenschaftliche Mitarbeiterin Helmholtz-Zentrum für Umweltforschung - UFZ, Department Catchment Hydrology, Halle
	Thema: *„Multi-Tracer-basierte Charakterisierung eines Einzugsgebiets (Fluss Gunt) im tadschikischen Pamir"* (BMBF-Projekt "PAMIR-Water")
09/2011	Tätigkeit als wissenschaftliche Hilfskraft Helmholtz-Zentrum für Umweltforschung - UFZ, Department Catchment Hydrology, Halle
07/2011-08/2011	Tätigkeit als studentische Hilfskraft Helmholtz-Zentrum für Umweltforschung - UFZ, Department Catchment Hydrology, Halle

Studium

10/2003-08/2011	Studium der Geographie an der TU Dresden
	Schwerpunkte: Physische Geographie, Hydrologie und Meteorologie
	Thema der Diplomarbeit: *„Isotopendendrochronologische Untersuchungen der Reaktionen von Fagus sylvatica L. und Picea abies [L.] H. Karst im Unterharz bei Harzgerode (Sachsen-Anhalt, Mitteldeutschland) auf Änderungen von Klima und Umwelt"*

09/2006-06/2007	ERASMUS-Auslandsstudium an der Université Joseph Fourier in Grenoble/Frankreich
10/2002-01/2003	Studium der Lebensmittelchemie an der TU Dresden

Schulbildung

1994-2002	Wilhelm-Adolph-von-Trützschler-Gymnasium Falkenstein
	Abschluss: Allgemeine Hochschulreife

Berufliche Weiterbildung

19.09.-22.09.2017	„Allgemeines Projektmanagement"
	QUI mbH, Leonhard Limburg, Bundesakademie für öffentliche Verwaltung (BAKöV)
05.04.-08.04.2016	„Kommunizieren und kooperieren"
	Dörthe Engelhardt, Bundesakademie für öffentliche Verwaltung (BAKöV)
01.06.-04.06.2015	Organische Hydrochemie
	• Organische Schadstoffe in der Umwelt
	PD Dr. Wolfgang Gossel, Martin-Luther-Universität Halle-Wittenberg
15.04.-17.04.2013	"Scientific Writing"
	Jana Kaiser, B. Sc. Hons, Coordinator for English, Language Resource Centre, TU Darmstadt
06.03.-08.03. 2013	„Introduction to Research in Environmental Technology"
	• Boden- und Grundwasserremediation
	PD Dr. L. Adrian, Helmholtz-Zentrum für Umweltforschung, Leipzig
19.10.-20.10.2012	"Academic Presenting in English"
	Millie Baker, Presence Training Ltd.
10/2009	Praktikum am Helmholtz-Zentrum für Umweltforschung – UFZ, Halle im Department Isotopenhydrologie

10/2005-02/2009   Teilnahme am Studienprogramm FLOODmaster der TU Dresden

07/2006-09/2006   Praktikum im Sächsischen Landesamt für Umwelt und Geologie
                       im Energieeffizienzzentrum

Publikationen   (nur Erstautor)

Juhlke, T.R.*, **Meier, C.***+, van Geldern, R., Vanselow, K.A., Wernicke, J., Baidulloeva, J., Bart, J.A.C., Weise, S.M., (2019): Assessing moisture sources of precipitation in the Western Pamir Mountains (Tajikistan, Central Asia) using deuterium excess, *Tellus B: Chemical and Physical Meteorology*, 71 (1), 1-16

   * diese beiden Autoren teilen sich die Erstautorenschaft
   + Corresponding author

Meier, C., Osenbrück, K., Seitz, H.-M., Weise, S.M., (2017): First Lithium Isotope Data from Rivers and Subsurface Water in the Pamirs, *Proc. Earth Plan. Sci.,* 17, 574-577

Meier, C., Knoche, M., Merz, R., Weise, S.M., (2013): Stable isotopes in river waters in the Tajik Pamirs: regional and temporal characteristics, *Isot. Environ. Health Stud*. 49 (4), 542 – 554

Konferenzteilnahme | Präsentationen (nur Erstautor)

27.-28.09.2018   Grundwassermonitoring und –probenahme 2018, Torgau   Eingeladener Vortrag: Einträge von Bioziden in das Grundwasser

13.-17.05.2018   SETAC Europe Annual Meeting, Rom   Poster: Monitoring of Biocides in German Sewage Treatment Plant Effluents – First Results

25.-28.06.2018   International conference on emerging contaminants (EmCon), Oslo   Vortrag: Monitoring of Biocides in German Sewage Treatment Plant Effluents – First Results

19.-20.06.2018   River Basins, Wien   Poster: Monitoring of Biocides in German Sewage Treatment Plant Effluents

20.-21.11.2017	Symposium "Beregnete Fassaden", Ober-Ramstadt	Eingeladener Vortrag: Welche Rolle spielen Labor- und Felddaten bei der Zulassung von Biozidprodukten?
17.-21.10.2016	Water-Rock-Interactions, Évora	Poster: First lithium isotope data from rivers and subsurface water in the Pamirs; (1. Platz, Posterpreis)
17.11.2015	HIGRADE Fall Conference, Leipzig	Poster: Panta rhei – sources and flow paths of river water in the Pamir Mountains; (2. Platz, Posterpreis)
04.-08.10.2015	Mountains of our Future Earth, Perth (UK)	Vortrag: What are the controlling factors on water composition in the Amu Darya headwaters?
28.-30.09.2015	Jahrestagung der Arbeits-gemeinschaft Stabile Isotope e.V., Heidelberg	Vortrag: What does δ^7Li tell us about flow paths in an alpine catchment?
11.-15.05.2015	International Symposium on Isotope Hydrology, IAEA Wien	Poster: Monitoring of stable isotopes in precipitation in the Tajik Pamirs Poster: δ^7Li for detecting ground water contributions and underground passages of river water
13.-17.04.2015	European Geosciences Union General Assembly 2015, Wien	Vortrag: What can δ^7Li tell us about sources and flow pathes of river water (Western Pamir, Tajikistan)? Poster: Single or multiple source(s) of precipitation in the Western Pamirs, Tajikistan?
15.-17.10.2014	Jahrestagung der Arbeitsgemeinschaft Stabile Isotope e.V., München	Poster: Erforschung von Abflusskomponenten im Tadschikischen Pamir mittels δ^7Li und ^{87}Sr/^{86}Sr

07.-12.04.2013	European Geosciences Union General Assembly 2013, Wien	Vortrag: Regional stable isotope patterns of river waters in an arid catchment in Central Asia
04.-06.04.2013	Tag der Hydrologie, Bern	Poster: Identifizierung und Quantifizierung von Abflusskomponenten in einem nival-ariden Einzugsgebiet in Zentralasienmittels stabiler Isotope
15.-17.11.2012	44. Jahrestreffen des Arbeitskreises Hydrologie, Lunz am See	Vortrag: Regional isotope patterns and hydrograph separation of an ungauged basin in Central Asia
20.-21.09.2012	Annual Meeting of the Joint Programme CAME, Frankfurt am Main	Vortrag: Project report: PAMIR
02.-07.09.2012	Joint European Stable Isotope Users Group Meeting - JESIUM 2012, Leipzig	Vortrag: Regional isotope patterns and hydrograph separation of an ungauged basin in Central Asia
16.-20.05.2012	Tagung der Fachsektion Hydrogeologie 2012, Dresden	Poster: Determining the water budget of the Gunt (semi-arid Tajik Pamir) using stable water isotopes, hydrochemical- and remote sensing data
22.-27.04.2012	European Geosciences Union General Assembly 2012, Wien	Poster: Isotopic and hydrochemical characterisation of a (semi)-arid catchment in the Tajik Pamirs
22.-23.03.2012	Tag der Hydrologie, Freiburg im Breisgau	Poster: Charakterisierung des Abflussverhaltens eines Flusses (Gunt) im semi-ariden Pamir Tadschikistans mittels stabiler Isotope, Hydrochemie und Fernerkundung

Sonstige Kenntnisse und Fähigkeiten

Führerschein	Klasse B seit Januar 2002
Sprachkenntnisse:	Deutsch: Muttersprache

Englisch: Fließend in Wort und Schrift

Französisch: Konversationssicher

Latein: Latinum

IT-Kenntnisse   MS Office: Umfassende Kenntnisse

Mathcad: Anwenderkenntnisse

FOCUS Pearl: Anwenderkenntnisse

ArcGIS: Anwenderkenntnisse

GIMP: Anwenderkenntnisse

Private Interessen

Kammerchor CantART Halle e.V. (Vorstandsvorsitzende seit 2012)

05.07.2019

Datum/*Date*   Unterschrift */Signature*